DEVELOPMENT OF A MANDREL SYSTEM WITH MACRO-TO-MICRO ANALYSIS FOR PREFABRICATED VERTICAL DRAIN INSTALLATION: REDUCING SMEAR ZONE IN SOFT SOIL

メイラニ, アデリヤティ

出版情報：Kyushu University, 2023, 博士（工学）, 課程博士
バージョン：
権利関係：

DEVELOPMENT OF A MANDREL SYSTEM WITH MACRO-TO-MICRO ANALYSIS FOR PREFABRICATED VERTICAL DRAIN INSTALLATION: REDUCING SMEAR ZONE IN SOFT SOIL

MEILANI ADRIYATI

SEPTEMBER 2023

DEVELOPMENT OF A MANDREL SYSTEM WITH MACRO-TO-MICRO ANALYSIS FOR PREFABRICATED VERTICAL DRAIN INSTALLATION: REDUCING SMEAR ZONE IN SOFT SOIL

九州大学

A THESIS SUBMITTED

IN PARTIAL FULFILLMENT OF THE REQUIREMENTS

FOR THE DEGREE OF

DOCTOR OF ENGINEERING

BY

MEILANI ADRIYATI

TO THE

DEPARTMENT OF CIVIL AND STRUCTURAL ENGINEERING

GRADUATE SCHOOL OF ENGINEERING

KYUSHU UNIVERSITY

FUKUOKA, JAPAN

2023

GEOTECHNICAL ENGINEERING LABORATORY
DEPARTEMENT OF CIVIL AND STRUCTURAL ENGINEERING
GRADUATE SCHOOL OF ENGINEERING
KYUSHU UNIVERSITY
FUKUOKA, JAPAN

CERTIFICATE

The undersigned hereby certify that they have read and recommended to the Graduate School of Engineering for the acceptance of this dissertation entitled, "**DEVELOPMENT OF MANDREL SYSTEM WITH MACRO-TO-MICRO ANALYSIS FOR PREFABRICATED VERTICAL DRAIN INSTALLATION: REDUCING SMEAR ZONE IN SOFT SOIL"** in partial fulfillment of the requirements for the degree of **DOCTOR OF ENGINEERING**.

Date: June 2023

Supervisor:

____

Prof. Noriyuki YASUFUKU, Dr. Eng.

Examining Committee:

____

Prof. Kyoshi OMINE, Dr. Eng

____

Prof. Masaru YAMASHIRO, Dr. Eng

ACKNOWLEDGMENT

Foremost, I would like to express my gratitude to the Almighty "Allah SWT", the God of all mankind, for giving me the health, strength, patience, and faith to complete the three years of the doctoral degree and to my beloved Parents (Muhammad Fatoni and Titin Priyatini), Sister (Fitri Setyowati H), Brother (Sonny Atmajaya), and Takeru Mitsuoka who have always been by the side through and thin. Their support for completing of this work, as always, for which my mere expression of thanks does not suffice.

I wish to express my sincere thanks and gratitude to my supervisor, Prof. Noriyuki YASUFUKU, for his kindness, precious time, constant support, guidance, and patience. He always looked for areas in my work which I could still improve. His good advice and encouragement have been invaluable both on an academic and personal level.

I would like to express my gratefulness to members of the examining committee Prof. Kiyoshi OMINE and Prof. Masaru YAMASHIRO for their treasured time, attentive evaluation, and valuable comments on my research.

I would also like to express my thankfulness to Assoc. Prof. Ryohei ISHIKURA for his guidance and valuable advice to improve my research.

My grateful appreciation to Mr. Michio NAKASHIMA for his support and logical insights when carrying out my experimental work.

My thankyou also addressed to Assoc. Prof. Ahmad RIFA'I and Assoc. Prof. Xue-Ting WU for kindness in guiding and precious advice during my research.

I would also like to extend my sincere appreciation to Mrs. Aki ITO, Mrs. Mayumi KUGIMOTO and Mrs. Yasura OIWA for their support in all administrative works.

I am ineffably indebted to the JICA-MEXT Scholarship in Innovative Asia program for providing the opportunity to study at Kyushu University.

Special thanks are given to present and past research colleagues of Geotechnical Engineering laboratory (Specially M. Akmal P., Rosy E. A. R., M. Gobin., and Erik H. G., for helping experimental works and reviewed my publications) and Indonesian Students Association in Fukuoka (Dilla, Cindy, Alvin, Ilma, Basoka, Wili, Dania, Egi, Laras) for their friendship and support throughout my time at Kyushu University and Fukuoka.

Meilani Adriyati

PUBLICATIONS

Adriyati, M., Yasufuku, N., Ishikura, R., Rifa'i, A. (2021). Numerical analysis of combined surcharge preloading using prefabricated vertical drain and stone column on runway construction. In: *Proceedings of 4th International Conference on Sustainable Infrastructure (ICSI 2021). (Virtual conference) Yogyakarta State University, Indonesia, October 5, 2021, pp. 1-9.* **(*International Conference*)**.

Adriyati, M., Yasufuku, N., Ishikura, R., Rifa'i, A. (2022). A simulation of embodied CO2 Emission of ground improvement technique using life-cycle assessment in runway construction. In: *Proceedings of 7th World Congress on Civil, Structural, and Environmental Engineering (CSEE 2022). (Virtual conference) Lisbon, Portugal, April 10-12, 2022, pp.236.1-5, ISSN 2371-5294, ISBN 9781927877999. DOI:* 10.11159/icgre22.236.
(*International Conference*).

Adriyati, M., Yasufuku, N., Ishikura, R., Rifa'i, A. (2022). Optimizing modified large-scale consolidation testing for describing smear zone caused by mandrel-driven prefabricated vertical drain. In: *Proceedings of 2022 GeoAsia7 conference & IGS First Young Engineering conference (GeoAsia7) - Taipei International Convention Center (TICC), Taipei, Taiwan, 2022, (ID: D-005) pp.1-4.* **(*International Conference*)**.

Adriyati, M., Yasufuku, N., Ishikura, R., A. Rifa'i, R. E. (2023). Microstructure analysis methods on clogging effect of PVD combined with vacuum preloading in soft ground. In: *The 58th Annual Meeting of the Japan National Conference on Geotechnical Engineering*. **(*National Conference*)**.

Adriyati, M., Yasufuku, N., Ishikura, R., Wu, X., Rifa'i, A. (2023). Improved Mandrel System for Prefabricated Vertical Drain Installation: A Macro to Micro Analysis. In*: Applied Sciences. 2023; 13(11):6673.* https://doi.org/10.3390/app13116673 **(*Journal)***.

ABSTRACT

In archipelagic countries such as Indonesia, airport infrastructure is becoming more important to increase connectivity and economic growth. Air transportation is one of the priority sectors in the ASEAN Economic Community (AEC). In particular, more airport facilities have been rebuilt and expanded in Indonesia. However, most of the airports are located on soft soil because the limited areas of stable soil are designated for urban use. Therefore, finding an effective method for engineering design in soft soil areas has become an important issue.

Soft soil has low strength, high compressibility, high water content, and it requires a far longer time to completely consolidated. Rapid and effective treatment of soft soil is needed to increase shear strength, increase permeability, reduce the post-construction differential settlement, and save construction costs. Therefore, ground improvement methods using a prefabricated vertical drain (PVD) combined with vacuum preloading have been utilized to accelerate the consolidation of soft soil by improving the mechanical properties since the early 1970s. However, the PVD performance is influenced by several factors. Firstly, the effect of PVD installation creates a smear zone in which the surrounding soft soil area is disturbed due to the mandrel's influence. Moreover, various types of PVD cores are related to the influence zone. In addition, the particle migration induces a binding effect which significantly weakens in which clay particles in smear zone surrounding the PVD, while also remarkably affecting the consolidation rate. Lastly, the smear zone acts as a barrier to the flow towards the PVD by reducing the permeability and affecting the consolidation requires a far longer time.

The objective of this research is to evaluate the effectiveness of a newly developed mandrel system in reducing the smear zone caused by installation of PVD and vacuum preloading conducted through a macro-to-micro analysis. To conduct this study, a mandrel system and three types of PVD cores were utilized. The performance of PVD combined with vacuum preloading technique in field conditions through 1g model testing in laboratory setting are investigated as macro level. In addition, to evaluate the performance of mandrel system and PVD, microstructure analysis was conducted using a scanning electron microscope (SEM) for micro-level investigation. Furthermore, this study was subjected to new Runway 3 construction in Soekarno-Hatta International Airport project in Indonesia. To achieve those missions, this dissertation includes seven chapters, as follows:

Chapter 1 provides an introduction of this research and focuses on the new Runway 3 Soekarno-Hatta International Airport in Indonesia. It highlights current issues and the motivation behind laboratory testing based on Standard National Indonesia (SNI), American Society for Testing and Materials (ASTM), and Japanese Geotechnical Society (JGS). This chapter also outlines the original contribution of this thesis along with the description of the ground improvement technology, objective, scope, limitation, and the framework of the thesis.

Chapter 2 offers a brief literature review associated with the present work. To covers various aspects such as the present theories of PVD, vacuum preloading, and factors affecting consolidations, including the equivalent diameter effect of mandrel, PVD filter and core, tensile strengths, discharge capacity, mandrel size and shape, installation procedure, PVD spacing, influence zone, the smear zone effect, clogging effect due to vacuum preloading, and microstructure analysis. These aspects, including the problem to be solved based on previous research, have been reviewed in detail.

Chapter 3 focuses on field observations and the implications of embodied CO_2 emissions concerning PVD material. Firstly, the finite element method (FEM) is conducted to present a performance of PVD combined with preloading. This analysis results propose a conversion of the axisymmetric to plane-strain condition to approach for accurate analysis of the advantages of PVD spacing in accelerating consolidation. It was found that the proposed formula can predict the results closed with the field measurement data. Therefore, the formula proved for analyzing the proper consolidation rate using FEM. Secondly, the life cycle assessment (LCA) is conducted on the implications of embodied CO_2 emissions for PVD materials based on their embodied carbon value. The analytical results found that PVD materials have lower embodied emissions than other ground improvement methods.

Chapter 4 presents the methodology of the laboratory experiment (1g model) and Scanning Electron Microscopy (SEM). The 1g model test is used to understand the development mandrel system during the installation of PVD material and can be utilized to measure the mechanical behavior of soft soil during and after vacuum preloading as a macro-level analysis. The SEM image analysis can be used to measure the chemical composition and structure of soft soil and PVD, before and after vacuum preloading as a micro-level analysis. The following subsection explains the important functions of apparatus and remarks the specific test procedures including the apparatus set up and model ground preparation to obtain accurate results.

Chapter 5 evaluates the effect of developed mandrel system using a 1g model test on the performance of soil improvement. The effect of water content, shear strength of soft soil, permeability, water flow rate, discharge capacity, soft soil settlement, excess pore water pressure, and consolidation rate has been discussed to examine the performance of PVD. The effectiveness of the mandrel system can be observed in its impact on the consolidation rate through the evaluation of an inner smear zone, transition zone and undisturbed zone. Furthermore, extended inner smear zone in the transition zone can be observed in its influence on the physical and mechanical indices of soft soil such as water content, shear strength of soft soil, and permeability. The results show that the water content, shear strength of soft soil, and permeability gradually increased in the inner smear zone and transition zone, while both decreased in the radial distance. It is concluded that the 1g model test can demonstrated the effect of developed mandrel system.

Chapter 6 describes the microstructure analysis using a SEM. The analysis of micro-level images clarifies the effect of the developed mandrel system in reducing the smear zone by examining the structure of soft soil with PVD. A microstructure analysis allowed examining the clogging effect by estimating the pore area and the particle area of the structure before and after consolidation. The results clarify the clogging effect due to mandrel system related to pore area and the particle area. In addition, the correlation between shear strength of soft soil and permeability of soft soil, and pore area revealed an inverse relationship, which can characterize the effect of the mandrel system.

Chapter 7 summarizes the main findings and provides recommendations for future research.

TABLE OF CONTENTS

LIST OF FIGURES

LIST OF TABLES

LIST OF NOTATIONS AND ABBREVIATIONS

k_p	Permeability of the prototype (m/s)
k_m	Permeability of the model (m/s)
k_v	Permeability of the PVD (m/s)
z_p	The embedded length of the PVD prototype (m)
z_m	The embedded length of the PVD model (m)
n_k	Scale factor of the permeability
n_z	Scale factor of embedded length
F	Scale factor
Δv	The change in initial specific volume (m^3/s)
Δe	The change in void ratio
E	Young's modulus (kPa)
w_p	Plastic limit (%)
w_L	Liquid limit (%)
I_p	Plasticity index
G_s	Specific Gravity
w	Water content (%)
$r_{w\,(\text{Type A})}$	The radius of PVD type A (mm)
$r_{w\,(\text{Type B})}$	The radius of PVD type B (mm)
$r_{w\,(\text{Type C})}$	The radius of PVD type C (mm)
$r_{w.eq}$	The radius of an equivalent drain system (mm)
a	Width of the mandrel (m)
x_1	The thickness of PVD type A (mm)
x_2	The thickness of PVD type B (mm)
x_3	The thickness of PVD type C (mm)
x_i	Different types of PVD thickness variants (mm)
y_i	The factor variant of PVD
s	Extended smear zone (mm)
r_s	The radius of the transition zone (mm)
r_w	The radius of PVD with mandrel (mm)

L	The length of the chamber apparatus (mm)
D_e	The diameter of the chamber apparatus (mm)
Q	The amount of water flow (g/s)
Q_{cal}	General form for amount of water flow (g/s)
β'	Slope of the water flow rate (°)
t_0	elapsed time of the actual water flow rate (s)
$Q_{t=1}$	initial value or sort-term value of the water flow rate in elapsed time
i	dimensionless hydraulic gradient
Δh	the head difference (m)
q_w	discharge capacity (m^3/s)
q_{w0}	The initial value of the discharge capacity (m^3/s)
A_0	The coefficient with respect to the time-dependent discharge capacity in elapsed time (s)
t	Elapsed time (s)
U	The average consolidation rate (non-unit)
T	Time factor (non-unit)
μ	The factor (non-unit) that takes soil disturbance surrounding the PVD
c_h	The coefficient of consolidation in the horizontal direction
k_{hs}	Hydraulic conductivity in transition zone of smear zone in axisymmetric conditions (mm/s)
k_s	Hydraulic conductivity of smear zone (mm/s).
k	Permeability
r_s	The radius of the smear zone (mm)
r_w	The radius of PVD with mandrel (mm)
η	smear zone permeability ratio
$-p0$	The vacuum pressure (kPa)
S	Torque
D	Diameter of vane (mm)
H	Height of vane (mm)
n	Total area of soil pores as a percentage (%)
n	Pore area (μm2)

n_0	Total area of soil pores (μm2)
n'	Total area of PVD and pores as a percentage (%)
n'	PVD and pore area (μm2)
n'_0	Total area of PVD and pores (μm2)
n_{total}	Total area of SEM image (μm2)
$s_{u.cal}$	Initial shear strength (kPa)
β	Slope of the strength (°)
r_{d0}	Radial distance (mm)
$\emptyset'$	Particle area (μm)
α	Slope of the pore area (°)
s_u	Vane shear strength (kPa)
PVD	Prefabricated vertical drain
SEM	Scanning electron microscope
AEC	ASEAN Economic Community
PWP	Pore water pressure
LVDT	Linear variable differential transformers
PC	Personal computer
ASTM	American Standard for Testing and Materials
CAIA	Advanced instrumental analysis
AOS	Apparent opening Size
O_{95}	The AOS of filter
D_{85}	The size which is larger than 50% of the fabric pores
D_{50}	The size for 85% and 50% of passing of soil particle by weight

This Page Intentionally Left Blank

CHAPTER I INTRODUCTION

Increasing development of infrastructure in Indonesia has driven the need for effective ground improvement methods to accelerate the consolidation of soft soil, which is estimated to occupy around 10% of the country's land area. Therefore, finding an effective ground improvement method for engineering design in soft soil areas has become a critical issue, especially in Indonesia. Therefore, ground improvement methods using a prefabricated vertical drain (PVD) combined with vacuum preloading to accelerate the consolidation of soft soil by improving the mechanical properties have been used since the early 1970s (Bergado et al., 1993).

This chapter serves as an introduction to the research and provides a detailed discussion on the field conditions, materials, and laboratory testing from macro-to-micro levels. Additionally, it concludes with a comprehensive description of the ground improvement technology, outlining the objectives and scope of the research, limitations, framework, and original contributions of the thesis.

1.1 BACKGROUND

The air transport facility is becoming an increasingly important sector, especially for an archipelagic country like Indonesia, as it enhances connectivity and boosts economic growth. Air transport is also a critical priority sector in the ASEAN Economic Community (AEC) (Saraswati & Hanaoka, 2013). In particular, Indonesia has recently undergone extensive development in its aviation infrastructure, including the expansion and rebuilding of airport facilities and runways (Laksono et al., 2018; Refaldi et al., 2018; Wibowo & Hamzah, 2022). Despite these efforts, the proportion of air traffic relative to population size in Indonesia remains lower compared to neighboring countries such as Malaysia, Thailand, and Singapore. Figure 1. 1 show that the Indonesia airport facility has an enormous opportunity to be develop, showing of 34% of proportion of population and air traffic. Therefore, it is essential to continue developing and expanding Indonesia's aviation infrastructure to keep pace with its economic growth and improve connectivity.

The construction of soft soil areas is a significant concern for geotechnical engineeri-

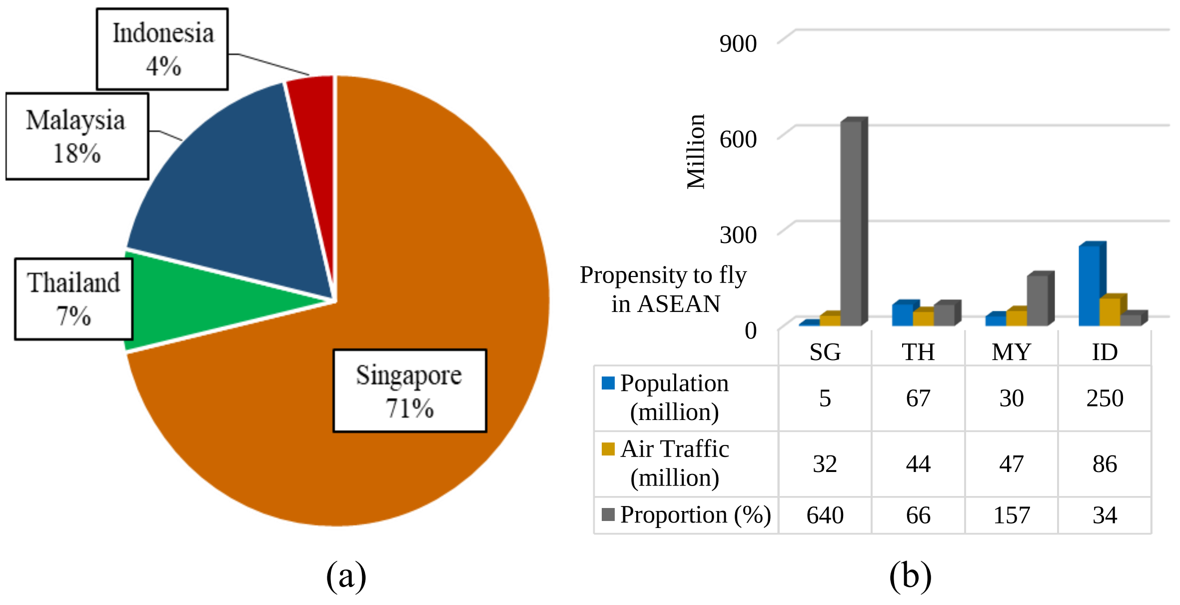

Figure 1. 1. (a) Air transportation data; (b) Proportion data in ASEAN.

ng design. Indonesia, a country consisting of over ten thousand islands, faces various difficult ground conditions including soft soil, peats, expansive soils, loose sands, highly weathered and fragmented rocks, and clay shales. As illustrated in Figure 1. 2 the research area is composed of alluvial deposits, beach ridge deposits, and banten tuff (Turkandi et al., 1992). Around 10% of the total land area of Indonesia are estimated to be soft soil (Cox JB, 1970; Gouw, 2020). Due to the limited availability of stable soil for urban use (Adriyati et al., 2020), most airports are located on soft soil.

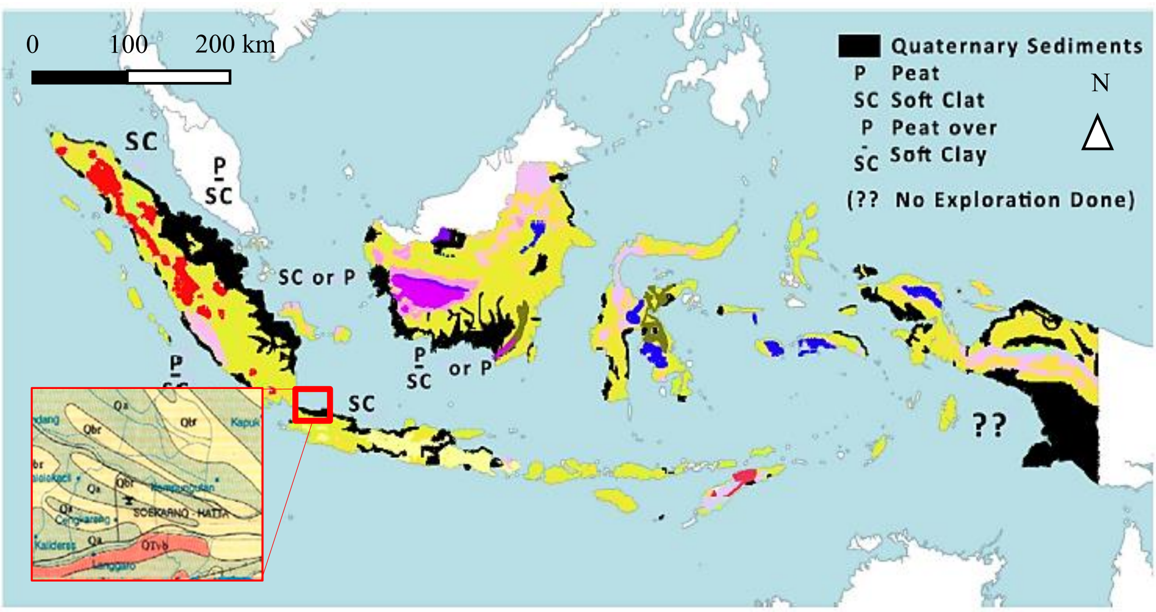

Figure 1. 2. Soft soil and geology map of Indonesia (Gouw, 2020; Turkandi et al., 1992).

A new Runway and Taxiway construction development at Soekarno-Hatta International Airport Indonesia is shown in Figure 1. 3, getting the impact of passenger's growth was studied in 2016. The Runway and Taxiway service will be serving wide-body aircraft types, such as the Airbus A380 and the B 777-300 ER aircraft type, which require the largest pavement structural strength capacity (Nur straits Engineering, 2017).

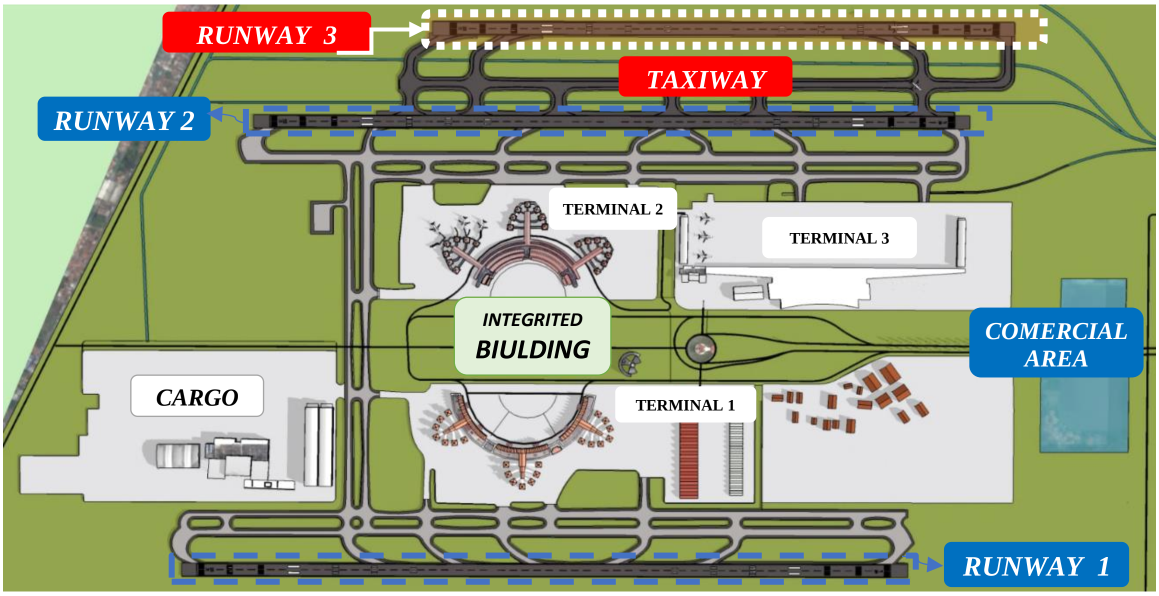

Figure 1. 3. Map of New Runway 3 at Soekarno-Hatta International Airport Indonesia (Nur straits Engineering, 2017).

1.2 GROUND IMPROVEMENT TECHNOLOGY IN INDONESIA

Ground improvement technology has been implemented in Indonesia since 1983 (Gouw, 2020). In the last 5 years, government initiatives to enhance housing and infrastructures have led to the construction of facilities such as housing, power plants, highways, railways, seaports, and airports, many of which have been built on soft soil regions requiring consolidation. To accelerate the consolidation process, either surcharge or vacuum preloading techniques have been implemented due to their faster construction time compared to conventional preloading with PVD.

The PVD combined with vacuum preloading installation is an effective, economic, and environmentally friendly method for improving soft clayey deposits, as illustrated in Figure 1. 4. This method involves applying a vacuum to the ground through a sealing membrane, perforated by PVDs installed within the ground mass under treatment, to accelerate consolidation.

The PVD combined with vacuum preloading method involves applying a vacuum to the ground through a sealing membrane that protects it from ground-surface pressure losses and is installed along PVD in the treated ground mass. The vacuum pump creates negative pressure with respect to atmospheric pressure in a permeable soil cushion located directly beneath the membrane. The main issue found in PVD combined with vacuum preloading installation are found as follows: a) the effect of PVD installation creates a smear zone in which the surrounding soil area is disturbed due to the mandrel's influence (Adriyati et al., 2022a, 2022b; Perera et al., 2017); b) apparent clogging around the PVD due to migration of soil particles to the zone around the PVD (Bergado et al., 1993, 2020; P. Wang et al., 2020); and c) the effect of discharge capacity decrease due to smear zone and vacuum preloading (Bo et al., 2016; Shin et al., 2008). Therefore, finding an effective method for engineering design in soft soil by using PVD combined with vacuum preloading has become an important issue especially in Indonesia.

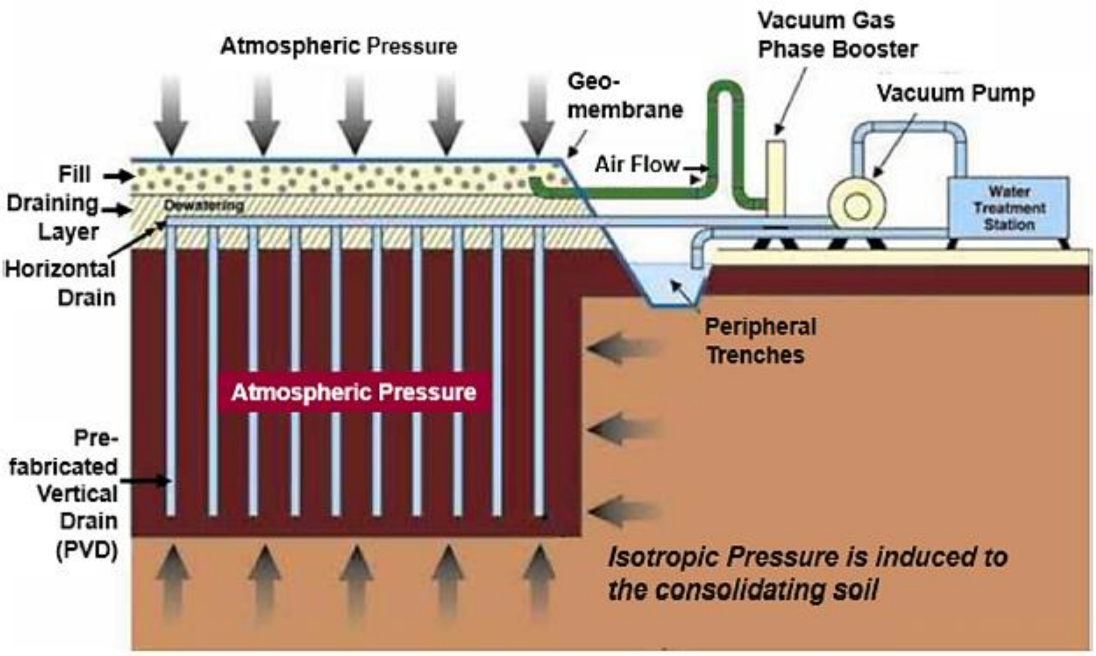

Figure 1. 4. Configuration of the vacuum preloading in Indonesia (Nur straits Engineering, 2017).

1.3 RESEARCH OBJECTIVES

This research aims to investigate the PVD performance combined with vacuum preloading method using a designed rectangular mandrel system and three types of PVD cores. The study involved large-scale consolidation testing in the laboratory to analyze the method's performance at the macro level. Additionally, microstructure analysis using a scanning electron microscope (SEM) examined the effect of the mandrel system and PVD combined with vacuum preloading performance at the micro level. Furthermore, this study was subjected to new Runway 3 construction in Soekarno-Hatta International Airport project in Indonesia, as follows:

1. To conduct a comprehensive analysis of a project in Indonesia through numerical and empirical methods, including axisymmetric to plane-strain conversion and involve an analysis of the environmental impact of PVD material, specifically its embodied CO_2 emissions.
2. To develop a laboratory experiment using a 1g model and microstructure analysis method, and provide a detailed explanation of the experimental procedure, scaling law, and apparatus functions. In addition, ImageJ software was used to support SEM image analysis.
3. To evaluate the effect of an extended inner smear zone in the transition zone on consolidation rate using a 1g model test and empirical analysis.
4. Microstructure analysis is conducted following vacuum preloading and discuss the pores and particle of PVD and soil interaction.

To achieve the aims to this thesis, several objectives were formulated, as described in Figure 1. 5.

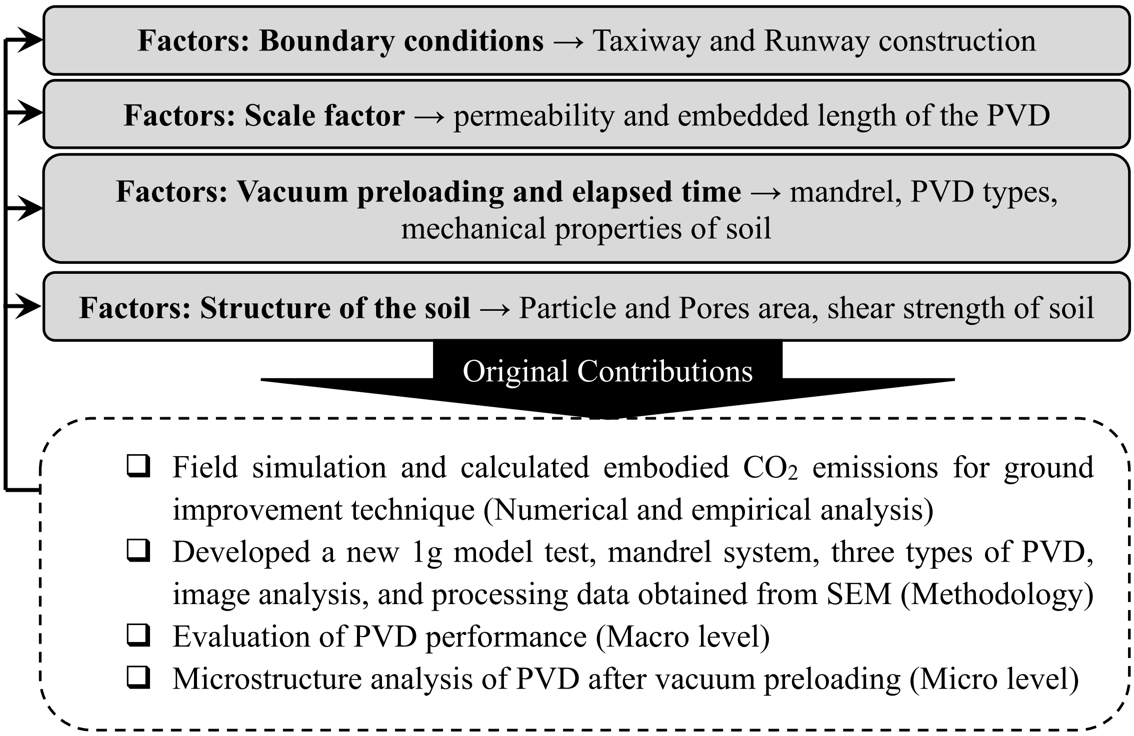

Figure 1. 5. Original contribution.

1.4 ORIGINAL CONTRIBUTIONS

This thesis presents a novel mandrel system to reduce the smear zone caused by installing prefabricated vertical drain (PVD) in soft soil ground. The research employs field conditions, laboratory experiments, analytical approaches, and proposes new findings that contribute to the field of soil mechanics. Several novel findings are obtained, which are considered to be the original contributions of this research, as follows:

Firstly, a formula for converting axisymmetric to plane-strain equivalents based on field conditions to accurately model the behavior of prefabricated vertical drains (PVD) in soft soil ground using FEM in PLAXIS2D. In addition, empirical analysis is employed to calculate the environmental implications of PVD material, specifically its embodied CO_2 emissions.

A newly 1g model experimental has been designed. The experiment evaluates the effectiveness of the combination of a prefabricated vertical drain (PVD) and vacuum preloading and includes the fabrication of a designed mandrel, conforming to the standard guidelines set by several national and international agencies such as standard national Indonesia (SNI), American society for testing and materials (ASTM), and Japanese geotechnical society (JGS).

To examine the laboratory results, the thesis proposes a three-zone theory of large-scale consolidation and modifies the formula for evaluating the consolidation rate based on empirical observations for understanding the behavior of soft soil ground under the influence of PVD.

Finally, microstructure analysis using a scanning electron microscope (SEM) is carried out to examine the effect of the mandrel system and smear zone by estimate the pores and particle size structure after consolidation, enabling an assessment of clogging effects on PVD behavior. By analyzing the microstructure of the soil, this study helps to identify the mechanisms that influence the behavior of PVD in soft soil ground.

1.5 FRAMEWORK AND OUTLINES OF THE THESIS

To accomplish the objectives and scopes, this thesis is structured into seven chapters as depicted in Figure 1. 6 and succinctly explicated in the subsequent sections as follows:

Chapter 1 provides an introduction of this research and focuses on the new Runway 3 Soekarno-Hatta International Airport in Indonesia. It highlights current issues and the motivation behind laboratory testing based on Standard National Indonesia (SNI), American

Society for Testing and Materials (ASTM), and Japanese Geotechnical Society (JGS). This chapter also outlines the original contribution of this thesis along with the description of the ground improvement technology, objective, scope, limitation, and the framework of the thesis.

Chapter 2 offers a brief literature review associated with the present work. To covers various aspects such as the present theories of PVD, vacuum preloading, and factors affecting consolidations, including the equivalent diameter effect of mandrel, PVD filter and core, tensile strengths, discharge capacity, mandrel size and shape, installation procedure, PVD spacing, influence zone, the smear zone effect, clogging effect due to vacuum preloading, and microstructure analysis. These aspects, including the problem to be solved based on previous research, have been reviewed in detail.

Chapter 3 focuses on field observations and the implications of embodied CO_2 emissions concerning PVD material. Firstly, the finite element method (FEM) is conducted to present a performance of PVD combined with preloading. This analysis results propose a conversion of the axisymmetric to plane-strain condition to approach for accurate analysis of the advantages of PVD spacing in accelerating consolidation. It was found that the proposed formula can predict the results closed with the field measurement data. Therefore, the formula proved for analyzing the proper consolidation rate using FEM. Secondly, the life cycle assessment (LCA) is conducted on the implications of embodied CO_2 emissions for PVD materials based on their embodied carbon value. The analytical results found that PVD materials have lower embodied emissions than other ground improvement methods.

Chapter 4 presents the methodology of the laboratory experiment (1g model) and Scanning Electron Microscopy (SEM). The 1g model test is used to understand the development mandrel system during the installation of PVD material and can be utilized to measure the mechanical behavior of soft soil during and after vacuum preloading as a macro-level analysis. The SEM image analysis can be used to measure the chemical composition and structure of soft soil and PVD, before and after vacuum preloading as a micro-level analysis. The following subsection explains the important functions of apparatus and remarks the specific test procedures including the apparatus set up and model ground preparation to obtain accurate results.

Chapter 5 evaluates the effect of developed mandrel system using a 1g model test on the performance of soil improvement. The effect of water content (w), shear strength of soft soil (s_u), permeability (k), water flow rate (Q), discharge capacity (q_w), soft soil settlement, excess pore water pressure, and consolidation rate (U) has been discussed to examine the performance of PVD. The effectiveness of the mandrel system can be observed in its impact on the consolidation rate ($\boldsymbol{U}$) through the evaluation of an inner smear zone, transition zone and undisturbed zone. Furthermore, extended inner smear zone in the transition zone can be observed in its influence on the physical and mechanical indices of soft soil such as w, s_u and k. The results show that the w, s_u and k gradually increased in the inner smear zone and transition zone, while both decreased in the radial distance. It is concluded that the 1g model test can demonstrated the effect of developed mandrel system.

Chapter 6 describes the microstructure analysis using a SEM. The analysis of micro-level images clarifies the effect of the developed mandrel system in reducing the smear zone by examining the structure of soft soil with PVD. A microstructure analysis allowed examining the clogging effect by estimating the pore area (n) and the particle area (Ø) of the structure before and after consolidation. The results clarify the clogging effect due to mandrel system related to n and Ø. In addition, the correlation between s_u and k of soft soil, and n revealed an inverse relationship, which can characterize the effect of the mandrel system.

Chapter 7 summarizes the main findings and provides recommendations for future research.

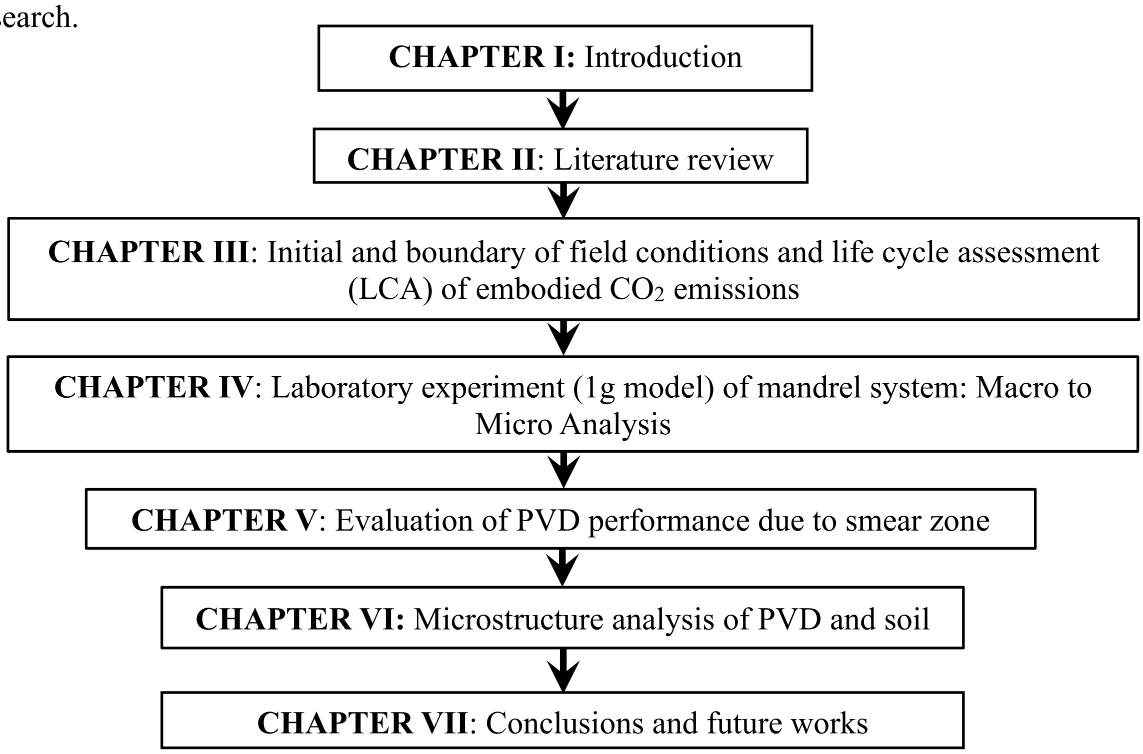

Figure 1. 6. Flowchart of dissertation.

1.6 REFERENCES

Adriyati, M., Rifa'i, A., & Fikri, F. (2020). Analysis of settlement prediction due to preloading and vertical drain applications on runway construction. *E3S Web of Conferences*, *156*, 2–6. https://doi.org/10.1051/e3sconf/202015602002.

Adriyati, M, Yasufuku, N., Ishikura, R., & Rifa, A. (2022a). Numerical Analysis of Combined Surcharge Preloading using Prefabricated Vertical Drain and Stone Column on Runway Construction. *Proceedings of 4th International Conference on Sustainable Infrastructuture* (ICSI 2021), 1, 1, 1-9, 2021. 10.

Adriyati, M., Yasufuku, N., Ishikura, R., & Rifa, A. (2022b). Optimizing modified large-scale consolidation testing for describing smear zone caused by mandrel- driven prefabricated vertical drain. *2022 GeoAsia7 Conference & IGS First Young Engineers Conference (GeoAsia7)*, 5–8.

Bergado, D. T., Alfaro, M. C., & Balasubramaniam, A. S. (1993). Improvement of soft Bangkok clay using vertical drains. *Geotextiles and Geomembranes*, *12*(7), 615–663. https://doi.org/10.1016/0266-1144(93)90032-J

Bergado, Dennes T., Chaiyaput, S., Artidteang, S., & Nguyen, T. N. (2020). Microstructures within and outside the smear zones for soft clay improvement using PVD only, Vacuum-PVD, Thermo-PVD and Thermo-Vacuum-PVD. *Geotextiles and Geomembranes*, *48*(6), 828–843. https://doi.org/10.1016/j.geotexmem.2020.07.003

Bo, M. W., Arulrajah, A., Horpibulsuk, S., Chinkulkijniwat, A., & Leong, M. (2016). Laboratory measurements of factors affecting discharge capacity of prefabricated vertical drain materials. *Soils and Foundations*, *56*(1), 129–137. https://doi.org/10.1016/j.sandf.2016.01.010

Cox JB. (1970). The distribution and formation of recent sediment in South East Asia. *Proceeding of 2nd South Asia Conference on Soil Engineering*, 30–47. http://seags.ait.asia/publications/2nd-SEAC-1970-Singapore.pdf

Gouw, T. L. (2020). Case Histories on the Application of Vacuum Preloading and Geosynthetic-Reinforced Soil Structures in Indonesia. *Indian Geotechnical Journal*, *50*(2), 213–237. https://doi.org/10.1007/s40098-019-00391-5

Laksono, T. D., Kurniasih, N., Hasyim, C., Setiawan, M. I., & Ahmar, A. S. (2018). The Impact of Airport Performance towards Construction and Infrastructure Expansion in Indonesia. *J. Physics: Conference Series*, *954*(1).

https://doi.org/10.1088/1742-6596/954/1/012015

Nur straits Engineering. (2017). *Detail Engineering Design (DED) Runway 3 International Airport Soekarno-Hatta*.

Perera, D., Indraratna, B., Leroueil, S., Rujikiatkamjorn, C., & Kelly, R. (2017). Analytical model for vacuum consolidation incorporating soil disturbance caused by mandrel-driven drains. *Canadian Geotechnical Journal*, *54*(4), 547–560. https://doi.org/10.1139/cgj-2016-0232

Refaldi, A., Emraldi, M., & Rizaldy, W. (2018). Impact of passenger of growth in Soekarno-hatta Airport. *Proceedings of the Conference on Global Research on Sustainable Transport (GROST 2017)*, *147*(Grost 2017), 808–816. https://doi.org/10.2991/grost-17.2018.71

Saraswati, B., & Hanaoka, S. (2013). Aviation policy in Indonesia and its relation to ASEAN Single Aviation Market. *Journal of the Eastern Asia Society for Transportation Studies*, *10*, 2161–2176. https://doi.org/https://doi.org/10.11175/easts.10.2161

Shin, E. C., Nazarova, Z., Cho, K. Y., Kim, S. H., & Kang, J. K. (2008). Evaluation of discharge capacity with various vertical drain core types. *Proceedings of the 4th Asian Regional Conference on Geosynthetic*, 420–421.

Turkandi, T., Sidarto, A, S. A., & Purbo H, M. M. (1992). *Peta Geologi lembar Jakarta dan kepulauan Seribu, Jawa, skala 1:100.000 (Bahasa Indonesia)*. https://pdfcoffee.com/peta-geologi-jakarta-tangerang-pdf-free.html

Wang, P., Han, Y., Zhou, Y., Wang, J., Cai, Y., Xu, F., & Pu, H. (2020). Apparent clogging effect in vacuum-induced consolidation of dredged soil with prefabricated vertical drains. *Geotextiles and Geomembranes*, *48*(4), 524–531. https://doi.org/10.1016/j.geotexmem.2020.02.010

Wibowo, S. M., & Hamzah, M. Z. (2022). Development Policy Impact of Soekarno-Hatta International Airport on The Sustainability of PT. Angkasa Pura II. *OIDA Journal of Sustainable Developmentf*, *15–07*, 11–26.

CHAPTER
II
LITERATURE REVIEW

2.1 INTRODUCTION

Ground improvement methods for accelerated consolidation have been widely used to improve the mechanical properties of soft soil. Prefabricated vertical drain (PVD) combined with vacuum preloading is one of the effective methods for engineering design in soft soil to accelerate consolidation by improving mechanical properties. The following sections are classified as the experimental test from the Macro level by using Large-scale consolidation testing in the laboratory. This chapter introduced the PVD combined with vacuum preloading characteristics and factors affecting consolidation, including mandrel system, PVD filter, equivalent diameter, discharge capacity, and installation procedure. Microstructure analysis by scanning electron microscopy (SEM) was also introduced. The main objective was to evaluate the effectiveness of the mandrel system in reducing smear effects resulting from installation PVD and due to combination with vacuum preloading.

2.2 CONSOLIDATIONS OF SOFT SOIL

2.2.1 Terzaghi's one dimensional consolidation theory

Terzaghi, K., (1943) described consolidation as any process that involves a decrease in the water content of a saturated soil without replacing it by water or air. The principle of the consolidation process for one-dimensional compression of a saturated soil is divided into three broad categories known as initial compression, primary consolidation, and secondary consolidation. Initial compression caused by the elastic deformation of dry and saturated soil without any change in the water content.

Primary consolidation caused by pore water pressure of a saturated soil increases immediately after applying as external load such as surcharge or vacuum preloading, as the excess pore pressure dissipates pore water is expelled, which results in a change in the volume of saturated cohesive soil. Secondary consolidation in saturated cohesive soils after the end of primary consolidation. Figure 2. 1 shows the three phases of settlement due to consolidation.

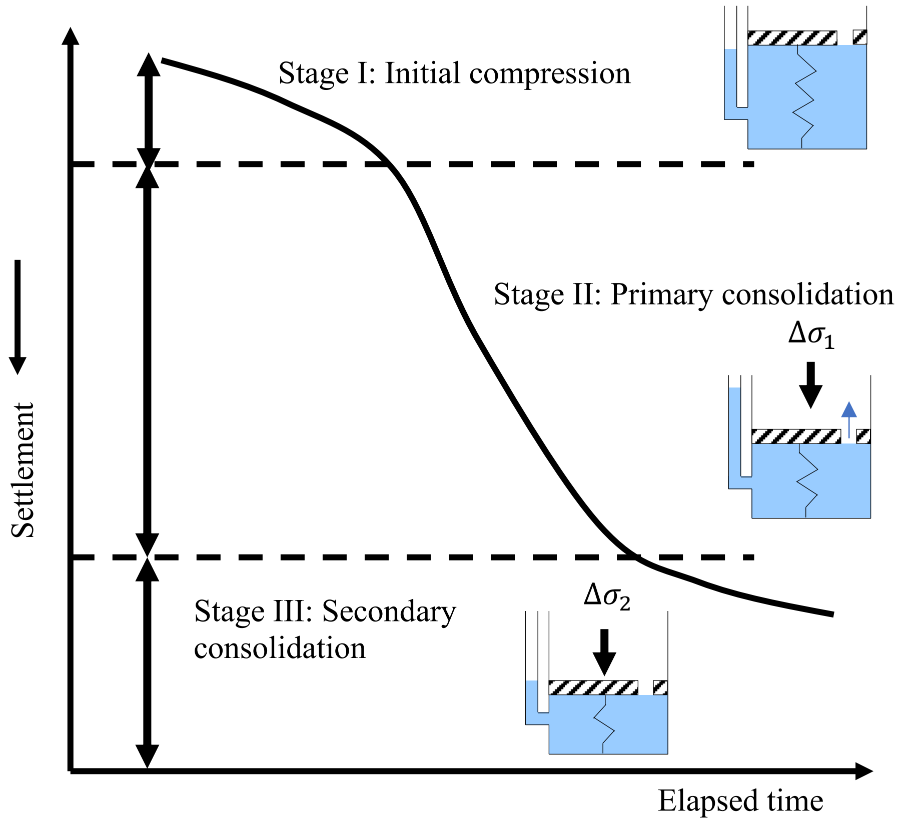

Figure 2. 1. Schematic of one-dimensional consolidation including spring analog.

The theory of consolidation based on Karl Terzaghi are assumption behind the original theory as follows. First, soil is saturated and homogeneous, and compressibility of solid grains of the soil and the compressibility of the pore water are negligible. A unique linier relationship exists between the vertical effective stress (σ) and the void ratio (e) that is independent of the loading and time. The coefficient of permeability is assumed to be constant during the consolidation process. The Darcy's law is valid. Lastly, the water flow is only one in vertical direction. Considering the above assumptions and the continuity equation, the following relationship between the void ratio and excess pores pressure can be expressed as:

$$\frac{k_v}{\gamma_w}\frac{\partial^2 e}{\partial z^2} = \frac{1}{1+e_0}\frac{\partial e}{\partial t} \tag{2. 1}$$

$$c_v\frac{\partial^2 u}{\partial z^2} = \frac{\partial u}{\partial t} \tag{2. 2}$$

Appropriate boundary condition gives an expression for degree of consolidation can be expressed as:

$$U = 1 - \exp^{\frac{-8T_v}{\mu}} \quad (2.3)$$

$$T_v = \frac{c_v t}{H^2} \quad (2.4)$$

Where, u is the excess pore pressure, t is the elapsed time, e_0 is void ratio, $k_v$is the permeability of consolidation in the vertical direction, c_v is the coefficient of consolidation in the vertical direction, γ_w is unit weight of water, $\mu = \ln n - \frac{3}{4}$ is the factor influence of vertical drain, and T_v is the time factor. Terzaghi's consolidation theory assumes a constant permeability throughout the consolidation process, however the permeability of the soil decreases as the pore within the soil mass shrinks.

2.2.2 Barron's and Hansbo's theory on radial consolidation using PVD

Barron R. A., (1948) presented the solution for radial consolidation using vertical drain. The vertical drain was incorporated with smear zone were also considered in this study. The assumptions on which solution made by Terzaghi for consolidation theory. However, the considered two possible cases of analysis based on Barron theory, known as equal vertical strain and free strain. For equal vertical strain the Barron's approach was consolidation developed different settlement of the upper surface of the soil mass and shear strains within the mass. For free strain, it was assumed that these effects did not influence the redistribution of load due to consolidation rate. It is obvious, however, that these effects will redistribute the load to some extent, depending on material in compressible soil. It can be obtained in the laboratory by use a rigid loading flatform, and probably is approach in the field if the ration of H to d_e is large, can be expressed as:

$$c_h\left(\frac{1}{r}\frac{\partial u}{\partial r} + \frac{\partial^2 u}{\partial r^2}\right) = \frac{\partial u}{\partial t} \quad (2.5)$$

He assumed that the soil in the smeared zone was an incompressible solid having the coefficient of permeability (k_{hs}), with a smeared zone can be expressed as:

$$U_h(T_h) = u_0 \exp\left(\frac{-8T_v}{\mu s}\right) \quad (2.6)$$

$$\mu s = \frac{n^2}{n^2 - m^2}\ln\left(\frac{n}{m}\right) - \frac{3}{4} + \frac{m^2}{4n^2} + \frac{k_h}{k_{hs}}\left(\frac{n^2 - m^2}{n^2}\right)\ln m \quad (2.7)$$

where, $T_h = \frac{c_h t}{{d_e}^2}$ is the time factor, $n = \frac{r_e}{r_w}$ is spacing ratio, $m = \frac{r_s}{r_w}$ is ratio of the smeared zone radius, and u_0 is the initial excess pore water pressure. Barron also presented a solution which consider both the smear and well resistance.

Hansbo et al., (1981) introduced some approximation and produced a simple closed-form solution of the degree of consolidations at a given depth. The consolidation rate is $U_h\ (z, T_h)$, involving both the disturbed and undisturbed zone is expressed as:

$$U_h\ (z, T_h) = 1 - \exp\ (\frac{-8T_h}{\mu sw}) \tag{2. 8}$$

$$\mu sw = \mu s + \mu w \tag{2. 9}$$

$$\mu s = \frac{n^2}{n^2-1}\left(\ln\ \left(\frac{n}{m}\right) + \eta \ln m - \frac{3}{4}\right) + \frac{m^2}{n^2-1}\left(1 - \frac{m^2}{4n^2}\right) + \eta \frac{m^2-1}{n^2-1}\left(\frac{m^2+1}{4n^2} - 1\right) \tag{2. 10}$$

$$\mu w = \pi z(2H - z)\frac{k_h}{q_w}\left(1 - \frac{1}{n^2}\right) \tag{2. 11}$$

where, $\eta = \frac{k_h}{k_{hs}}$ is the equivalent permeability, $q_w = \pi {r_w}^2 k_w$ is the equivalent discharge capacity. Although the model used by Hansbo is more realistic than that of Barron because the smeared zone is still assumed to be equal to that of the undisturbed soil. However, the general increased by disturbed area due to compressibility of the soft soil. Compressibility of clay is, however, generally increased by disturbance (Long & Covo, 1994). Furthermore, Hansbo also assumed as Barron did that the radial strain and tangential strain are equal to zero, for the vertical strain is independent of the radius in the cylindrical area of soil. These assumptions are equivalent to the volumetric strain being also independent of radius.

2.3 VACUUM PRELOADING WITH PVD

Kjellman W., (1952) was first proposed the concept of a vacuum preloading method (VPM). Since then, the vacuum preloading method has evolved into a mature and efficient technique for treating soft clays. This method has been successfully used for soil improvement or land reclamation projects in a number of countries (Bergado et al., 1996; J.-C. Chai et al., 2001; CHU et al., 2006; Indraratna, 2008).

The PVD combined with vacuum preloading involves applying a vacuum perdured into ground has been protected from ground-surface pressure losses to atmosphere by a sealing membrane shows in Figure 2. 1. The vacuum pump procedures a negative pressure

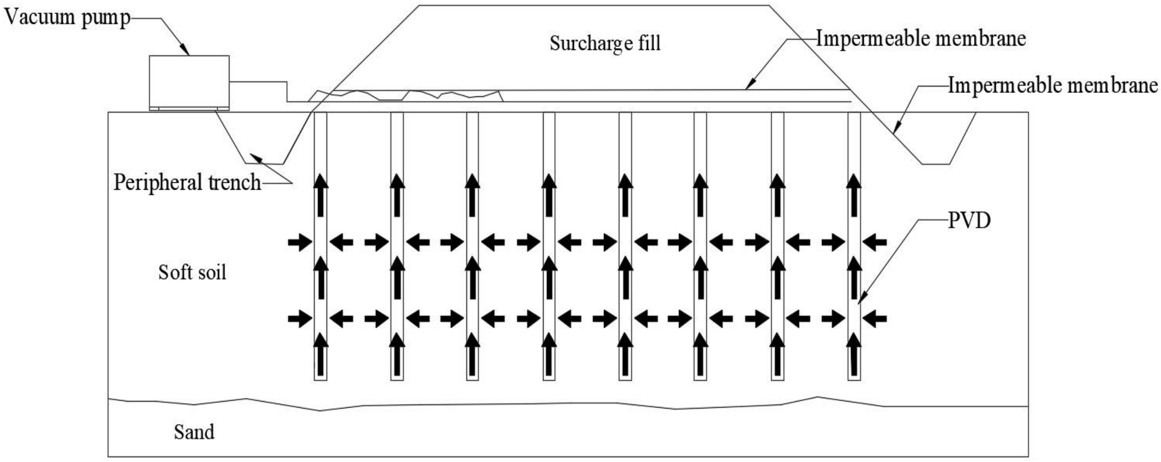

Figure 2. 1. Schematic diagram of typical membrane vacuum preloading.

PVD with tubing arrangement (Griffin & O'Kelly, 2014; Seah TH, 2006) with respect to atmospheric pressure in a permeable soil cushion, located directly beneath the membrane, and along PVD installed within the ground mass under treatment is shown. The vacuum preloading method utilizes atmospheric pressure as a surcharge load to accelerate soil consolidation to enhance soft soil conditions, including high compressibility, high water content, lack of shear strength, and lower hydraulic conductivity. Consequently, this technique generates promising results.

2.4 FACTORS AFFECTING CONSOLIDATION OF SOFT SOIL WITH PVD

The design of PVD varies according to the specific applications. The key parameters and factors influencing the PVD combined with preloading are explained in detail: mandrel system PVD material, Soil disturbance due to installation, discharge capacity due to vacuum preloading, and clogging due to vacuum preloading, all of which are explained in detail in the following section.

2.4.1 Mandrel system

2.4.1.1. Designed mandrel system

The PVD are installed by pushing a steel mandrel, designed rectangular mandrel is proposed in this study made from iron steel, with a length of 750 mm, and a width of 90 mm. The material of the PVD is protected inside the mandrel. Generally, any disturbance increases with the total cross-sectional area of the mandrel, which means the size of the mandrel should be as close as possible to the drain to minimize the smearing effects. The common types of mandrel cross sections are shown.

Basu et al., (2010) was investigated analytically to understand the effect of the shape of the mandrel using different size mandrels: 125 mm×50 mm, 150 mm×50 mm, 120 mm×120 mm, and 150 mm×150 mm. The results clearly showed that the rate of consolidation decreased as the size of the mandrel increased. Furthermore, square mandrels disturbed a much larger area than rectangular mandrels, which means that PVD installed with square mandrels are less effective. However, to understand another effect such as different PVD core in rectangular mandrels are studied.

2.4.1.2. Equivalent diameter of mandrel system

Barron's (1948) radial consolidation theory assumed a circular cross-section drain in the analysis. This can easily be calculated when PVD have been installed because the mandrel used has a circular cross section. Due to the increased usage of PVD in ground improvement technique projects it was necessary to come up with a method to estimate an equivalent diameter for a PVD and mandrel. Kjellman (1948) suggested that the circumference of a drain is more important than its cross-sectional area when assessing its water discharge capacity, and if the circumference of the drains is the same then it will lead to the same consolidation response. Hansbo (1979) later verified this using finite element analysis and proposed an equivalent diameter for PVD having a width of "*a*" and a thickness of "*b*" is expressed as:

$$2\times(a+b)/\pi \tag{2. 12}$$

Rixner et al (1986) using the finite difference method, proposed the equivalent drain diameter, can be expressed as:

$$0.5\times(a+b) \tag{2. 13}$$

Pradhan et al (1993) proposed an equation for the equivalent drain diameter based on the flow nets around the drain influenced area and determined the simple form, as follow:

$$(2\times(a+b))/\pi \tag{2. 14}$$

Long & Covo (1994) determined an equivalent diameter for drain with rectangular cross section using an electrical analogue field plotter, can be expressed as:

$$0.5a+0.7b \tag{2. 15}$$

In addition, to elaborate on the proposed newly developed mandrel system for the original contribution. However, it is important to investigate other factors, such as the use of different PVD cores in rectangular mandrels.

2.4.2 PVD material

2.4.2.1. Drain filter and core

The drain material and the filter jacket of PVD have two basics but contrasting roles, which are: retaining the soil particles, and the same time allowing the pore water to pass through (Hansbo, 1980). The characteristics of the filter that affect the functionality of the vertical drain reported as follows; permeability of the filter jacket, filtration (effective filtration can minimize movement of soil particles through the filter), retention ability of the filter, and filter clogging (filter material may be clogged when the soil particles are trapped within the filter fabric).

The pore size or the apparent opening size (AOS) must be small enough to prevent the fine particles of the soil from entering the filter and the drain. The parameter O_{95} indicates the approximate largest particle that would effectively pass through the filter. The standards Carroll, (1983) and Chu et al., (2004) commonly used can be expressed as:

$$O_{95} \leq (2-3)D_{85} \tag{2. 16}$$

$$O_{95} \leq (4-7.5)D_{85} \tag{2. 17}$$

$$O_{50} \leq (10-12)D_{50} \tag{2. 18}$$

where O_{95} is the AOS of filter, D_{85} is the size which is larger than 50% of the fabric pores, and D_{85} and D_{50} refer to the sizes for 85% and 50% of passing of soil particle by weight. $O_{95} \leq 0.075$ m, or 75 mm, is often specified for prefabricated vertical drain. As a result, to achieve the goals of vacuum preloading effect, it is critical to select a suitable pores size of the filter.

2.4.2.2. Drain tensile strength and durability

The PVD should be strong enough to sustain the tensile stresses subjected to handling and installation. Therefore, the tensile strength of core and filter on entire drain and the spliced drain should be specified in both wet and dry conditions (Bo, 2004). Kremer et al., (1983) reported that a drain should be able to withstand at least 0.5 kN of tensile force without exceeding 10% of elongation. It is common nowadays to specify the tensile strength of the entre drain at wet and dry conditions to be large than 1 kN at a tensile strain of 10% (Bo, 2004). A spliced vertical drain should also be required to have a tensile strength comparable to an unplaced drain. Durability of the geosynthetic materials throughout the consolidation period is generally a concern. However, if the vertical drain contains solvents or other chemical pollutants, the drain integrity needs to be checked.

2.4.2.3. Drain length

Vertical drain length should be sufficient to consolidate the soft soil layer to extent necessary to achieve the design objectives (R. Radhakrishnan & C. Gunasekaran, 2019). The drain should be installed to a depth where the excess pore water pressure can dissipate quickly, leading to accelerate consolidation.

In addition, some cases it may not be necessary to fully penetrate the compressible stratum to achieve the necessary shear strength gain and to accelerate consolidation. Furthermore, additional length greater than 25m, the vertical drain may not improve the consolidation rate considering the effects of the drain resistance. Therefore, it is important to determine the appropriate length of the vertical drain based on the specific soil conditions and design objectives. The design and installation of vertical drains should be guidelines set by industry associations such as the American Association of State Highway and Transportation Officials (AASHTO) or local department of transportation (Patrick J. Hannigan et al., 2016).

2.4.3 Soil disturbance due to installation

2.4.3.1. Effect of PVD spacing

The appropriate spacing of PVD depends on a variety of factors, including the soft soil layer depth, the load and settlement requirements, and the duration of construction. There are several methods include analytical, numerical, and empirical based on previous study. Typically, PVD may be installed at regular intervals in a square, rectangular pattern (Bergado et al., 1996), which center to center distance (s) varying from about 1.0 to 3.5 m. As illustrated, the radius of the influence zone (R) is a controlled variable because it is a function of the drain spacing (s). The zone of influence can be determined, as follows:

$$R = 0.546 \times \text{Spacing (Square pattern)} \tag{2. 19}$$

$$R = 0.525 \times \text{Spacing (Triangular pattern)} \tag{2. 20}$$

Adriyati et al., (2020) proposed the drain spacing based on field conditions, can be determined based on the required degree of consolidation and work timeframe by adopting analytical solutions. According to the practical recommendations the drain spacing should usually be more than 0.8 m. However, it is important to note that the appropriate drain spacing.

2.4.3.2. Smear zone

Installation PVD with mandrel causes a significant disturbance of the subsoil, especially near the mandrel. This disturbed zone is called the smear zone (Sharma & Xiao, 2000), the permeability of the soil around the drain can be decreased significantly by smearing and retarding the rate of consolidation.

Two parameters are needed to characterize the smear effects, by the three-zone hypothesis that introduced in this study to investigate the smear zone influence is determined in Figure 2. 3. The smear zones are dependent on the size and shape of the mandrel cross-section. The inner smear zone, the transition zone, and the undisturbed zone is disturbed soil conditions (Madhira R. Madhave, et al., 1993). The values in the transition area of the smear zone are essential to describe the extended smear zone during consolidation, which is determined as follow:

$$s = \frac{r_s}{r_w} \tag{2. 21}$$

where r_s is the radius of the transition zone and r_w is the radius of PVD with mandrel. The installation of PVD using a mandrel disturbs the soil around the drain, which results in a smear zone of reduced permeability that adversely affects the consolidation process.

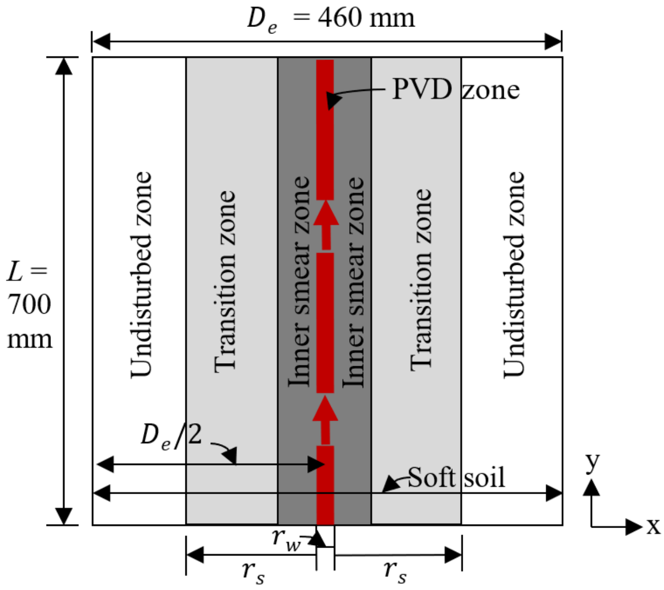

Figure 2. 2. Full illustration of three-zone hypothesis for smear zone.

2.4.3.3. Installation method

The PVD should be installed using approved equipment which can insert the material into the ground with the minimum possible disturbance to the soils while keeping the mandrel vertical during installation. In the field, the PVD is forced into the soil with the hollow mandrel, and once a firm layer is encountered or the target dept is reached, the mandrel is retracted and the PVD, which is held in the ground by the anchor, stay in place. Once the bottom of the mandrel reaches the surface, the PVD is cut and the anchor for next drain is attached. The mandrel is a part of a mast assembly, which is supported and powered by a hydraulic excavator or crane, and it is then removed leaving the PVD in place.

The illustration picture in the field is shown in Figure 2. 4. The detailed of the filed procedure of PVD installation involves several steps. Here is a detailed explanation of the process based on Figure 2. 5: (a) measuring angles to the target point using the theodolite, this measurement helps to ensure that the PVDs are installed at the correct angle and depth (b) drilling the hole based on design target (c) the PVD is installed into the hole, (d) cut the PVD based on the target depth.

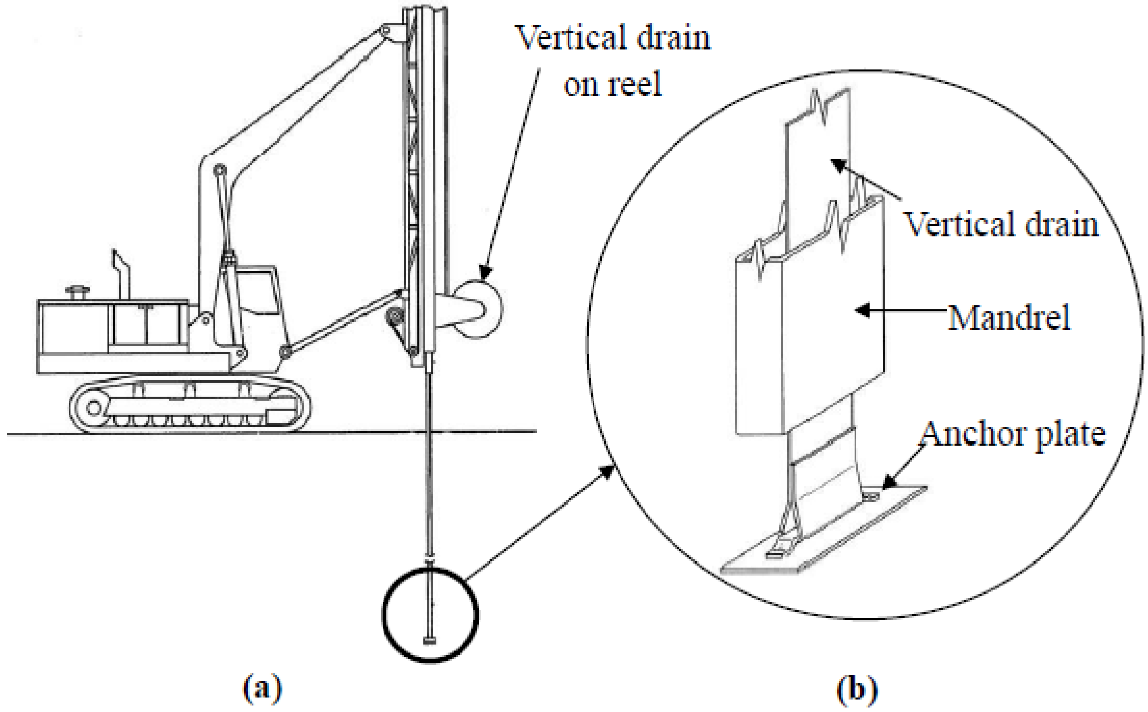

Figure 2. 3. (a) drain delivery arrangement; (b) drain attached to the anchor plate at bottom.

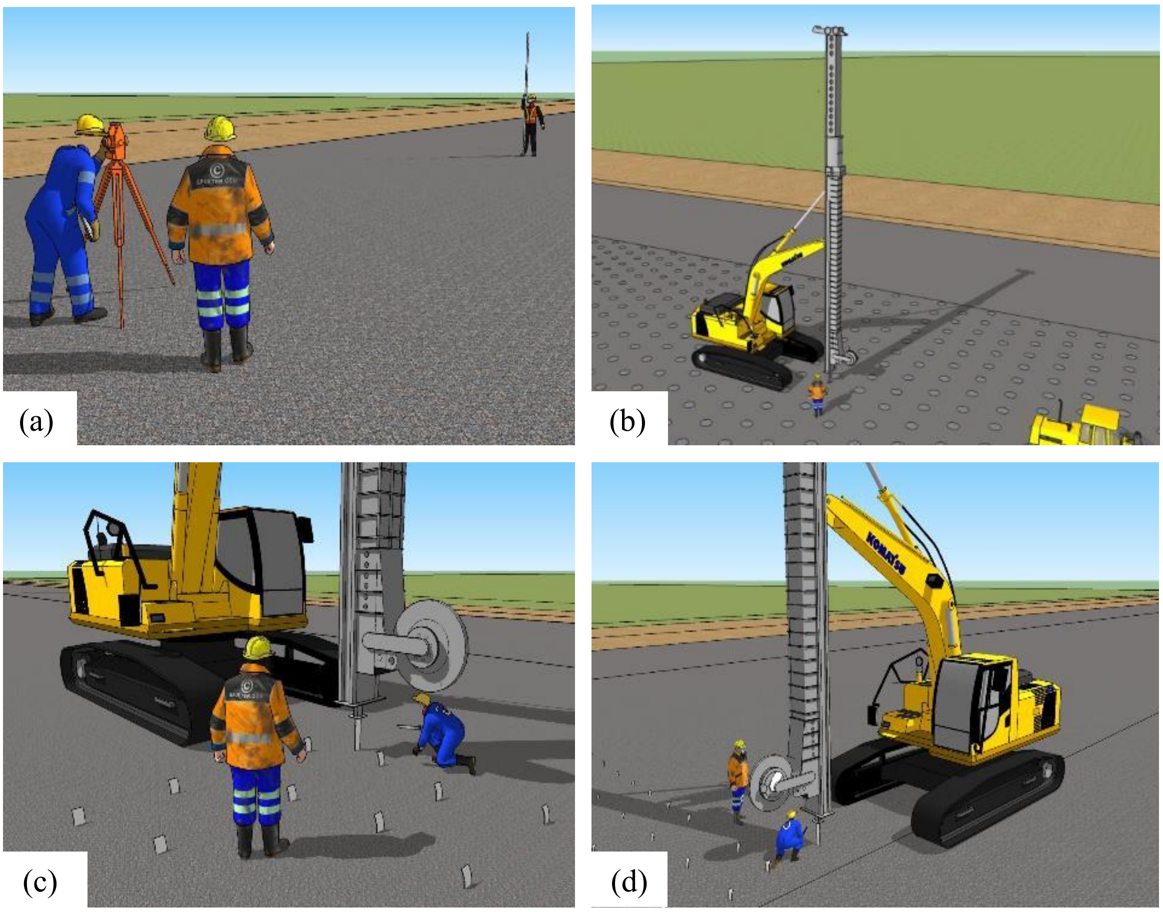

Figure 2. 4. Schematic installation of PVD in the field: (a) measuring; (b) drilling; (c) installing PVD; (d) cut the PVD based on the target depth.

2.4.4 Permeability of soil due to preloading

Terzaghi's consolidation theory assumes a constant permeability throughout the consolidation process, but as consolidation progresses the permeability of the soil decreases as the pore within the soil shrinks (Terzaghi, K., 1943). Permeability is a fundamental soil property affecting water movement and deformation behavior in response to loading. Preloading induces consolidation of the soil through the application of PVD combined with either surcharge or vacuum method, leading to increased density and reduced porosity.

The permeability of soft clay could also be obtained indirectly (Taylor's, 1948) method a using the coefficient of consolidation derived from the step loading consolidation tests, but the permeability values derived from these methods were not representative of the actual field permeability encountered.

Literature on this topic involves a comprehensive examination of previous studies and associated methodologies to identify the factors affecting permeability, the mechanisms driving soil deformation under preloading, and the methods available for measuring soil permeability. The falling head permeability apparatus by using JGS standard is widely employed for such evaluations, wherein the time required for a fixed volume of water to pass through a soil sample under a constant head is measured by using Darcy's formula:

$$k = \frac{a \times L}{A \times t} \ln\left(\frac{h_0}{h_1}\right) \tag{2. 22}$$

where a is $(\frac{\pi \times d^2}{4})$ inside cross-sectional area of the water tank, A is $(\frac{\pi \times D^2}{4})$ inside cross-sectional area of the sample, L is the length of the sample, t is the time taken for the water to pass through the sample, h_0 is distance to bottom of the beaker before the test, and h_1 is distance to bottom of the beaker after the test. A thorough literature review on the permeability of soil following preloading provides an essential basis for understanding and quantifying the response of soils to static loading.

2.4.5 Discharge capacity due to preloading

The PVD are used to dissipate excess pore water pressure in the soil and discharge water, and therefore the higher their discharge capacity the better they perform. The discharge capacity of a band drain, denoted as q_w, is defined as the rate of flow through the drain at a hydraulic gradient of unity. Based on (Bergado et al., 1996) the discharge capacity can be expressed as the product of the longitudinal permeability of the drain and its cross sectional area. The discharge capacity of vertical drains can be affected by factors such as the consolidation stress, deformation of the drain, time, clogging, and the hydraulic gradient and temperature.

$$i = \frac{\Delta h}{L} \tag{2. 23}$$

$$q_w = \frac{Q}{i} \tag{2. 24}$$

where i is the dimensionless hydraulic gradient, Δh is the head difference (m), L is the length of the chamber apparatus (m), q_w is the discharge capacity (m^3/s), and Q is the rate of water flow per unit of elapsed time (m^3/s). The discharge capacity of PVD is smaller than the amount of water that needs to be discharged, well resistance will occur. However, the discharge capacity of the PVD should be large enough to ignore the well resistance in the design because the well resistance increases as the length of the drain increases and reduces the rate of consolidation. Well resistance retards the dissipation of pore water pressure, which means that settlement is retarded.

The observed that discharge capacity is affected by the lateral confining pressure. According to Bo (2004) states that it is unnecessary to use an excessively high reduction factor for the discharge capacity with the deformation of the vertical drain and time, the permeability of the soil reduces with consolidation, so the amount of water discharges also reduces over time. Different studies have been carried out to determine the value of q_w and they are summarized in Table 2. 2.

Table 2. 1. The discharge capacity references.

References	Discharge capacity (q_w)	Remarks
Hansbo et al (1981)	50-100	Lab Test
Kremer et al (1982)	160	Lab Test (σ_c=100 kPa)
Jamiolkowski et al (1983)	10-15	Lab Test (σ_c=300-500 kPa)
Mesri and Lo (1991)	2-80	Back analysis
Indraratna (2002)	100	Back analysis
Bo (2004)	27-405	Back analysis
This study	**13-171**	**Lab Test**

A new type of PVD, called integrated PVD where the core and filter adhered together due to heat melting, was introduced (Liu & Chu, 2009). The integrated PVD offers a number of advantages over the separable PVD. Bothe the tensile strength and the discharge capacity of the integrated PVD were higher than the separable one made from the same material.

2.4.6 Clogging due to vacuum preloading

Historical analysis of clogging has been restricted to a physical modeling of the particle interface interactions and migration. Considering mass and momentum conservation principles one can relate properties such as particle size distribution, mass flow rate and filter capacity to changes in permittivity of the filter medium (Xiao & Reddi 2000).

Sun et al., (2021) and Xu et al., (2020) Clogging due to vacuum preloading occurs when the soil particles around prefabricated vertical drains (PVD) become trapped in the filter sleeve, reducing drainage capacity, and causing the PVD to become less effective in consolidating soft soil. PVDs are commonly used in vacuum preloading applications to improve the drainage capacity of soft soil and accelerate consolidation times. However, clogging of the filter sleeves is a common problem that can significantly reduce the effectiveness of the PVDs and lead to longer consolidation times. Figure 2. 6 shows the schematic diagram of the soil and fine particle movement. The PVD filter surrounding the core primary serves two functions during consolidation: (1) Prevent soil particles from entering the core (2) Allow maximum flow of water inside the core to allow for maximum

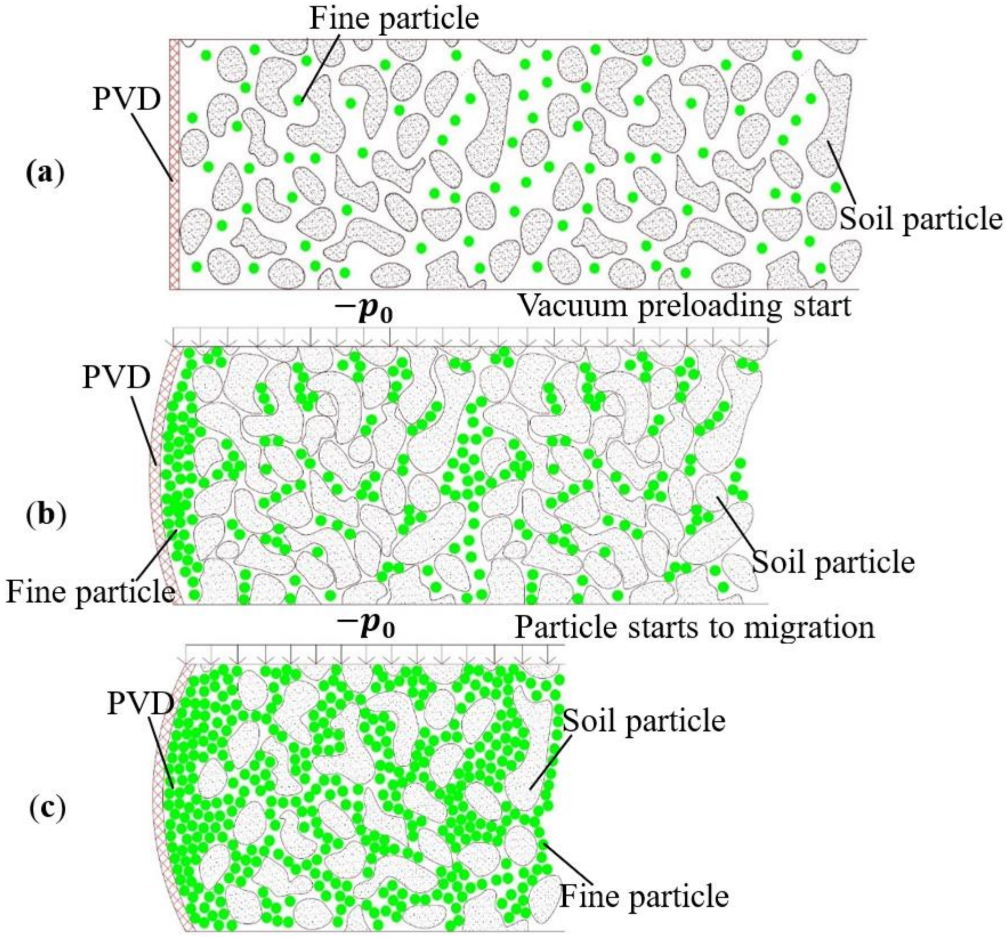

Figure 2. 5. (a) Initial conditions of the soil; (b) The fine particles migrate through the void pores; (c) The fine particle start to migrations to the surrounding PVD.

possible drainage through the core in minimum amount of time. To understand the effectiveness of drainage system, typically the soil filtration system develops around the drain filter as water flow through the filter so that any further transport of particles to the core is prevented. The development of such a filtration system is critical to the long-term performance of the drain. Holtz et al (1991) is the ability of development for the filtration system is dependent upon a several factors such as:

1. Physical & chemical characteristics of the filter jacket
2. Soil Characteristics
3. Magnitude of external loads or stresses applied on the system
4. Hydraulic conditions in and around the filter jacket

To achieve the required filtration system several criteria were proposed as to what should be the ideal ratio of filter opening to that of the particle size distribution of the soil.

Carroll (1983) has given one criteria of filter, which states that the O_{95} value of the filter, also referred to as the apparent opening size (AOS), should be less than approximately 2-3 times the D_{85} of the soil. Here D_{95} refers to the 95% of the opening size of the geotextile and D_{85} refers to the soil grain diameter at 85% passing on the No 200 sieve.

2.5 NUMERICAL MODELLING USING PLANE STRAIN CONSOLIDATION METHOD

Previous study models were developed by considering the consolidation of a single drain in a unit cell in axisymmetric conditions, However, when analyzing an embankment built on soft soil improved using PVD, it is necessary to use plane strain conditions to accurately reflect consolidation responses. Thus, the development of a method that can convert existing axisymmetric models to equivalent plane strain in 2D models is imperative to give the same consolidation response (PLAXIS, 2015).

Indraratna (2010) suggested achieving equivalent plane strain conditions using a geometric approach, permeability approach, or combined permeability and geometry approach. While Hird et al., (1992) presented a solution to convert the axisymmetric model to a plane strain model that can be incorporated in finite element methods, it tends to average out the effects of the smear zone across the unit cell, thus implicitly incorporating smear effects. However, Indraratna & Redana (1997, 1999) were able to explicitly include smear effects in the plane strain model, enhancing its accuracy in predicting the effects of smear and consolidation when vertical drains are used in ground improvement projects shown in Figure 2. 7. This literature review explores how to accurately determine the permeability of soft soils subjected to preloading, specifically in embankment construction, and the methods used to convert axisymmetric models to equivalent plane strain 2D models to reflect consolidation responses accurately.

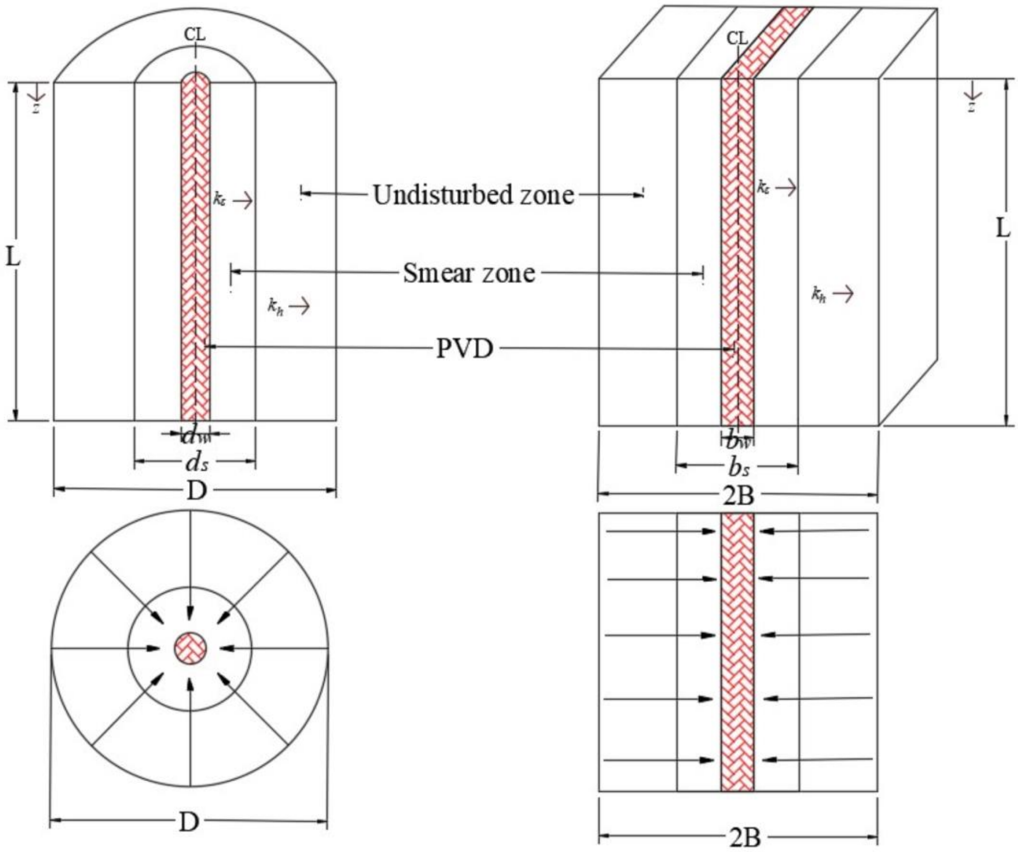

Figure 2. 6. Conversion of an axisymmetric unit cell into a plane strain conditions (Indraratna et. al, 1997)

2.6 EMBODIED CO_2 EMISSIONS IN GROUND IMPROVEMENT

Several studies have suggested that ground improvement techniques offer a more sustainable alternative for geotechnical construction compared to traditional foundation systems. This can be attributed to their potential to reduce construction time, material usage, fuel consumption, and labor (Chau et al., 2008; Dixit et al., 2012; G. P. Hammond & Jones, 2008; Menzies et al., 2007; Shillaber et al., 2016). To investigate the embodied CO_2 emissions of ground improvement techniques, a study proposes a calculation based on the combination of technology, such as the prefabricated vertical drain combined with stone column design, relative to other techniques with the same function.

In geotechnical construction, considering both economic cost and environmental impact when selecting design alternatives that meet performance criteria can lead to more sustainable projects. Therefore, it is proposed that life cycle embodied CO_2 emissions be considered relevant factors for quantifying the global environmental impact of ground improvement simply and transparently.

By factoring in CO_2 emissions along with monetary cost and final performance requirements in geotechnical design decisions, the profession can advance towards achieving sustainable development goals. As indicated by (Geoff Hammond, 2008; Shillaber et al., 2015), the life cycle should be considered from raw material extraction to the completion of construction, and the study provides an example to illustrate the application of embodied CO_2 emissions associated with ground improvement projects.

2.7 MICROSTRUCTURE ANALYSIS BY USING SEM

Microstructure analysis by using SEM (Scanning Electron Microscopy) is a common method in material science research. It involves the use of high-resolution imaging to investigate the microscopic structure and morphology of a material. SEM can provide images with much higher resolution than optical microscopy, which can reveal fine details of the sample being analyzed. Perhaps the main reason for their wide use is that SEM image generally are easily recognizable. SEM were used as further evidence to correlate the corresponding levels of improvements by using PVD combine with vacuum preloading (Bergado et al., 2020).

SEM analysis can be used to examine the microstructure of a material in detail. This can include identifying the size and shape of the constituent particles, their distribution within the matrix, and any defects or imperfections present in the material. These observations can then be used to draw conclusions about the properties and behavior of the material. ImageJ is an open-source software program commonly used in SEM analysis to process and analyze the images obtained from the SEM. The software includes a wide range of image analysis tools, such as measuring particle size and shape, performing color analysis, and generating three-dimensional reconstructions of the microstructure. In summary, SEM analysis with the use of ImageJ can provide valuable information for a literature review in a thesis, allowing detailed examination of the microstructure of a material, and providing insight into its physical and mechanical properties.

2.8 PROBLEM TO BE SOLVED BASED ON PREVIOUS RESEARCHER

This chapter discusses the practical and academic aspects of a persistent problem in geotechnical engineering. The research aimed to simulate field conditions using numerical analysis, empirical analysis, model testing using a large-scale consolidation apparatus, and microstructure analysis using SEM to address the fundamental issue. The results are summarized as follows:

1. Based on the gaps identified in previous research, this study aimed to solve the problem of accurately predicting soil behavior under different spacing. To accomplish this, the research developed an accurate equivalent formula from axisymmetric to plane strain and an efficient numerical method based on field conditions using PLAXIS2D. Additionally, engineering properties were provided, which offer reliable predictions and potential solutions to this issue.
2. This study builds on previous research to explore ways to reduce carbon emissions in ground improvement techniques, which can support sustainable infrastructure development for economic growth and well-being in countries like Indonesia that align with the SDGs and NDCs. Using an emissions assessment model and LCA in empirical analysis, the study compares prefabricated vertical drains with other techniques that have a similar function, considering their potential to reduce material use, fuel consumption, and improve sustainability.
3. Building upon previous research, this study aimed to solve the problem of accurately measuring the efficiency of the mandrel system and the behavior of vertical drains during the consolidation process. To accomplish this, the modified apparatus of large-scale consolidation testing was optimized to go beyond the scope of conventional small consolidation equipment. The methodology of the experiment setup is proposed and explained in detail, thereby providing potential solutions to this issue.
4. Expanding on previous research, this study aimed to solve the problem of accurately evaluating the factors that influence the smear zone in the area close to PVD (Prefabricated Vertical Drain). To accomplish this, the research utilized experimental model tests and empirical analysis to study the effects of reducing water content, water flow rate, discharge capacity, and consolidation rate on the performance of PVD. By y examining these factors in detail, the study provides potential solutions to improve the effectiveness of PVD and reduce construction risks.
5. Building on earlier studies, this research aimed to solve the problem of accurately evaluating the performance of the mandrel system due to PVD (Prefabricated Vertical Drains) combined with vacuum preloading at a micro level. Using SEM (Scanning Electron Microscopy), the microstructure was analyzed to examine the pores area, particle area, the relationship between pores and shear strength, and correlation between

pores and permeability. By discussing these factors in detail, the study provides practical solutions to minimize the smear zone and improve the performance of the mandrel system with PVD combined with vacuum preloading.

2.9 REFERENCES

Adriyati, M., Rifa'i, A., & Fikri, F. (2020). Analysis of settlement prediction due to preloading and vertical drain applications on runway construction. *E3S Web of Conferences*, *156*, 2–6. https://doi.org/10.1051/e3sconf/202015602002

Barron R. A. (1948). Consolidation of fine-drained soils by drain well. *Transactions of ASCE*, *113*, 718–754.

Basu, D., Prezzi, M., & Madhav, M. R. (2010). Effect of Soil Disturbance on Consolidation By Prefabricated Vertical Drains Installed in a Rectangular Pattern. *Geotechnical and Geological Engineering*, *28*(1), 61–77. https://doi.org/10.1007/s10706-009-9279-7

Bergado, D.T, Manivannan, R., & Balasubramaniam, A. (1996). Proposed criteria for discharge capacity of prefabricated vertical drains. *Geotextiles and Geomembranes*, *14*(9), 481–505. https://doi.org/10.1016/S0266-1144(96)00028-3

Bergado, Dennes T., Chaiyaput, S., Artidteang, S., & Nguyen, T. N. (2020). Microstructures within and outside the smear zones for soft clay improvement using PVD only, Vacuum-PVD, Thermo-PVD and Thermo-Vacuum-PVD. *Geotextiles and Geomembranes*, *48*(6), 828–843. https://doi.org/10.1016/j.geotexmem.2020.07.003

Bo, M. W. (2004). Discharge capacity of prefabricated vertical drain and their field measurements. *Geotextiles and Geomembranes*, *22*(1–2), 37–48. https://doi.org/10.1016/S0266-1144(03)00050-5

Chau, C., Soga, K., Nicholson, D., O'Riordan, N., & Inui, T. (2008). *Embodied Energy as an Environmental Impact Indicator for Basement Wall Construction*. 867–874. https://doi.org/10.1061/40971(310)108

Carroll, R. . (1983). *Geotextile Filter Design*. Transportation Research Recors, 916: 46-53. https://onlinepubs.trb.org/Onlinepubs/trr/1983/916/916-008.pdf

Chai, J.-C., Shen, S.-L., Miura, N., & Bergado, D. T. (2001). Simple method of modeling PVD-Improved subsoil. *Journal of Geotechnical and Geoenvironmental Engineering*, *127*(November), 965–972. https://doi.org/10.1061/(ASCE)1090-0241(2001)127:11(965)

Chu, J., Bo, M. W., & Choa, V. (2004). Practical considerations for using vertical drains in soil improvement projects. *Geotextiles and Geomembranes*, *22*(1–2), 101–117. https://doi.org/10.1016/S0266-1144(03)00054-2

CHU, J., BO, M., & CHOA, V. (2006). Improvement of ultra-soft soil using prefabricated vertical drains. *Geotextiles and Geomembranes*, *24*(6), 339–348. https://doi.org/10.1016/j.geotexmem.2006.04.004

Dixit, M. K., Fernández-Solís, J. L., Lavy, S., & Culp, C. H. (2012). Need for an embodied energy measurement protocol for buildings: A review paper. *Renewable and Sustainable Energy Reviews*, *16*(6), 3730–3743. https://doi.org/10.1016/j.rser.2012.03.021

Geoff Hammond, C. J. (2008). *Inventory of Carbon & Energy (Ice)*. http://www.emccement.com/pdf/Full-BSRIA-ICE-guide.pdf

Griffin, H., & O'Kelly, B. C. (2014). Ground improvement by vacuum consolidation – a review. *Proceedings of the Institution of Civil Engineers - Ground Improvement*, *167*(4), 274–290. https://doi.org/10.1680/grim.13.00012

Hammond, G. P., & Jones, C. I. (2008). Embodied energy and carbon in construction materials. *Proceedings of Institution of Civil Engineers: Energy*, *161*(2), 87–98. https://doi.org/10.1680/ener.2008.161.2.87

Hansbo, S. (1979). Consolidation of clay by band-shaped prefabricated vertical drains. Ground Engineering, 12, pp. 16-25.

Hansbo, Sven. (1980). Consolidation of clay by band-shaped prefabricated drains. *International Journal of Rock Mechanics and Mining Sciences & Geomechanics Abstracts*, *17*(1), A10. https://doi.org/10.1016/0148-9062(80)90141-2

Hansbo, S., Jamiolkowski, M., & Kok, L. (1981). Consolidation by vertical drains. *Geotechnique*, *31*(1), 45–66. https://doi.org/10.1680/geot.1981.31.1.45

Hird, C. C., I. C. Pyrah and D. Russell (1992). Finite element modelling of vertical drains beneath embankments on soft ground. *Geotechnique*, 42(3),pp. 499- 511.

Holtz, R. D., Jamiokowski, M., Lancellotta, R. and Pedroni, R. (1991). Prefabricated vertical drains: Design and Performance, CIRIA Ground Engineering Report, Butterworth-Heinemann Ltd., London.

Indraratna, B. and I. W. Redana (1997). Plane strain modeling of smear effects associated with vertical drains. J. Geotech. Eng., ASCE, 123(5),pp. 474-478.

Indraratna, B. and I. W. Redana (1999). Closure: Plane strain modeling of smear effects associated with vertical drains. *J. Geotech. Eng*., ASCE, 123(5),pp. 474-478

Indraratna, B. and Radampola, S. (2002). Analysis of Critical Hydraulic Gradient for Particle Movement in Filtration. *J. Geotech and Geoenvirob Eng*., ASCE, 128(4),pp. 347-350.

Indraratna, B. (2008). Recent advancements in the use of prefabricated vertical drains in soft soils. *Australian Geomechanics Journal*, *43*(1), 29–46. https://ro.uow.edu.au/cgi/viewcontent.cgi?article=1430&context=engpapers

Indraratna, B. (2010). Recent advances in the application of vertical drains and vacuum preloading in soft soil stabilisation. *Australian Geomechanics Journal*, 45(2),pp. 1-44.

Jamiolkowski, M, and Lancellotta, R. (1984). Embankment on vertical drains: Pore pressure during construction. *Proc., Int. Conf. Case Histories in Geotechnical Engineering, St. Louis*, 275-278.

Kjellman, W. (1952). Consolidation of clay soil by means of atmospheric pressure. *Proceedings of a Conference on Soil Stabilization, Massachusetts Institute of Technology, Boston*, pp. 258-263.

Kjellman, W. (1948). Accelerating consolidation of fine grained soils by means of cardboard wicks. *Proceedings 2nd International Conference on Soil Mechanics and Fondation Engineering*. Vol 2, Rotterdam, pp. 302-5.

Kremer, R., de Jager, W., Magdenberg, A., Meyvogel, I., and Oostveen, J. (1982). Quality standards for vertical drains. *Proceedings 2nd International Conference on Geotextile, Las Vegas*, pp. 319-324.

Kremer, R. H. J., Oostveen, J. P., van Weele, A. F., De Jager, W. F. J., and Meyvogel, I. J. (1983). The quality of vertical drainage. Proceedings Eighth European Conference on Soil Mechanics and Foundation Engineering, Vol. 129, No. 9, September 2003, 858-860.

Liu, H. long, & Chu, J. (2009). A new type of prefabricated vertical drain with improved properties. *Geotextiles and Geomembranes*, *27*(2), 152–155. https://doi.org/10.1016/j.geotexmem.2008.09.006

Long, R. P. ., & Covo, A. (1994). Equivalent diameter of vertical drains with an Oblong cross section. *Journal of Geotechnical Engineering*, *120*(9), 296–300. https://doi.org/https://doi.org/10.1061/(ASCE)0733-9410(1994)120:9(1625)

Madhira R. Madhave, Yeong-mog park, N. miura. (1993). Modelling and study of smear zones around band shaped drains. *Soils and Foundations*, *33*(4), 135–147.

https://doi.org/https://doi.org/10.3208/sandf1972.33.4_135

Menzies, G. F., Turan, S., & Banfill, P. F. G. (2007). Life-cycle assessment and embodied energy: A review. *Proceedings of Institution of Civil Engineers: Construction Materials*, *160*(4), 135–143. https://doi.org/10.1680/coma.2007.160.4.135

Mesri, G., Lo, D. O. K. and Feng, T-W. (1991). Field performance of Prefabricated Vertical Drains. *In Proceedings of the International Conference on eotechnical Engineering for Coastal Development-Theory to Practice*, Yokohama, Japan, 1, pp 231-236.

Pradhan, T. B. S., Imai, G., Murata, T., Kamon, M., Suwa, S. (1993). Experiment study on the equivalent diameter of a prefabricated band-shaped drain. *Proceeding 11th Southeast Asian Geotech. Conf.* 391-396.

Patrick J. Hannigan, P., Frank Rausche, PhD, P., Garland E. Likins, P., Brent R. Robinson, PhD, P., & Matthew L. Becker, E. (2016). *Design and installation of vertical drains by American Association of the stage highway and Transportation Officials (AASHTO): Vol. I.*

PLAXIS (2015). PLAXIS 2D Reference Manual. R. B. J. Edited by Brinkgreve, Delft University of Technology and PLAXIS b.v., The Netherlands.

Rixner, J. J., Kraemer, S. R., Smith, A. D. (1986). Prefabricated vertical drain. Vol. I, Engineering guidelines, FWHA/RD-86/168. Federal Highway Administration, Washinton, D. C.

R. Radhakrishnan, & C. Gunasekaran. (2019). *Factors Influencing PVD Performance in Soft Clay Consolidation* (Vol. 14). *Springer Nature Singapore*. https://doi.org/https://doi.org/10.1007/978-981-13-0559-7_4

Seah TH. (2006). Design and construction of ground improvement works ad Suvarnabhumi airport. *Proceedings of the International Symposium on Geotechnial Aspects of the Second Bangkok (Suvarnabhumi) Airport in Thailand*, 89–112. http://seags.ait.asia/publications/International-Symposium-Suvarnabhumi-Airport-Thailand-2006.pdf

Sharma, J. S., & Xiao, D. (2000). Characterization of a smear zone around vertical drains by large-scale laboratory tests. *Canadian Geotechnical Journal*, *37*(6), 1265–1271. https://doi.org/10.1139/t00-050

Shillaber, C. M., Mitchell, J. K., & Dove, J. E. (2015). Energy and Carbon Assessment of Ground Improvement Works. II: Working Model and Example. *Journal of*

Geotechnical and Geoenvironmental Engineering, *142*(3), 04015084. https://doi.org/10.1061/(asce)gt.1943-5606.0001411

Shillaber, C. M., Mitchell, J. K., & Dove, J. E. (2016). Energy and Carbon Assessment of Ground Improvement Works. I: Definitions and Background. *Journal of Geotechnical and Geoenvironmental Engineering*, *142*(3), 04015083. https://doi.org/10.1061/(asce)gt.1943-5606.0001410

Sun, H., He, Z., Geng, X., Shen, M., Cai, Y., Wu, J., Yang, B., & Wang, W. (2021). Formation mechanism of clogging of dredge slurry under vacuum preloading visualized using digital image technology. *Canadian Geotechnical Journal*, *59*(November), 1292–1298.

Taylor, D. W. (1948). Fundamentals of soil mechanics, *John Wiley, New York.*

Terzaghi, K. (1943). Theoretical soil mechanics, John Wiley and Sons, New York.

Xiao, M., Reddi, L. N. (2000). Comparison of Fine Particle Clogging in Soil and Geotextile Filters. Proceedings GeoDenver 2000 in Advances in Transportation and Geoenvironmental Systems Using Geosynthetics. Denver, Corolado, August 5-8, 2000. pp 176-185.

Xu, B. H., He, N., Jiang, Y. Bin, Zhou, Y. Z., & Zhan, X. J. (2020). Experimental study on the clogging effect of dredged fill surrounding the PVD under vacuum preloading. *Geotextiles and Geomembranes*, *48*(5), 614–624. https://doi.org/10.1016/j.geotexmem.2020.03.007

This Page Intentionally Left Blank

CHAPTER III
INITIAL AND BOUNDARY OF FIELD CONDITIONS AND LIFE CYCLE ASSESSMENT (LCA) OF EMBODIED CO_2 EMISSIONS

3.1 INTRODUCTION

In archipelagic countries such as Indonesia, airport infrastructure is becoming more important to increase connectivity and economic growth. Air transportation is priority sectors in the ASEAN Economic Community (AEC) (Saraswati & Hanaoka, 2013). In fact, most of the airports are located in soft soil because the limited areas of stable soil are designated for urban use (Adriyati et al., 2020). In this chapter focuses on the initial conditions and boundary condition for PVD material application, based on field observations. The numerical analysis using PLAXIS2D software with finite element method (FEM) are conducted and assess the embodied CO_2 emission to understand the PVD material benefit.

3.2 NUMERICAL ANALYSIS USING FEM

3.2.1 Introduction

Prefabricated vertical drain (PVD) is one of the soft ground improvement techniques that have the advantage of accelerating consolidation rate of soft soil by providing a drainage path. Surcharge and vacuum preloading are common combinations method with PVD are mentioned in previous study (Adriyati et al., 2022a) and illustration in Figure 3. 1 and Figure 3. 2. The objective of this section is to determine the approximate method for modelling a real condition of ground improvement in Runway construction and simplified the conversion of axisymmetric to plane strain for finite element method analysis solution. Therefore, engineering design can use more realistic models to evaluate the environmental impacts and performance of ground improvement techniques, such as those discussed in the previous chapter. This will lead to better decision-making when selecting the most sustainable and efficient design alternatives for geotechnical construction projects.

The discussion of combined technologies has presented a significant time acceleration along with reducing the settlement due to preloading installation, and some limitations can be developed.

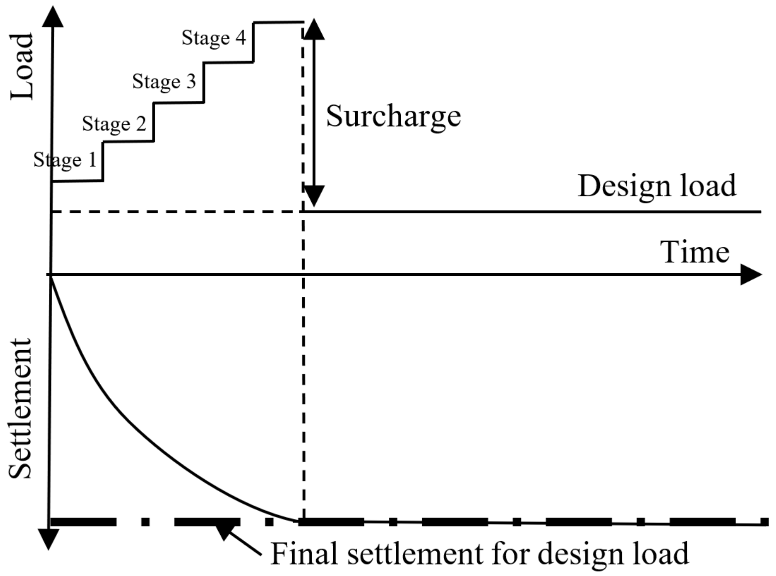

Figure 3. 1. Surcharge preloading concept of ground improvement (Adriyati et al., 2022a)

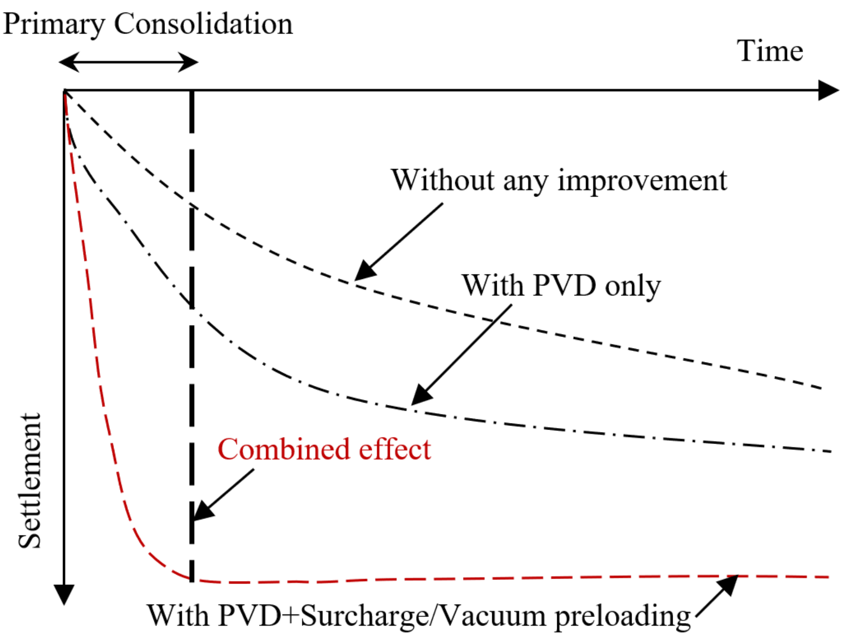

Figure 3. 2. Combined concept of ground improvement (Adriyati et al., 2022a).

3.2.2 Characteristics of soil and material

3.3.4.1 Geology structure of the study area

Geological structure of study area was covered by Alluvial (Qa), Beach Ridge Deposit (Qbr) and Banten Tuff (QTvb). The Alluvial formation consist of clay, silt, sand, gravel, pebble and boulder, the Beach Ridge Deposit consist of Coarse sand, well sorted with mollusk shells and the Banten Tuff consist of tuff, pumice tuff and tuffaceous sandstone (Bergado et al., 2002).

3.3.4.2 Soil profile in the field

A total of 58 test deep-bore tests and 160 laboratory tests were conducted for this project. However, not all the field test data will be used, and only relevant data will be selected. Based on observations from both the drill data and laboratory analysis, 3 points of drill data were identified and used to describe the soil layer at the study site. According to the soil investigation data, the research area is dominated by clayey in the surface less than 12 m, and the author used standards interpreting for stratigraphic analysis is American Society for Testing and Materials (ASTM D1586-1) and Standard National Indonesia (SNI 4153-2008). Based on an analysis of soil descriptions, drilling results, and N-SPT values, the interpretation yields a description of the soil conditions in the PVD area are shown in Figure 3. 3.

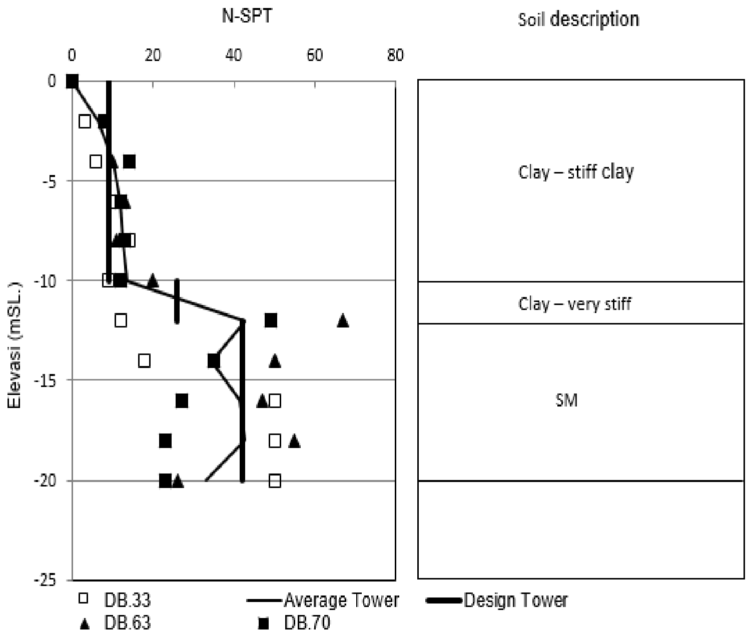

Figure 3. 3. Soil properties and profile (Adriyati et al., 2020).

3.3.4.3 Material of PVD

The prefabricated vertical drain well is increasingly being used in various ground improvement projects on soft soil deposits such as soft soil or marine clay, which has advantages to decreasing the overall time required for completion of primary consolidation, to decreases the amount of surcharge load required to achieve the same desired amount of consolidation. Other than that, there is a disadvantage, are a greater number of wick drains required to achieve the same rate of drainage, then is recommended to find a distance that can influence, as discussed in this study. The properties of PVD materials CT-D832 are shown in Table 3. 1.

Table 3. 1. Properties of PVD.

Core		Filter	
Thickness, t (mm)	5	Coefficient of permeability, 100 mm head (m/s)	2.99×10^{-4}
Width, *w* (mm)	100	Grab tensile strength (N)	68600
Discharge cap., 300 kPa, i =0.1 (m^3/s)	1.73×10^{-4}	Apparent Opening Size (O_{90}) (µm)	≤ 75

3.2.3 Equivalent conversion of PVD

The approximate method for modelling a real condition with a PVD combined with vacuum preloading involves using the classical axisymmetric solution for soil parameters, which is converted into an equivalent two-dimensional plane strain analysis (PLAXIS2D) for soft ground improvement techniques. Additionally, the unit cell theory in axisymmetric conditions which was proposed are shown in Figure 3. 4.

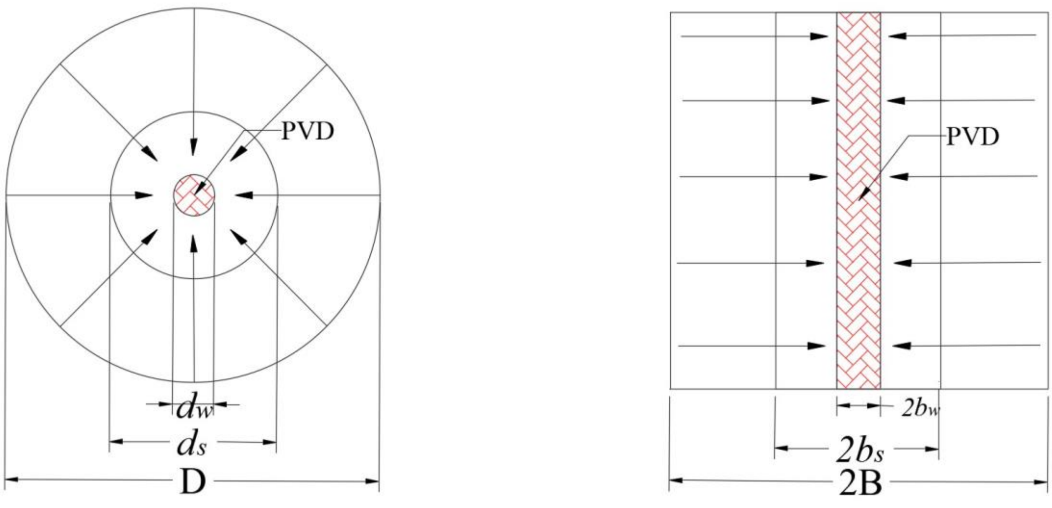

Figure 3. 4. Axisymmetric unit cell in plan view and plane strain unit cell (Modification from Adriyati et al., 2020).

$$X_{eq} = \left(\frac{L_{PVD}}{L_e} \times X_{PVD}\right) + \left(\frac{L_{soil}}{L_e} \times X_{soil}\right) \tag{3.1}$$

Where is X_{eq} is the equivalent parameter, L_e is the area of the equivalent element, L_{pvd} is the area of the PVD length, L_{soil} is the area of the soil, X_{PVD} is the equivalent parameter area of PVD permeability, and X_{soil} is the equivalent parameter area of soil permeability.

3.2.4 Methodology and limitations

The PVD represented by an equivalent value of vertical hydraulic conductivity (k) based on the equal average degree of consolidation, methodology of this study is shown in Figure 3. 5. The triangular configuration is chosen in this research to provide a more uniform consolidation between drains. Therefore, to determine the input required parameter in numerical analysis, design equations should pay attention to soil properties, boundary and drainage conditions, desired degree of consolidation, time available for consolidation and equivalent diameter of the material. The output obtained is the drain spacing, do varies to optimize the design. Closer spacings increase installation, which is often a most important design consideration.

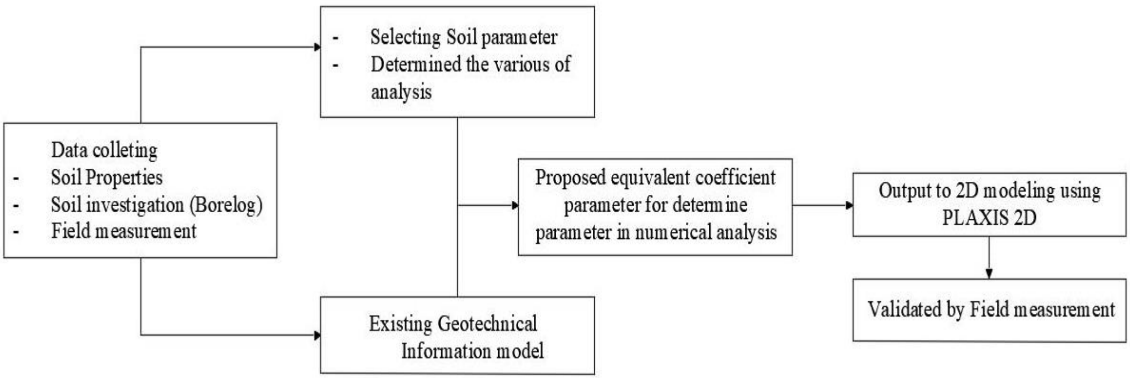

Figure 3. 5. The structure of numerical method.

However, this paper is required to have several limitations in the methodology, as described in the following, to simplify the problem. The factors that have been considered in this calculation has limitations: In the numerical study, the influence of the vertical component of pore-water flow is neglected because the column was penetrated up to the full depth of the soft clay bed and the isotropic consolidation caused by the surcharge preloading pressure.

The lateral strain at the boundary of the unit cell can be neglected in a representative element volume within the unit cell as per the numerical model. The laminar flow through the soil (Darcy's law) is adopted. Material model is Mohr-Coulomb. Numerical model using Finite element method with the static condition.

3.2.5 Results and discussion

The accurate prediction of the consolidation settlement of soil requires a comprehensive assessment of various soil parameters, such as grain size distribution, initial water content, and compressibility. To understand the impact of these parameters on settlement, we conducted FEM analysis in PLAXIS2D. Figure 3. 6 and Figure 3. 7 show the boundaries of the analysis and generated mesh, respectively, revealing the distribution of stresses and strains in the soil under different loading conditions. These results provide valuable insights into the behavior of the soil and can aid in optimizing engineering designs for soil settlement control

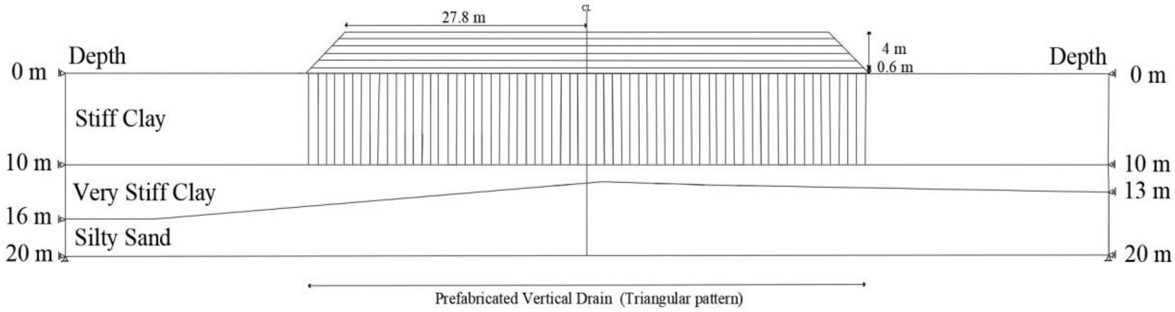

Figure 3. 6. Soil layer input in FEM for boundary conditions analysis.

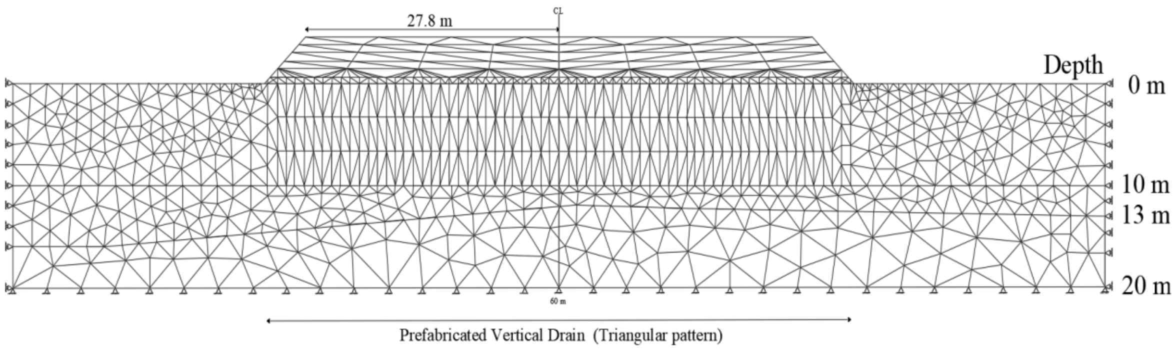

Figure 3. 7. Generated mesh in FEM for settlement analysis.

The results, presented in Figure 3. 8 and Figure 3. 9, reveal the impact of different PVD spacing on consolidation settlement over various durations. The analysis found that the spacing of 1.0 m led to a duration of 79 days and a settlement of 16.2 cm, while a spacing of 1.5 m resulted in a duration of 202 days and a settlement of 16.7 cm. Moreover, a spacing of 2.0 m resulted in a duration of 489 days and a settlement of 16.8 cm. Although the experimental and numerical study yields interesting observations and the results match well, there are several limitations in the numerical study model that uses the Finite Element Method with a static condition. Furthermore, to evaluate the behavior of the testing chamber and sensors and to record data using a data acquisition system, it is necessary to monitor the time-dependent settlement of the laboratory scale 1g model test setup needed to understand the mechanism of the influence effect. The combined ground improvement method accelerates the consolidation settlement.

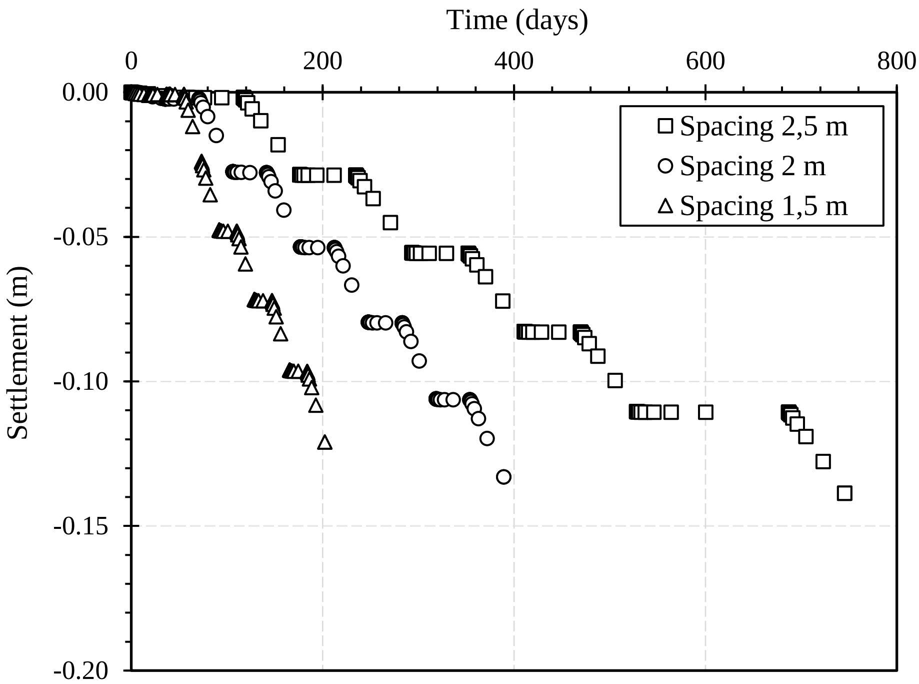

Figure 3. 8. The PVD spacing during the construction stages.

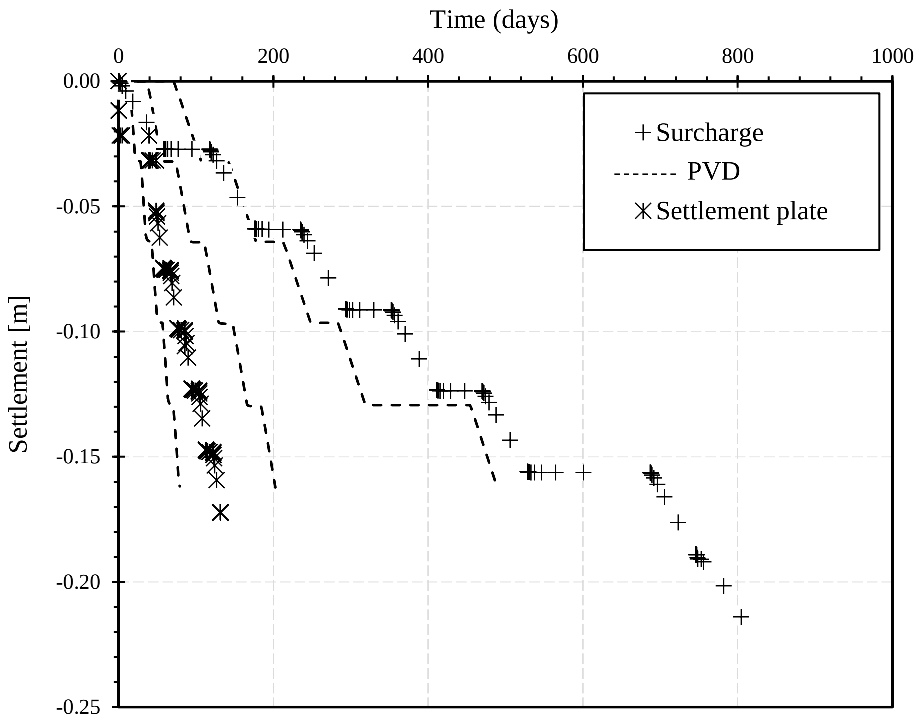

Figure 3. 9. The PVD spacing, surcharge and settlement plate results.

3.3 LIFE CYCLE ASSESMENT (LCA) OF EMBODIED CO_2 EMISSIONS IMPLICATIONS FOR PVD MATERIAL

3.3.1 Introduction

The Sustainable Development Goals (SDGs) target the development of quality, reliable, sustainable, and resilient infrastructure to support economic development and human well-being. By 2030, one of the targets is to upgrade infrastructure and retrofit industries to make them more sustainable, especially in countries like Indonesia, where alignment can be achieved between the SDGs and the countries' Nationally Determined Contributions (NDCs) (UNDP, 2018). This research uses an emissions assessment model to calculate the embodied carbon dioxide (CO_2) emissions for ground improvement techniques in runway construction. Life cycle assessment (LCA) is used to evaluate the environmental impacts of the techniques, which have the potential to reduce construction time, material use, fuel consumption, and labor, making them a more sustainable alternative to traditional foundation systems (Geoff Hammond, 2008; Menzies et al., 2007; Slocombe & Egan, 2010).

The study objective is to compare the embodied CO_2 emissions of prefabricated vertical drain with other ground improvement techniques with the same function. The LCA are applied in this study and illustrate the embodied CO_2 emissions associated with ground improvement projects (Shillaber et al., 2015). The purpose of these comparisons is to demonstrate the environmental benefits of each technique.

3.3.2 Methodology

3.3.2.1 Defining the boundary and quantities material of study

This study compares the embodied CO_2 of six commonly used ground improvement techniques in Indonesia, including prefabricated vertical drain (PVD), stone column, granulated blast furnace slag (GBFS), bored cast in situ pile, deep mixing soil, and sand drain. This study, simulated assumptions were made to examine the various ground improvement techniques. The project involves a runway of dimensions 3000 x 60 m in soft soil with a length of one kilometer. The quantities of the simulation assumptions materials for this design alternative are explained as follows:

1. Stone column quantities

Stone columns utilize much less raw material, consume much less fuel for installation of an equivalent by performance system, and the materials are less processing energy. This study, a design simulation was conducted for the installation of stone column in Area Runway 3 of the Soekarno-Hatta airport construction project. The diameter of the stone column using gravel material is 50 cm and the depth is 11 m. The total volume of the stone aggregate used in the project area is 148032.5 m^3 in total. The stone column material was assumed to be transported from the distance of 1529.45 km to the construction site.

2. PVD quantities

The design of PVD was used to accelerate consolidation in Area Runway 3 of the Soekarno-Hatta airport construction project. The soft soil in the construction area is approximately 11 m depth, and High Density Polyethylene (HDPE) was the material chosen for the PVD. For this project, PVD with a thickness of 0.5 cm and a width of 10 cm were simulated, with the total volume of 95.32 m^3. The PVD were assumed to be transported from the distance of 1897.52 km to the construction site.

3. GBFS quantities

Using GBFS in such as applications saves the energy that would be needed for line calcination in the manufacturing process of ordinary Portland cement. This also eliminates the release of carbon dioxide resulting from decomposition of limestone. GBFS is an environmentally friendly product. This project simulated by slag content up to 50% may replace the Portland cement. The density 2.8 g/cm^3, activity index 28 days old, Flow ration 95 %, magnesium oxide 10 %, sulfur trioxide 4 %, Ignition loss 3 %, and Chloride ions 0.02 %, respectively. The diameter of the pile by using GBFS admixture material is 50 cm, and the depth is 11 m. The total volume of in the project area is 148032.5 m^3 in total. The GBFS were assumed to be transported from the distance of 268.37 km to the construction site.

4. Bored cast in situ pile quantities

In general, bored cast in situ pile offer the most economic foundation as they can constructed in a wide choice diameter around 40 cm to 100 cm, depth generally up to 18 m with bigger drilling depths are possible. The advantage of this method is vibration free, reinforcement can push into the fresh concrete, and durability for earthquake resistance. The steel reinforcement the yield strength (fy) is 375 N/mm^2 or as per bored pile specification, concrete fcu is 35 N/mm^2, binding wire, concrete spacers approximately 75 mm or equivalent, and flooring steel plates. This study, diameter of the bored cast in situ pile is 50 cm with the depth is 11 m. The total volume of in the project area is 296065 m^3 in total.

5. Deep mixing soil quantities

The deep mixing soil method was developed in 1970's in Japan (Takahashi et al., 2023). This method does not need long curing or waiting time to obtain the strength. Mixing the soil with binders offers environmental and economic advantages and contributes vastly to sustainability. The large amount of cement, and the strength of the treated soil is high, at 1500 kN/m^2 or more and solidifying clayey soil. This study, diameter of deep mixing soil is 50 cm with the depth is 11 m. The total volume of in the project area is 148032.5 m^3 in total. The material was assumed to be transported from the distance of 272 km to the construction site.

6. Sand drain quantities

The sand drain method consists of driving sand drains into the clay layer to let the water out of the clay layer as fast as possible. The method speeds up the settlement process and hardens the clay layer. The sand drain method was first used in Japan 1952, one of project are used sand drain is Kansai Airport in Japan. By referring the project, this study simulated diameter of sand drain is 50 cm with the depth is 11 m. The total volume of in the project area is 148032.5 m^3 in total. The material was assumed to be transported from the distance of 1529.45 km to the construction site. Figure 3. 10 shows the location where the ground improvement technique was applied. The embodied carbon values and average fuel consumption for this study based on field conditions and based on Table 3. 2 and Table 3. 3.

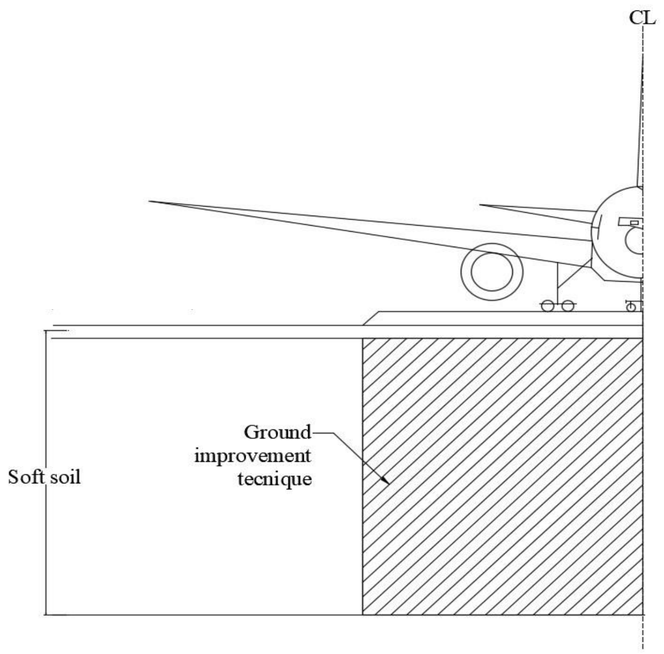

Figure 3. 10. Application of Ground Improvement Techniques in this study (unscaled).

3.3.2.2 Calculation methodology

The stages describing the life cycle assessment include (1) Material and Equipment; (2) Ground improvement construction with transportation between and within sites and processes constructions, including an allocation of the machinery manufacturing, operation and maintenance processes, and disposal or recycle energy after the demolition. The following methods of ground improvement and piling considered shows in Figure 3. 11 this study is shown in the boundaries and methodology are used for quantifying environmental impact factors for geotechnical construction for embodied CO_2 emission, based on site-specific in Runway construction.

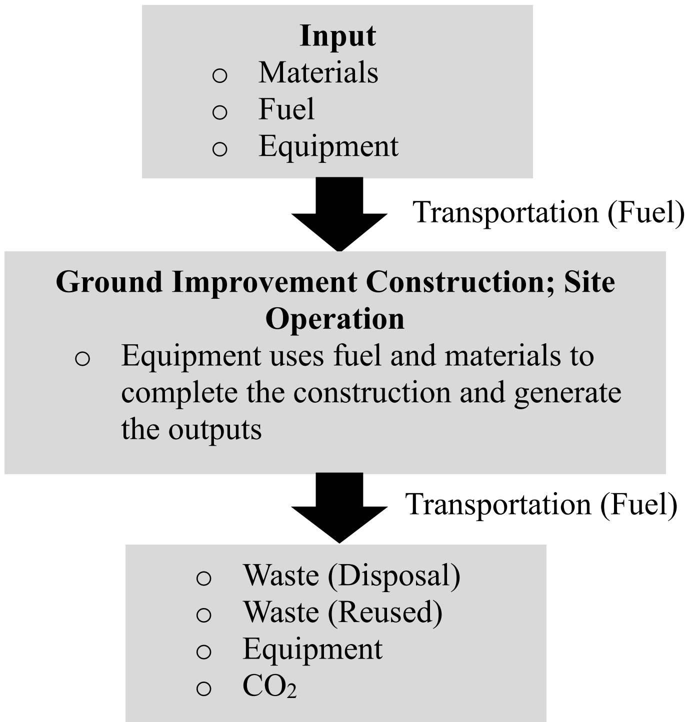

Figure 3. 11. Flow chart of the boundary condition for analysis (modified from Shillaber et al, 2015).

Material and equipment are evaluated by total volume of each material and equipment used, hence the weight and multiplying them by their respective embodied CO_2 emissions value. Construction and site operation are the amount of emissions consumed on site operate the machineries on site; this evaluated as the product of the amount of fuel. It includes the operation of installation. Transportation emissions includes moving machinery and materials used to and from sites; this is calculated by using the liter of fuel consumed. The quantities of fuel consumption based on (Davis et al., 2012; Dixit et al., 2012). Although a transportation vehicle rarely return empty from a work site, our analysis takes a conservative approach. Section 3.3.3 provides a list of distances between the site and the manufacturer. The analysis includes waste and equipment materials from site operations, as well as input materials associated with CO_2 emissions. Furthermore, waste disposal methods are similar throughout the United States, resulting in a consistent impact on energy and CO_2 emissions for a unit of disposed waste.

The embodied CO_2 emissions for material (CO_{2_m}) is computed by assuming the product of the quantity of each material for ground improvement technique and for construction site operation, on-site consumption fuel such as diesel are explained (CO_{2_T}) Since these terms are widely used, they are defined:

$$CO_{2_m} = \sum_{i=1}^{n} [(M_{mi} \times C_{mi})] \tag{3.2}$$

$$CO_{2_T} = \sum_{j=1}^{m} \left[\left(F_{cmi} \times C_{fmi}\right)\right] \tag{3.3}$$

The total quantity of a particular fuel (e.g., diesel), the average fuel consumption of construction. The CO_2 emissions are computed following the same approach used for embodied CO_2 emission. Overall total CO_2 emissions are determined in Equation. (3. 4).

$$Total_{CO_2e} = CO_{2_m} + CO_{2_T} \tag{3 .4}$$

where M_{mi} = Mass volume of material, C_{mi} = coefficient of material. where CO_{2_m}= total embodied CO_2 emission of consuming material; CO_{2_T} = total embodied CO_2 emission of consuming for transportation, F_{cmi} = Fuel consuming of transportation, C_{fmi} = coefficient of transportation from the supplier to the site.

3.3.2.3 Coefficients of fuel consumption and CO_2 emission

In terms of building and civil infrastructure construction, embodied CO_2 emission may be classified as either indirect or direct. Embodied energy may further be classified as either primary or delivered are shown in Table 3. 2 and Table 3. 3.

Table 3. 2. Average fuel consumption of construction (Davis et al., 2012; Dixit et al., 2012).

Description of vehicle	Truck class (1-8)	Average fuel consumption (km/L)
Light heavy-duty truck	7	2.72
Heavy-duty truck	8	2.42

Table 3. 3. Embodied carbon values used for analysis (G. Hammond & Jones, 2011; G. P. Hammond & Jones, 2008).

Material	EC-kg CO_2/kg	Reference
High Density Polyethylene (HDPE)/ PVD	1.60	
Stone Gravel	0.017	Inventory of Carbon & Energy (ICE) V.1.6a, University of Bath, UK
Concrete	0.130	
Steel (Reinforcement steel)	1.77	
Sand	0.005	
Soil-cement (DMS)	0.14	
Slag (U.S)	0.021	Slag cement Association 2014
Fuel – Diesel *Diesel density is taken as 0.83 kg/l	3.25	Carbon calculator V.3.1.1, Environmental Agency, UK

3.3.2.4 Limitation and analysis for CO_2 emissions

The following four factors can make it challenging to performed of calculation total embodied CO_2 emissions for material (CO_{2_m}) and total embodied CO_2 emission of consuming for transportation (CO_{2_T}) analyses of geotechnical designs (Inui et al. 2011):

1. Geotechnical design is strongly site specific;
2. Fewer design varieties area available;
3. The installation process described at the design stage often does not reflect what happens on site; and
4. The service life is often longer than that of buildings, and negligible operational energy is required.

The difference between the design assumptions and what occurs on site is the most difficult to address. Additional uncertainty is introduced into the analysis. While the coefficients represent typical industry average production for material and fuel are different.

3.3.3 Results and discussion

In the civil infrastructure and geotechnical works, there are standards that permit the use of emissions coefficients for GHGs. The Inventory of Carbon and Energy (ICE) version 2.0 is one of the largest available database for construction materials, developed by (Geoff Hammond, 2008) for construction materials are used in this study. The analysis results are represented in the total embodied CO_2 emissions is shown in Table 3. 4.

The database present many available studies for each material as possible, including minimum, maximum, average, and standard deviation of EECs for each material, giving an indication of the spread in the available data from published sources. G. Hammond & Jones (2011), indicated that the data from the ICE database can be used internationally as its EE values are considered more reliable than the CO_2 emission values used as the standard for calculating the volume in this study.

Table 3. 4. Calculation embodied carbon by ground improvement technique.

No	**Ground improvement technique**	**All Material Volume (m³)**	**The bulk density of material (kg/m³)**	**Material consumption (ton)**	**Embodied CO_2 (ton)**	**Distance between Project and Manufacturing Location (km)**	**Total Diesel density (kg)**	**Fuel consumption (kg/l)**	**Total Embodied CO_2 (ton)**
1	Stone column	148032.5	1420	210206	3573	1529.45	1269.44	3046	6997
2	Prefabricated vertical drain	95.32	0.5	0.047	0.076	1897.52	1574.94	4248	4248
3	Granulated Blast Furnace Slag	148032.5	3600	532917	11191.26	268.37	222.75	600	11792
4	Bored cast in situ pile	296065	8615.68	1275400	2120127	540.38	448.52	1209	2121337
5	Deep mixing soil	148032.5	1440	213166	29843	272.00	225.76	609	30452
6	Sand drain	148032.5	1600	236852	1184	1529.45	1269.44	600	4608

In this study, the coefficient of emissions for runway construction project was calculated using the ICE database. In this study, estimating the total embodied CO_2 emissions by comparing two commonly used ground improvement methods in Airport projects in Indonesia. The lower percentage in the results indicate a less accurate the estimate for total embodied CO_2 emissions. There is a recognized need to improve geotechnical construction materials and reduce transportation energy-related carbon dioxide (CO_2) emissions, which will

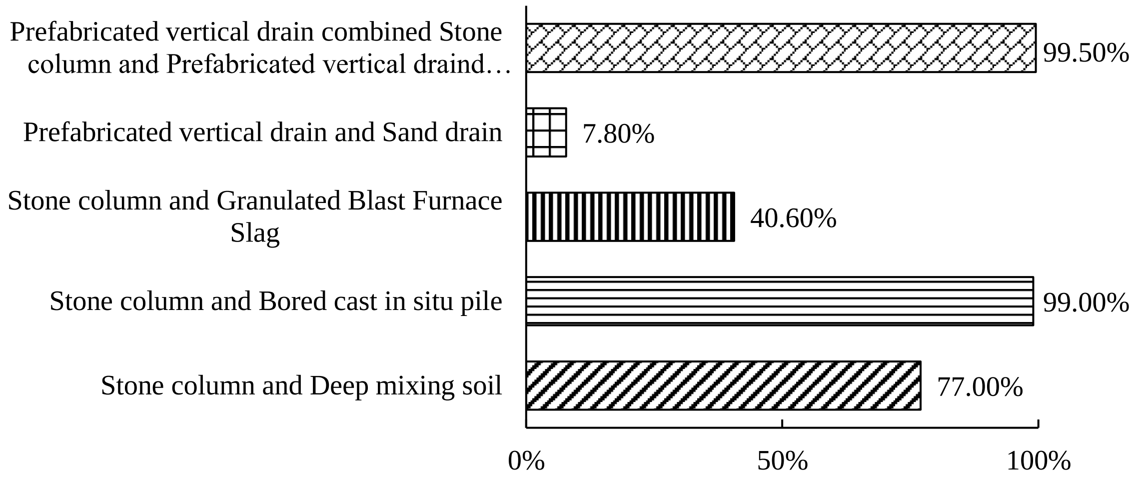

Figure 3. 12. The total saving embodied CO_2 emission.

3.4 SUMMARY

Accurately predicting consolidation settlement requires a careful evaluation of soil parameters. In this study, we carried out experiments to assess the settlement behavior of different PVD spacings and found that varying spacings resulted in different durations and settlement amounts. We also found that the use of combined ground improvement methods can accelerate consolidation settlement. However, we noted that the numerical study model that used Finite Element Method with a static condition had limitations, making it necessary to monitor the testing chamber and sensors to understand the mechanism of the influence effect.

Emissions coefficients for greenhouse gases (GHGs) are allowed in civil infrastructure and geotechnical works, and the Inventory of Carbon and Energy (ICE) version 2.0 is a comprehensive database that provides data on the embodied energy and carbon of different construction materials used in the UK. In this study, we calculated the embodied CO_2 emissions as an environmental impact factor to compare different alternatives for ground improvement. Our study shows that the prefabricated vertical drain design had higher CO_2 savings of up to 99.5%. We also found other ground improvement techniques yielded CO_2 savings ranging from 7.8% to 99%. By considering environmental impacts, ground improvement projects can become more sustainable. Additionally, we calculated the coefficient of emissions for runway construction using the ICE database and provide the estimated total embodied CO_2 emissions with high accuracy

3.5 REFERENCES

Adriyati, Meilani, Rifa'i, A., & Fikri, F. (2020). Analysis of settlement prediction due to preloading and vertical drain applications on runway construction. *E3S Web of Conferences*, *156*, 2–6. https://doi.org/10.1051/e3sconf/202015602002

Adriyati, M, Yasufuku, N., Ishikura, R., & Rifa, A. (2022a). *Numerical Analysis of Combined Surcharge Preloading using Prefabricated Vertical Drain and Stone Column on Runway Construction*.

Bergado, D. T., Balasubramaniam, A. S., Fannin, R. J., & Holtz, R. D. (2002). Prefabricated vertical drains (PVDs) in soft Bangkok clay: a case study of the new Bangkok International Airport project. *Canadian Geotechnical Journal*, *39*(2), 304–315. https://doi.org/10.1139/t01-100

Davis, S. C., Diegel, S. W., & Boundy, R. G. (2012). Transportation energy futures. In *Annual review of energy. Vol. 14*. https://doi.org/10.1146/annurev.eg.14.110189.002111

Dixit, M. K., Fernández-Solís, J. L., Lavy, S., & Culp, C. H. (2012). Need for an embodied energy measurement protocol for buildings: A review paper. *Renewable and Sustainable Energy Reviews*, *16*(6), 3730–3743. https://doi.org/10.1016/j.rser.2012.03.021

Geoff Hammond, C. J. (2008). *Inventory of Carbon & Energy (Ice)*. http://www.emccement.com/pdf/Full-BSRIA-ICE-guide.pdf

Hammond, G. P., & Jones, C. I. (2008). Embodied energy and carbon in construction materials. *Proceedings of Institution of Civil Engineers: Energy*, *161*(2), 87–98. https://doi.org/10.1680/ener.2008.161.2.87

Hammond, G., & Jones, C. (2011). Embodied Carbon: The Inventory of Carbon and Energy (ICE). *A BSRIA Guide*, 136. www.emccement.com.

Inui, T., Chau, C., Soga, K., Nicolson, D., and O'riordan, N. (2011). Embodied Energy and Gas Emissions of retaining Wall Structures. *Journal of Geotechnical and Geoenvironmental Engineering*, 137 (10), October 1, 2011.

Menzies, G. F., Turan, S., & Banfill, P. F. G. (2007). Life-cycle assessment and embodied energy: A review. *Proceedings of Institution of Civil Engineers: Construction Materials*, *160*(4), 135–143. https://doi.org/10.1680/coma.2007.160.4.135

Saraswati, B., & Hanaoka, S. (2013). Aviation policy in Indonesia and its relation to ASEAN

Single Aviation Market. *Journal of the Eastern Asia Society for Transportation Studies*, *10*, 2161–2176. https://doi.org/https://doi.org/10.11175/easts.10.2161

Shillaber, C. M., Mitchell, J. K., & Dove, J. E. (2015). Energy and Carbon Assessment of Ground Improvement Works. II: Working Model and Example. *Journal of Geotechnical and Geoenvironmental Engineering*, *142*(3), 04015084. https://doi.org/10.1061/(asce)gt.1943-5606.0001411

Slocombe, B. C., & Egan, D. (2010). Demonstrating environmental benefits of ground improvement. *Proceedings of the Institution of Civil Engineers: Ground Improvement*, *163*(1), 63–69. https://doi.org/10.1680/grim.2010.163.1.63

Takahashi, H., Sato, I., Morikawa, Y., and Ozawa, A. (2023). Long-Term Durability of Cement-Treated Soil Used in Offshore Airport Island Construction. Appl. Sci. 2023, 13, 8081. https://doi.org/10.3390/app13148081.

UNDP. (2018). *Aligning nationally determined contributions and sustainable development goals: Lessons learned and practical guidance*. *November 2017*, 15. https://www.undp.org/content/undp/en/home/librarypage/climate-and-disaster-resilience-/ndcs-and-sdgs.html

This Page Intentionally Left Blank

CHAPTER IV
LABORATORY EXPERIMENT (1G MODEL) OF MANDREL SYSTEM: MACRO TO MICRO

4.1 INTRODUCTION

This chapter presents a comprehensive description of the laboratory experiment (1g model) test setup and methodology for macro analysis. Moreover, it introduces the experimental setup and testing methodology of Scanning Electron Microscopy (SEM) for micro analysis.

For the 1g model test, the material of PVD and soil properties were scaled down from the prototype to the experimental model. The following subsection provides a step-by-step explanation of the detailed apparatus and testing procedure. Additionally, ImageJ software was used to support the SEM analysis of the image results.

4.2 MATERIAL AND EXPERIMENTAL APPARATUS

4.2.1 Material of PVD

The test is conducted in large-scale models to determine the response characteristics of a geometrically similar prototype structure, illustrating a process in Figure 4. 1 to correct the predictive results of the incomplete scale-down model for the prototype.

Figure 4. 1. Process for prediction of scale-down models.

Various scaling factors need to be chosen, and there may be a discussion about the most fundamental set to use (Wood, et al., 2002). The permeability factor is defined by the permeability of PVD in prototype times to model test per unit time. According to the similarity theory, the scaling factor of PVD is determined as:

$$\frac{k_p}{k_m} = n_k \quad (4.\ 1)$$

$$\frac{z_p}{z_m} = n_z \quad (4.\ 2)$$

where k_p is the permeability of the prototype, k_m is the permeability of the model, n_k is the scale factor of the permeability, z_p is the embedded length of the PVD prototype, z_m is the embedded length of the PVD model, and n_z is the scale factor of embedded length. The scale factor implies a necessary change in initial specific volume or void ratio was determined the scale factor (F=20) are describe as:

$$\Delta v = \Delta e = n_k \ln(\text{F}) \tag{4. 3}$$

where Δv is the change in initial specific volume and Δe is the change in void ratio. The scale factor parameter for three types of PVD is shown in Table 4. 1.

Table 4. 1. The properties of PVD.

Parameter	**Prototype**	**Model PVD**		
		Type A	**Type B**	**Type C**
Material	Polypropylene core			
Width (m)	0.1	0.09		
Thickness (m)	0.0050	0.0035	0.0040	0.0055
Young's modulus, E (kPa)	68.6	2.5	2.5	4.8
Permeability, $k_v = k_h$ (m/s)	2.99×10^{-4}	1×10^{-2}	1×10^{-2}	1×10^{-1}

The PVD consists of a core, drainage channel, and filter. A schematic illustration of PVD is provided in Figure 4. 2. The material of the PVD made by Polypropylene core. In the equivalent two-dimension design, it is necessary to convert the band shaped drain into

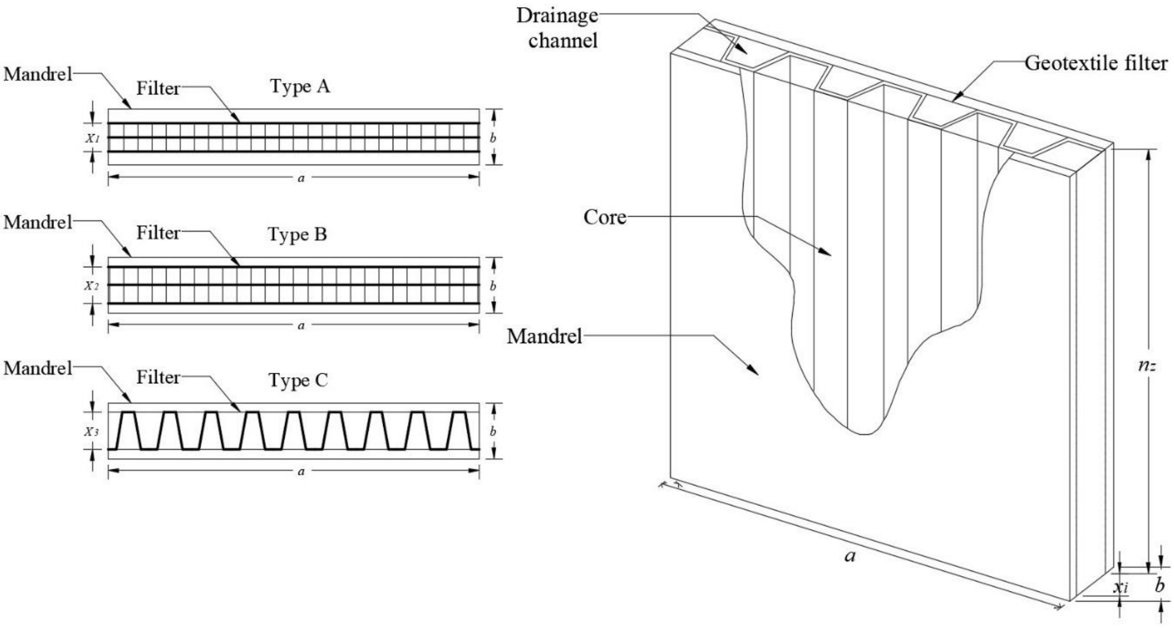

Figure 4. 2. The illustration of PVD types: (a) shapes of PVD types A, B, and C; (b) PVD type C structure.

an equivalent circular diameter called the “equivalent diameter”, as shown in Figure 4. 3 This dimension dictates the size of the inflow surface.

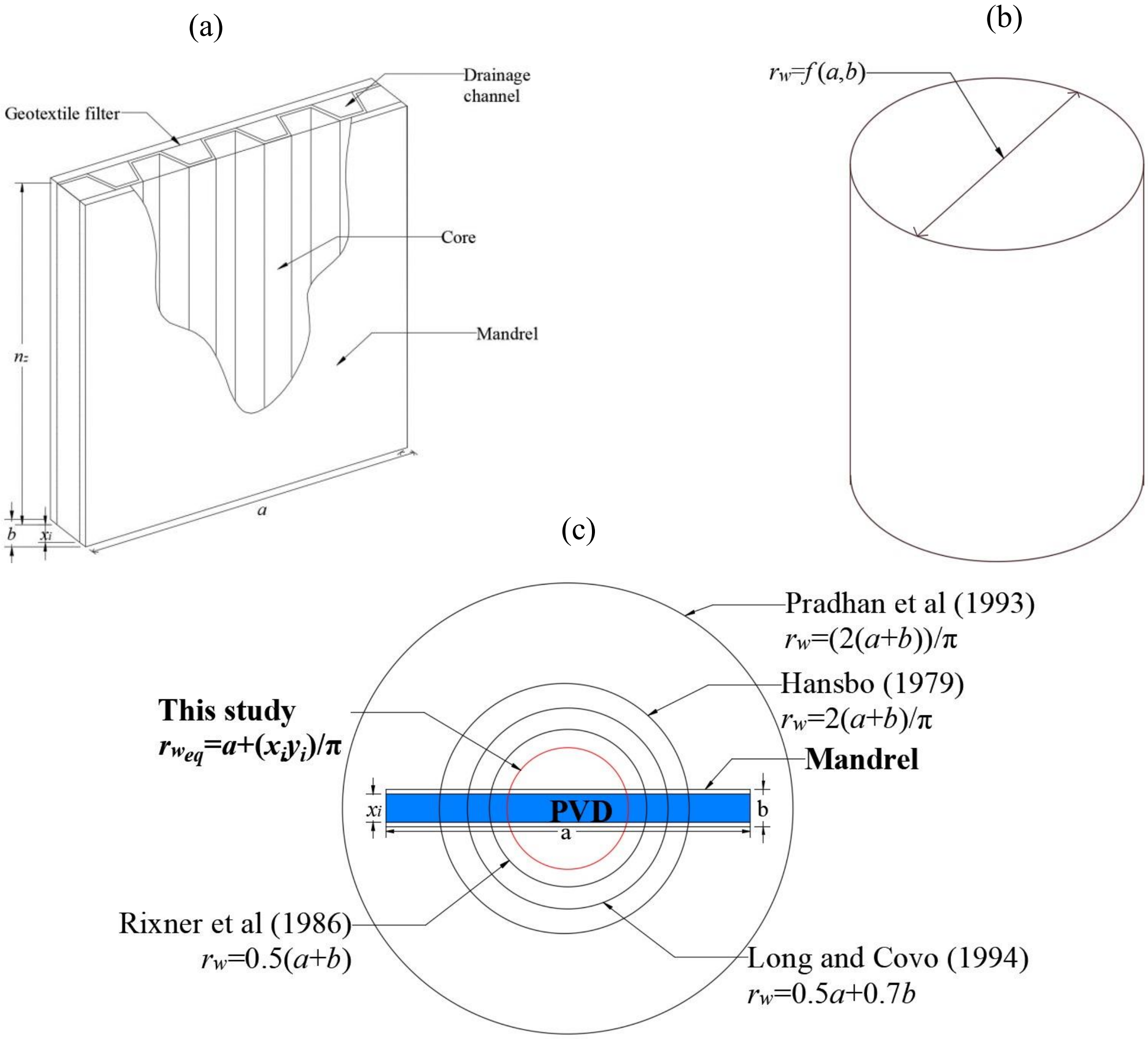

Figure 4. 3. Equivalent of PVD radius: (a) PVD structure; (b) cylindrical model; (c) Equivalent diameter.

The physical modeling is performed to study particular aspects of the behavior of prototypes. The mandrel has an influence on the resulting smear zone for the equivalent drain radius of PVD, as proposed in the chapter 2 section 2.3.1.2. Furthermore, were used to describe the drain radius of the smear zone’s influence on PVD with mandrel in this study:

$$r_{w\ (\text{Type A})} = \frac{a + 1.6\, x_1}{\pi} \tag{4. 4}$$

$$r_{w\ (\text{Type B})} = \frac{a + 1.4\, x_2}{\pi} \tag{4. 5}$$

$$r_{w\ (\text{Type C})} = \frac{a + x_3}{\pi} \tag{4. 6}$$

The model in a general form is expressed:

$$r_{w.eq} = \frac{a + (x_i y_i)}{\pi,} \tag{4. 7}$$

where $r_{w.eq}$ is the radius of an equivalent drain system, a is the mandrel width, x_i represents different types of PVD thickness variants, and y_i is the factor variant of PVD. In this study, x_1 is the thickness of PVD type A, x_2 is the thickness of PVD type B, x_3 is the thickness of PVD type C, and $r_{w.eq}$ was determined as 30 mm based on the designed rectangular mandrel.

Different equations for the equivalent drain diameter (r_w) of band shaped PVD have been proposed and are presented in Table 2. 1. The dimensions *a* and *b* are 900 mm, based on PVD type A is 3.5 mm, b for type B is 40 mm, b for type C is 5.5 mm are considered to compare the results of different equations.

Table 2. 2. The equivalent diameter of mandrel-driven prefabricated vertical.

References	Equivalent diameter (mm)
Hansbo (1979)	2×(*a*+*b*)/π
Rixner et al (1986)	0.5×(*a*+*b*)
Pradhan et al (1993)	(2×(*a*+*b*))/π
Long and Covo (1994)	0.5*a*+0.7*b*
This study	$\boldsymbol{a + (x_i y_i)/\pi}$

4.2.2 Soil properties

The experiment was carried out on a large-scale model to evaluate the influence and characteristics of mandrels with similar prototype structures. The specimen needs to be prepared appropriately to understand the reliable conditions. The soft soil sample used for this study is kaolinite for model the ground in the laboratory. The Indonesian soft soil, especially Runway project in Soekarno-Hatta Airport had similarity with kaolinite due to specific properties that are characteristic of natural soil such as particle size distribution, plasticity, relatively low permeability, and the existing database of its engineering properties are available. The apparatus can be used for very fine samples (less than 75 µm), also provides in Figure 4. 4. The laboratory results of grain size distribution using laser diffraction particle size analyzer apparatus in Figure 4. 5.

In order to evaluate the mechanical behavior of Indonesia soft soil to Runway project

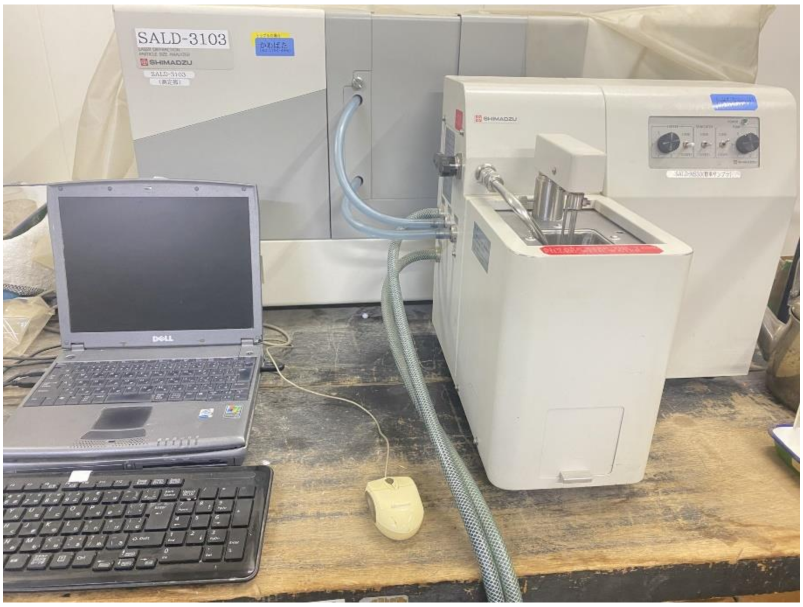

Figure 4. 4. Laser diffraction particle size analyzer apparatus.

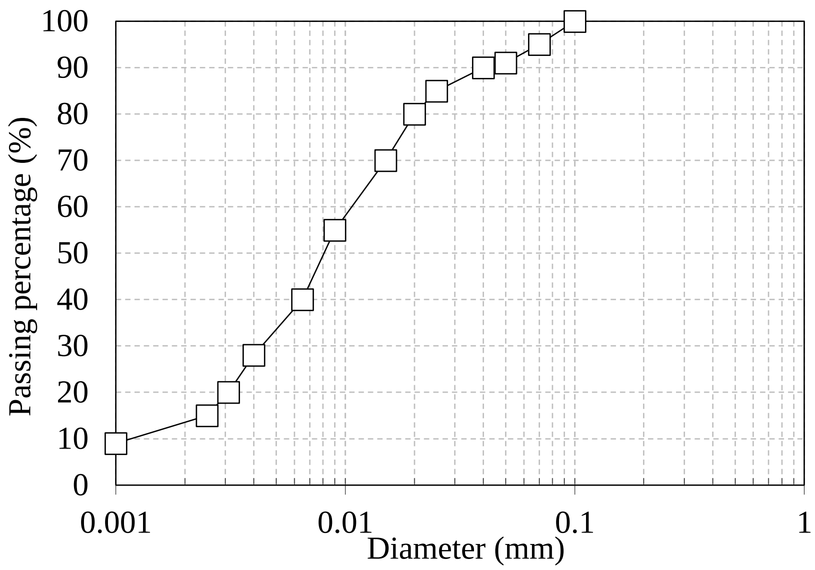

Figure 4. 5. Grain size distribution graph.

in Soekarno-Hatta Airport, based on the comparison of engineering properties, the ground can be simulated with kaolinite in laboratory. Based on the Japanese Geotechnical Society Standard, Indonesian soft soil and kaolinite are classified as a cohesive soil with a high liquid limit (C.H). The oedometer test was conducted the compressibility index and the consolidated pressure. Determination of water content are from the initial void ration and final void ratio. The formula change in void ratio is used in expressed:

$$\Delta e = \frac{V_{v_1}}{V_s} - \frac{V_{v_2}}{V_s} \tag{4. 8}$$

The formula change in water content is used in expressed:

$$\Delta w = \frac{\Delta e}{G_s} \bigg/ \frac{1}{\Delta e} \tag{4. 9}$$

$$w = w_1 + \Delta w \tag{4. 10}$$

where Δe is the change in void ratio, V_{v_1} is the change in volume of soft soil sample, V_{v_2} is the change in volume due to the compression of soft soil sample, V_s is the volume of soft soil, Δw is the change water content, G_s is the specific gravity, w is the water content, and w_1 is the initial water content before oedometer. The soil properties shown in Table 4. 2.

Table 4. 2. The soil properties

Soil properties	**Soekarno-Hatta International Airport, Jakarta**	**Kaolinite**
Grain size particle less than 0.002 mm (%)	96.54	100
Plastic limit, w_p (%)	17.1-29.86	28.8
Liquid limit, w_L (%)	33.8-69.8	48.1
Plasticity index, I_p	11.1-41.12	19.3
Specific Gravity (G_s)	2.41-2.58	2.58
Water content, w (%)	32-56	135
Soil classification	CH	CH
Soil particle density ρ_s (g/cm³)	2.65	2.69
Compression Index (Cc)	0.2-0.49	0.37
Coefficient of permeability (k) m/s	8.82×10^{-7}	7.81×10^{-6}

4.2.3 Detailed apparatus of 1g model (Macro level)

The details of consolidation test apparatus are explained as follows. The detail of experimental pictures is shown in Figure 4. 6 and the schematic apparatus in Figure 4. 7 including Table 4. 3. Sample chamber, the material is a thick glass cell of diameter 460 mm diameter and 700 mm height. Furthermore, the axial loading system, air jack-compressor system with a maximum axial loading capacity of 1000 kPa. The vacuum pump that can generate up to 100 kPa suction pressure is employed at the top of PVD. Pore water pressure (PWP) is placed at the bottom of the chamber and connected directly to the data logger. The LVDT is the settlement measurement of the axial displacement placed at the top of the acrylic plate. The water tank with a balance is a method used to measure the volume of water.

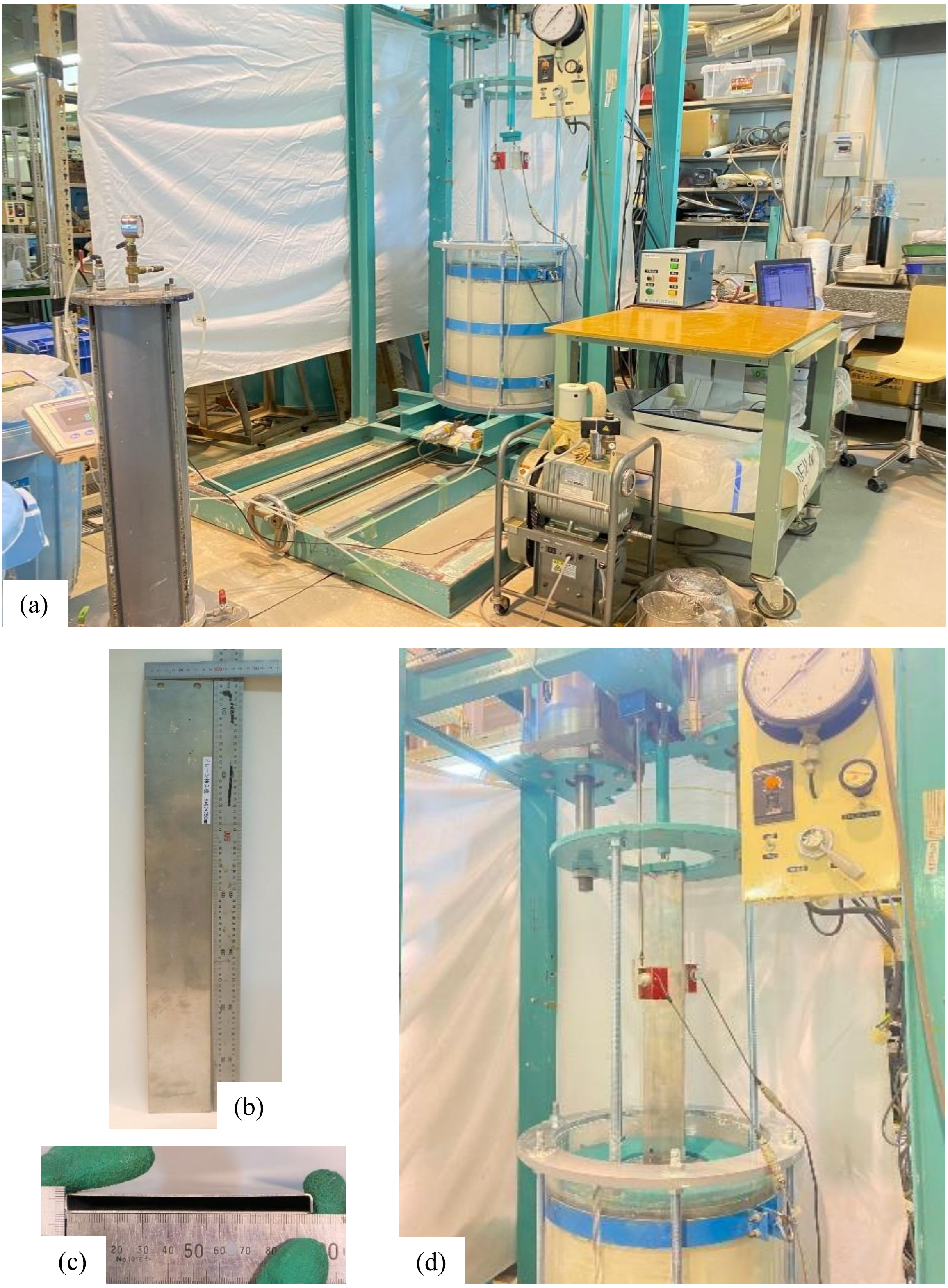

Figure 4. 6. (a) full pictures, (b) mandrel in cross section, (c) mandrel in top view (c) mandrel installation setup (not to scale).

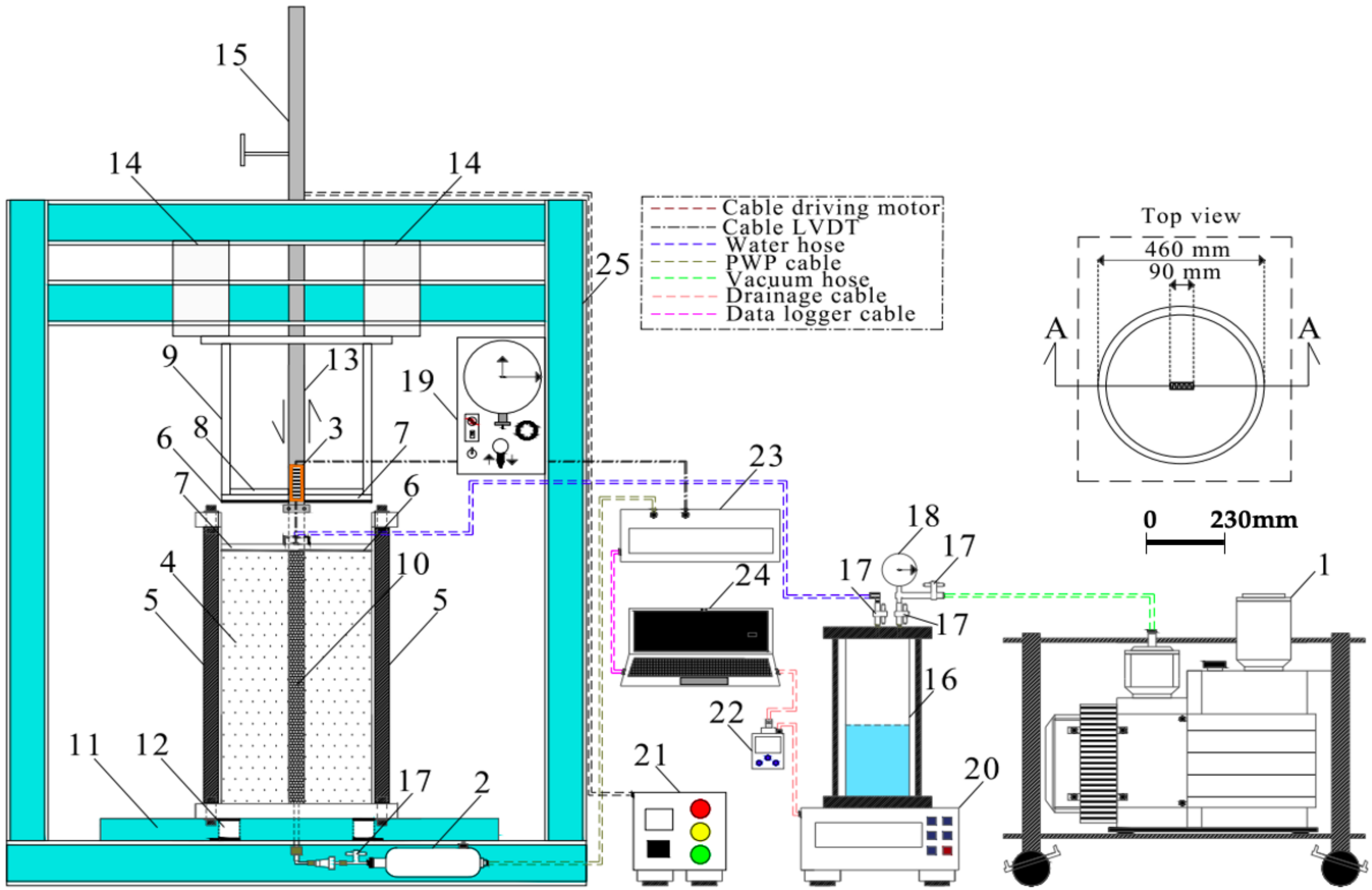

Figure 4. 7. Schematic of large-scale consolidation test setup used in the experiment.

Table 4. 3. The functions and remarks of schematic of large-scale consolidations.

No	Component	Functions and remarks
1	Vacuum pressure	The technique of applying a vacuum suction into an isolated soil mass to reduce the atmosphere pressure; measurement range: 100 kPa
2	Pore water pressure	Measuring the pore water pressure; measurement range: 200 kPa/0.0391 kPa/μ; accuracy: 0.9 kPa.
3	LVDT	Measuring displacement; accuracy: 100×10^{-6}/mm
4	Sample chamber	Contains the soil sample; diameter: 460 mm; height: 700 mm
5	Acrylic mold	The cell container is made of transparent acrylic tube
6	Sponge packing	Technique using sponge packing material for sealing to prevent air leaking
7	Acrylic plate	Hanging from the top of chamber and following volume changes during the test
8	Doughnut pressure chamber	Inner diameter: 190 mm; outer diameter: 450 mm; thickness: 12 mm
9	Hanging loading system	Steel frame, moveable up and down during the test
10	Three types of PVD	Ground improvement technique: three types of shape used in this study
11	Placemat frame chamber	Steel frame to support the chamber
12	Moveable placemat frame chamber	Horizontally moveable chamber for sample preparation
13	Mandrel actuator driving motor	Steel handle, which can move up and down during mandrel penetration
14	Loading device	Screw jack (max load: 1000 kPa)
15	Penetration supporting frame	Steel frame to support the steel handle for mandrel penetration
16	Water tank	Collecting the drained water
17	Valve	Controlling airflow and water through pipelines
18	Small pressure gauge	The instrument for controlling pressure during vacuum preloading in kPa
19	Big pressure gauge and controller	Speed controller by unit time and pressure controller loading
20	Balance	Continuously recording the amount of drained
21	Controller mandrel driver	A motor set to drive the mandrel penetrate to the sample chamber with velocity of 0.3 mm/s
22	Weighting data logger	A handheld device that collects weighting data without connecting to a PC
23	Data logger	Transmits commands to the regulator and measures data
24	Computer	Control and data acquisition
25	Frame	Steel frame system

4.2.4 Detailed apparatus of SEM (Micro Level)

The SEM equipment used for observing the microstructure of PVD and soil due to installation and vacuum preloading was the HITACHI SU3500, as shown in Figure 4. 8 and Table 4. 4. The HITACHI SU3500 is a high-resolution SEM that offers high-performance imaging and analysis capabilities. The microscope is equipped with various detectors such as in-lens SE, BSD (Back-Scattered Electron Detector), and a high-angle annular dark field (HAADF) detector that enables elemental mapping in SEM images. After consolidation testing, SEM analysis was performed to investigate the structure of soil and PVD interface side from three types of PVD conditions.

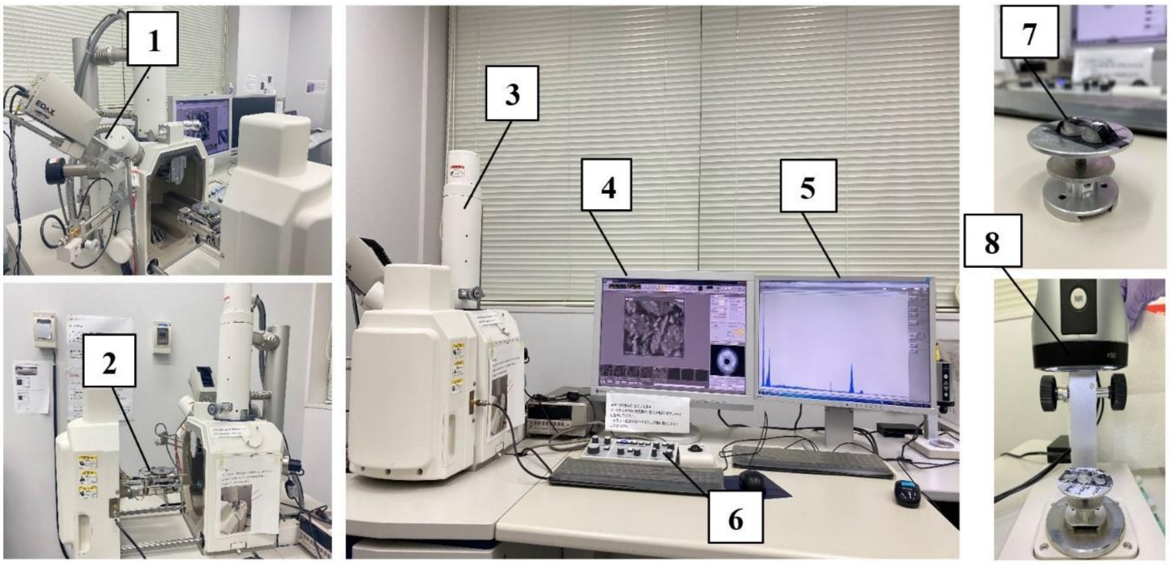

Figure 4. 8. Full pictures of Scanning Electron Microscope (SEM) SU3500.

Table 4. 4. Description of SEM apparatus.

No	Component	Functions and remarks
1	EDS, WDS and EBSD	• Used to detect and analyze the X-ray signals emitted from a sample under electron beam excitation • Used a crystal spectrometer to separate the X-ray emissions into discrete wavelengths • Used to study the crystallographic structure of materials at the microscale
2	Locations of specimen	Mounted on sample holder or stub to store sample

Table 4. 4. Description of SEM apparatus (Continue).

No	Component	Functions and remarks
3	Eucentric 5-axis Motorized stage	An important feature in modern SEM, providing exceptional control over the positioning of specimens and enabling high-quality imaging and analysis of materials
4	SEM screen	An essential component for imaging and analyzing samples in high resolution, providing real-time feedback and control over the imaging process.
5	EDX screen	An essential tool for analyzing the composition and structure of PVD and soil
6	Operation	Keyboard to direct the target location in the sample area and set the resolution manually or automatically
7	Specimens	Plate to put the samples PVD and Soil
8	Digitalupe	For capturing the samples before analysis

4.3 METHODOLOGY OF MACRO ANALYSIS

4.3.1 Soil preparation

As a preliminary step for testing on soft soil using a 1g model, it is customary to employ standard procedures. Firstly, collect the desired amount of kaolinite clay and ensure it is properly dried and sieved to remove any large particles or debris that may affect the experiment. Determine the optimal water content for the kaolinite clay by conducting a series of tests to find the Atterberg limits (i.e. the liquid limit and plastic limit) and calculate the corresponding water content at which the soil will be in its plastic state, the standard using (The Japanese Geotechnical Society, 2015). Mix the kaolinite clay with initial water content to achieve the desired water content and ensure it is thoroughly homogenized to minimize any variations in soil properties within the sample.

4.3.2 Testing procedure of 1g model

A two-step preloading test was conducted. The first step was pre-consolidation with 20 kPa using a loading system. The setup apparatus is shown in Figure 4. 9. All tests were carried out in three main stages: (1) preparation of soil samples, (2) drain installation, and (3) specimen sample collection after the process of consolidation. Firstly, a big mixer thoroughly mixed the soil sample with a water level slightly greater than the liquid limit; then, the sample was set up into the chamber. Controlling the water content and controlling saturation are common problems. Secondly, in order to optimize the method using the mandrel system, the PVD was installed with the driving motor system. After installing the mandrel with PVD into the ground, the PVD was left in place while the mandrel was slowly removed from the ground at a velocity of 0.3 mm/s. The specimen samples were collected such as water content, shear strength of the soil (ASTM D 4648-00, 2000), and permeability after the consolidation. In additions, during consolidation process the settlement and water flow are measured.

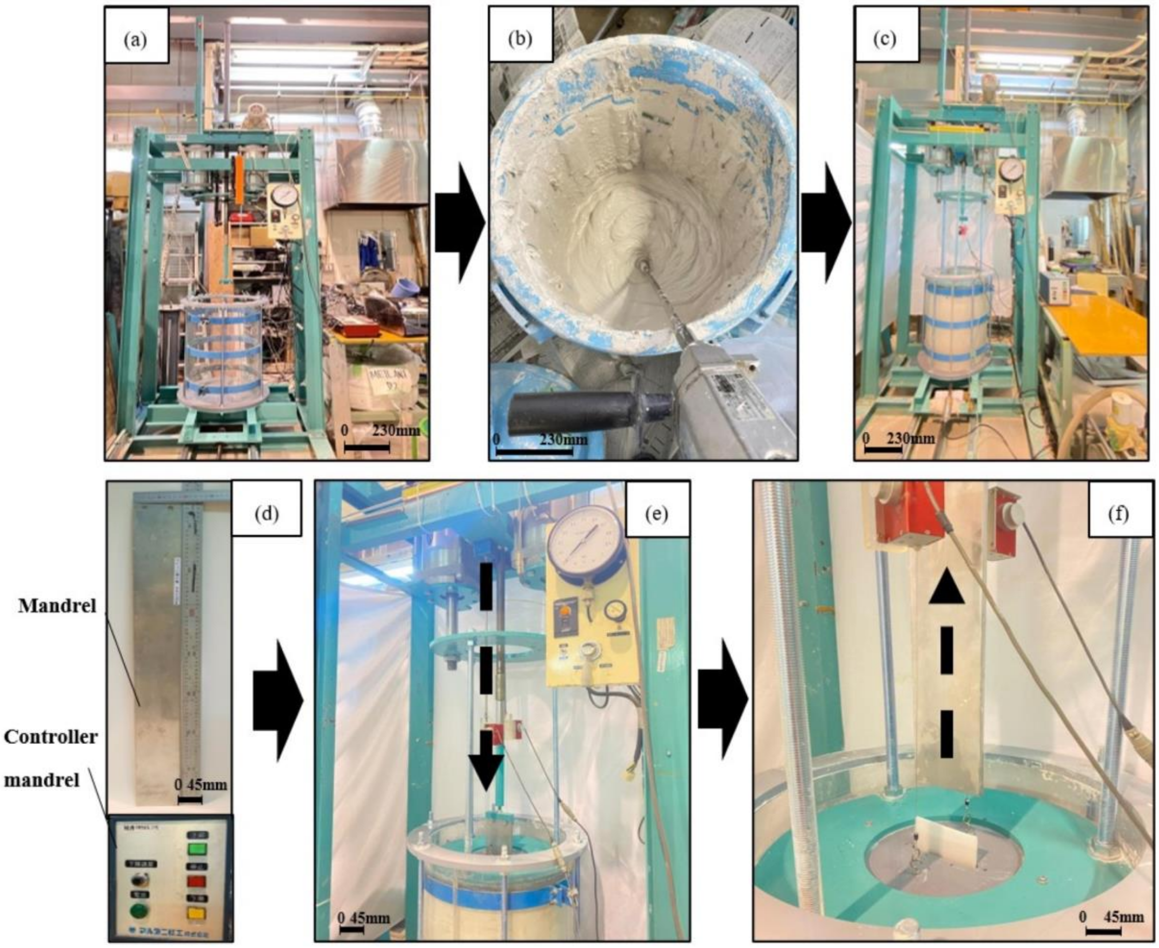

Figure 4. 9. The setup of large-scale consolidation apparatus: (a) preparation of the frame and chamber; (b) mixing of the kaolinite using a big mixer with initial water content; (c) setup of the kaolinite into the chamber; (d) preparation of the mandrel system including the controller; (e) insertion of the PVD with the mandrel with appropriate speed; (f) withdrawal of the mandrel and PVD already installed in the ground.

The conventional radial consolidation theory is a commonly used method for predicting the behavior of vertical drains in soft soil. In laboratory observations of vacuum pressure, it was found that the efficiency of the prefabricated vertical drain (PVD) depended on the magnitude and distribution of the vacuum. To quantify the loss of vacuum, a trapezoidal distribution of vacuum pressure along the length of the PVD was assumed. The detailed distribution patterns of vacuum pressure are illustrated in Figure 4. 10.

The distribution of vacuum pressure along the drain boundary varied linearly from $(-p0)$ at the top of the drain to (k_{p0}) at the bottom of the drain, where vacuum pressure was applied through the PVD. The suction head could decrease with depth and move laterally, resulting in a constant permeability smear zone (k_s) and horizontal permeability (k_h); hence, a trapezoidal vacuum pressure was assumed (Indraratna et al., 2005).

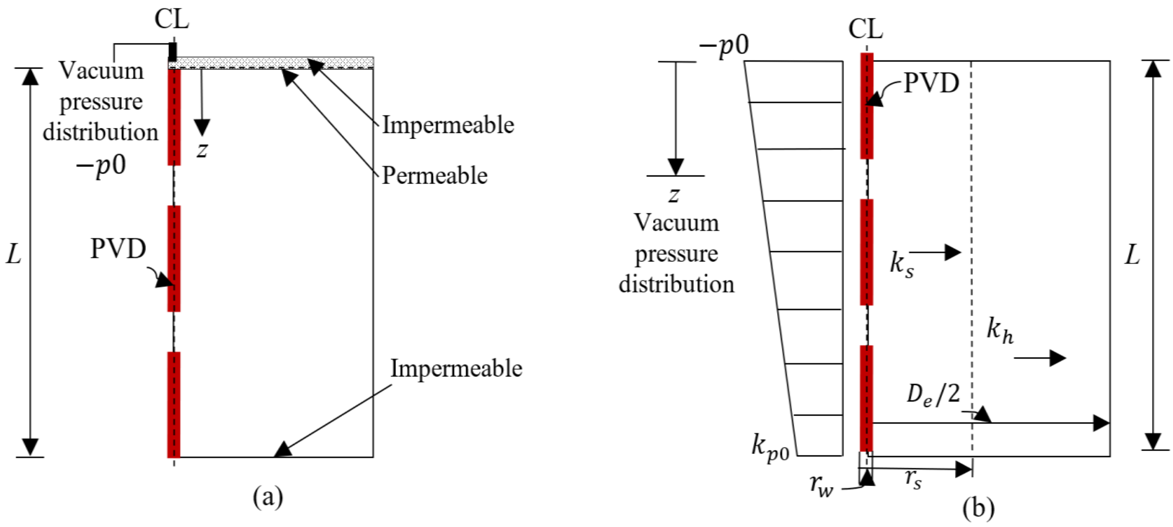

Figure 4. 10. Schematic of vacuum preloading: (a) vacuum system; (b) vacuum pressure distribution.

4.3.3 Sampling method

Figure 4. 11 (b) shows the top view of the sample area where the specimen samples were taken. The experimental test conditions and cases (including their average values and total number of samples) collected for pre-PVD installation for water content, vane shear strength, permeability, and SEM testing, are shown in section 4.3.5. Therefore, the number of samples collected before PVD installation, and the number of samples collected after PVD installation are provided. For water content, a total of 180 specimens were utilized for sections A-A and B-B undergoing consolidation. The diameter of each sample was 30 mm. The discharging capacity of the water through of the samples was measured; were taken

throughout the testing process, along with monitoring of pore water pressure and drainage.

The three-zone hypothesis established in a previous study by Adriyati et al., (2022b) was used to determine the sample locations for microstructure analysis, based on water content reduction in the top, middle, and bottom areas.

Furthermore, the permeability was measured through the use of a constant head apparatus. The SEM analysis was conducted to determine the chemical composition of the soil samples before and after PVD installation.

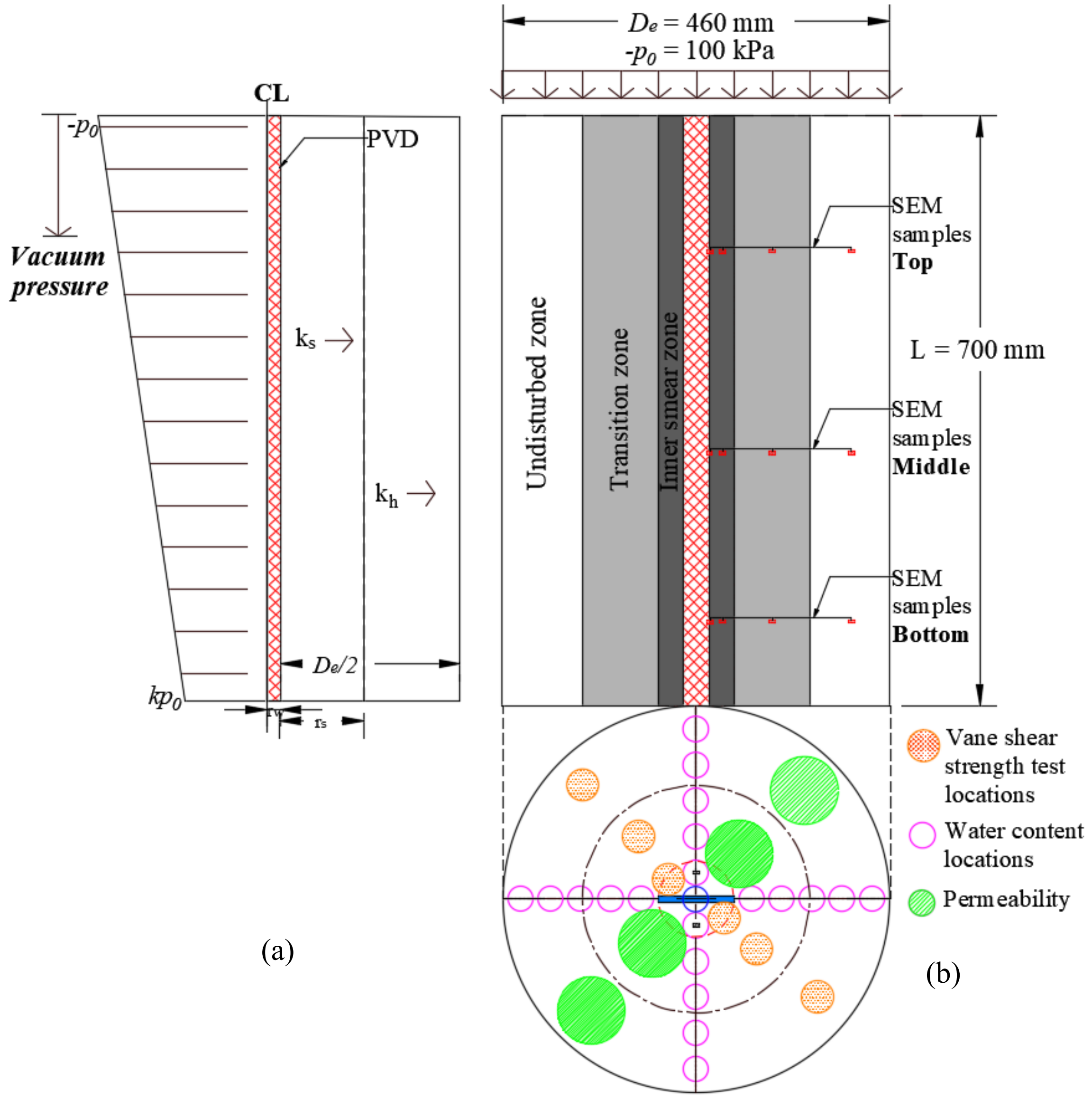

Figure 4. 11. Schematic of analysis area and measurement point: (a) vacuum pressure distribution; (b) cross section of three zone hypothesis and half illustration locations of sampling specimens in this study; (c) top view the sampling locations.

4.3.4 Permeability apparatus

The falling head test is commonly used for measuring the permeability of cohesive soils, such as clay. The test involves using a permeameter with a fixed cross-sectional area and known height and placing a sample of the soil to be tested in the permeameter. The permeameter is then filled with water and the time taken for water to flow through the soil sample is measured. The falling head test is considered a quick and straightforward method for estimating the permeability of cohesive soils.

The basic theory behind the falling head test is Darcy's law, which states that the rate of flow of fluid through a permeable medium is directly proportional to the hydraulic gradient. The apparatus is shown in Figure 4. 12, the step-by-step falling head apparatus for permeability in accordance with JGS.

Firstly, take a sample from the 1g model test by using the container specimen to keep being undisturbed. Furthermore, falling head permeability apparatus on a levelled surface ensures that the apparatus is properly grounded and secured. Place the mold in the permeability apparatus, making sure that it is levelled and center under the falling head.

Release the falling head by opening the valve at the top of the apparatus, and allow it to fall through the tube, perforating the soil sample. When the free fall of the head stops due to a constant water level, start the stopwatch to measure the time taken for water to pass through the soil sample. Measure the water passage time up to 60 seconds or until a volume of water has passed through the specimen. Repeat the step for three more trials, and obtain the average time taken for water to pass through the soil sample. Lastly, calculate the permeability coefficient using the formula:

$$k = \frac{a \times L}{A \times t} \ln\left(\frac{h_0}{h_1}\right) \tag{4. 11}$$

where a is $(\frac{\pi \times d^2}{4})$ inside cross-sectional area of the water tank, A is $(\frac{\pi \times D^2}{4})$ inside cross-sectional area of the sample, L is the length of the sample, t is the time taken for the water to pass through the sample, h_0 is distance to bottom of the beaker before the test, and h_1 is distance to bottom of the beaker after the test.

The permeability coefficient is then compared with the standard values to determine the permeability of the soil.

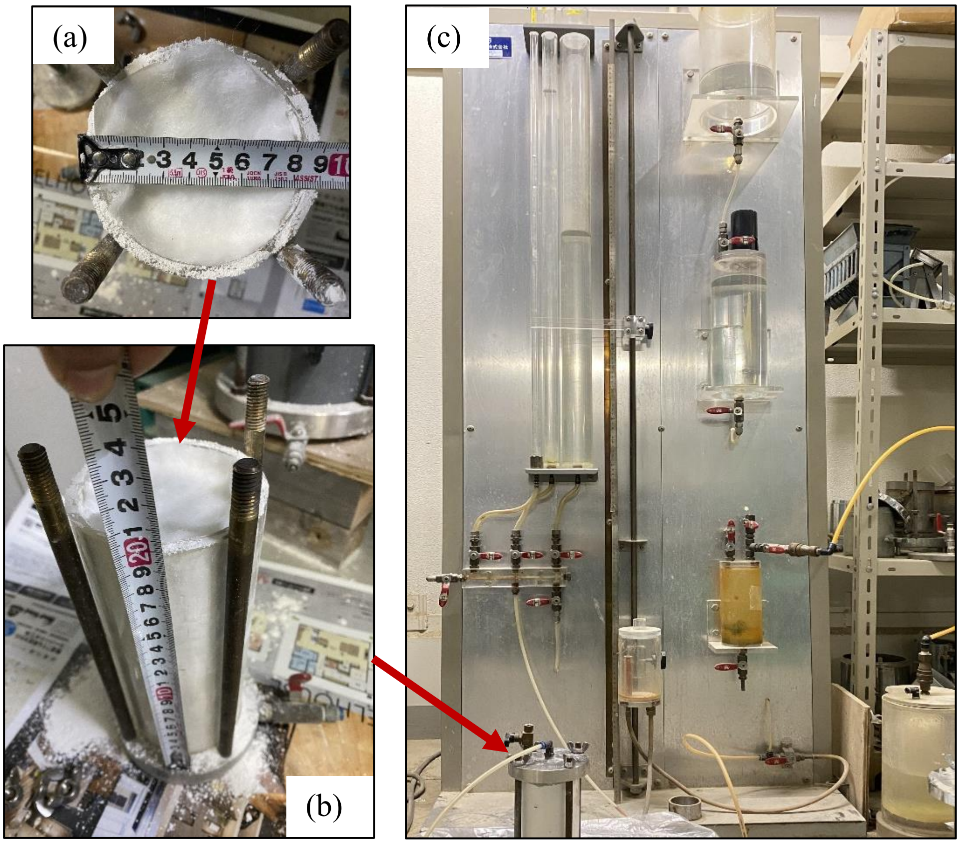

Figure 4. 12. The permeability test apparatus: (a) top view of container specimen; (b) side view of container specimen; (c) top view the sampling locations.

4.3.5 Vane shear apparatus

The vane shear equipment was used to measure the undrained shear strength before and after consolidation tests based on ASTM 4648. The vane shear blade was made of stainless steel; it was 20 mm in diameter and 40 mm in height. The adjustable stainless-steel rod diameter was 5 mm, capable of measuring the shear strengths at different locations; its height was 500 mm from the top of the chamber, 300 mm from the middle, and 100 mm from the bottom area. In the radial distance based on the three-zone hypothesis, the inner smear zone was 9.25 mm, transition zone was 46.25 mm, and undisturbed zone was 145.5 mm.

The test procedure of the vane shear test is described as follows: firstly, the apparatus was cleaned, and grease was applied to the lead screw for smoother handle movement. Subsequently, the soil surface was leveled, and the container was mounted on the base of the vane shear test apparatus using the provided screws. Gradually, the vane was lowered into the soil specimen until it was 10 to 20 mm below the surface, and the initial reading of the pointer was recorded on the circular graduated scale. The vane was rotated inside the soil specimen using the torque-applying handle at a rate of 0.1° per second. When the specimen fails, the strain indicator pointer moves backward on the circular graduated scale. At this point, the test must be stopped, and the final reading of pointer is noted. Lastly, the procedure must be repeated at different specified points.

The details of the vane shear testing apparatus are shown in Figure 4. 13, and the shear strength could be obtained by calculation using Equations are describe as:

$$T = \frac{Spring\ constant}{180} + (Initial\ reading - final\ reading) \tag{4. 12}$$

$$S = \frac{\mathrm{T}}{\pi\left(\frac{D^2H}{2} + \frac{D^3}{6}\right)} \tag{4. 13}$$

where T is torque, S is shear strength of soil, D is the diameter of vane (mm), and H is the height of vane (mm).

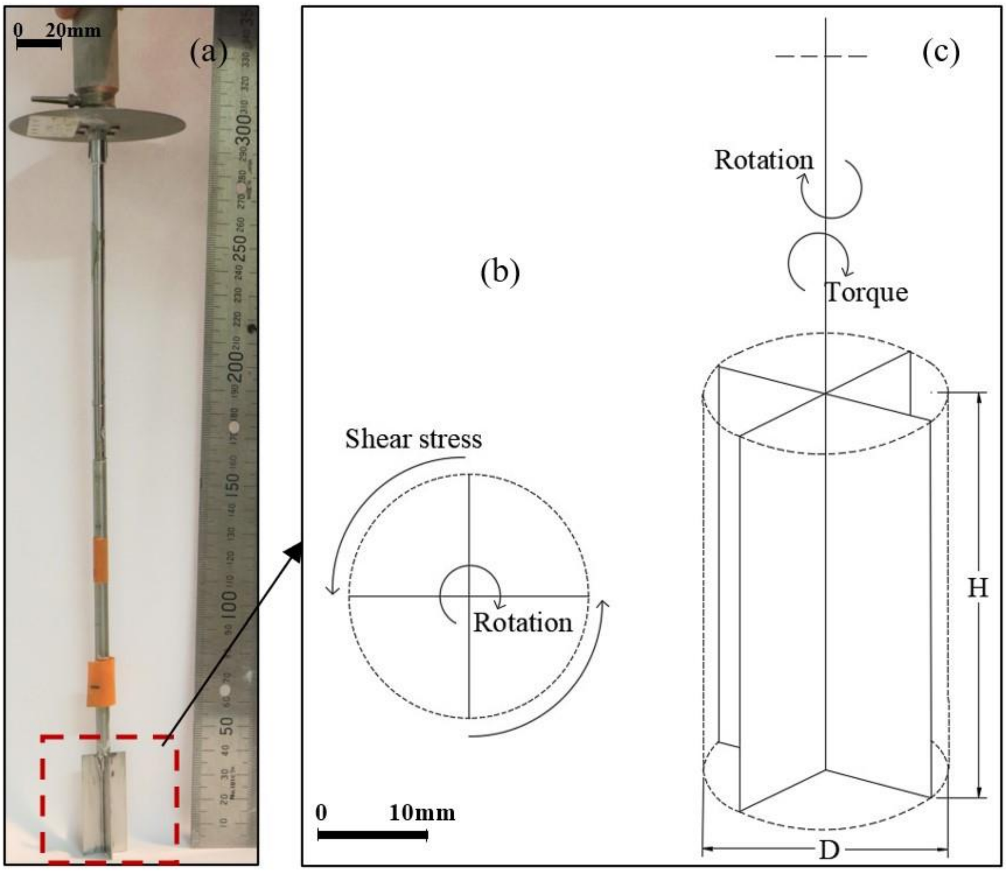

Figure 4. 13. The schematic of vane shear apparatus: (a) real pictures of vane shear apparatus; (b) bottom view of vane shear apparatus; (c) vane shear blade cross.

4.4 METHODOLOGY OF MICRO ANALYSIS

4.4.1 Sample preparation of SEM

The samples, including those with initial water content and degraded drain samples, were subjected to analysis using a SEM. In additions, to determine potential variation in elemental decomposition and structural changes caused by installation and vacuum preloading, samples were analyzed using a SEM. The samples, including those with initial water content and degraded drain samples, were subjected to analysis using a SEM to determine potential variation in the elemental decomposition and structure due to installation and vacuum preloading.

SEM is a useful tool for identifying changes in the elemental composition and structure caused by clogging in certain applications, as it can provide high-resolution images of the surface of a material. Such changes or their effects may include deposit formation or degradation of PVD material. Examining the microstructure of clogged material using SEM can help researchers gain insight into the mechanisms behind clogging, and potentially develop strategies to prevent or mitigate its occurrence. However, it should be noted that specific methodologies for analyzing clogging can vary depending on the material and application, and SEM is just one tool in this analysis area.

4.4.2 Test procedure of SEM analyses

The three-case microstructure analysis (initial conditions, PVD and soil interactions, and soil structure). The first step was to cut the PVD filter to size 10 mm × 10 mm before and after the consolidations at specified positions. Soil samples before and after the test were also prepared in the three-zone area with different depths. The second step involved a PVD filter brought to the Central of Advanced Instrumental Analysis (CAIA) laboratory to conduct SEM tests.

After these two steps, the specimens were ready for testing. Subsequently, the samples were added to a plate with a diameter of 5 cm to capture pictures for observation. Furthermore, the main step was to put the samples into the SEM machine and start with a low-vacuum setting. The last step was to analyze structure of the PVD and soil from the screen (units = μm), captured with ×300, ×500, and ×3000 magnification and a voltage of 15 kV. The most appropriate image for interpreting the overall morphological characteristics of the PVD, soil and pore microstructure, and their respective ratios was selected on the basis of the magnification results.

In this study, ImageJ was utilized for image processing, as shown in Figure 4. 14 and the microstructure was characterized using quantitative analysis. The objective of image processing was to extract information from the image and the output data of pores and particles. Observations of pore diameters are a basic feature in ImageJ. The percentage of the measured area of the pore to the total area of the image can be expressed:

$$n\,(\%) = \frac{n_0}{n_{total\ area}} \times 100 \tag{4. 14}$$

$$n'(\%) = \frac{n'_0}{n_{total\ area}} \times 100 \tag{4. 15}$$

where n is the total area of soil pores as a percentage, n_0 is the total area of soil pores, n' is total area of PVD and pores as a percentage, n'_0 is the total area of PVD and pores, and $n_{total\ area}$ is the total area of SEM image.

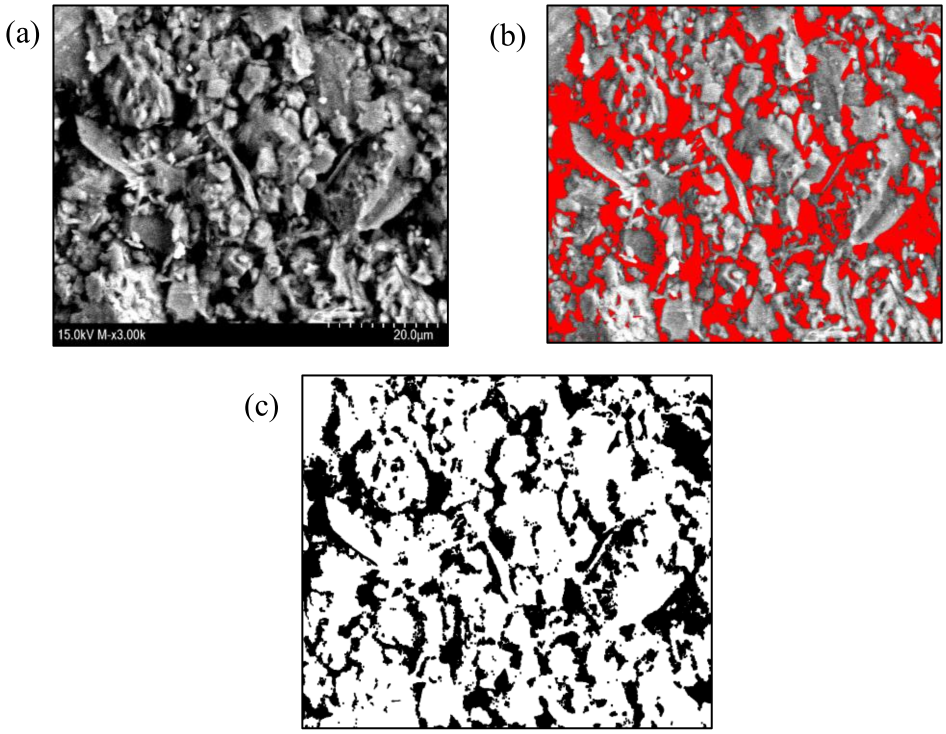

Figure 4. 14. Image analysis processing: (a) SEM image; (b) interpretation the pores and particle using clip studio plot; (c) ImageJ processing the analyze.

4.5 EXPERIMENTAL TEST CONDITIONS AND CASES

An experimental study was performed using rectangular mandrel and three types of PVD. The laboratory test outline is shown in Figure 4. 15, consisting of three aspects: the 1g model test, the soil properties, and microstructure analysis. The detailed test cases and the associated test conditions are presented in Table 4. 5 and Table 4. 6.

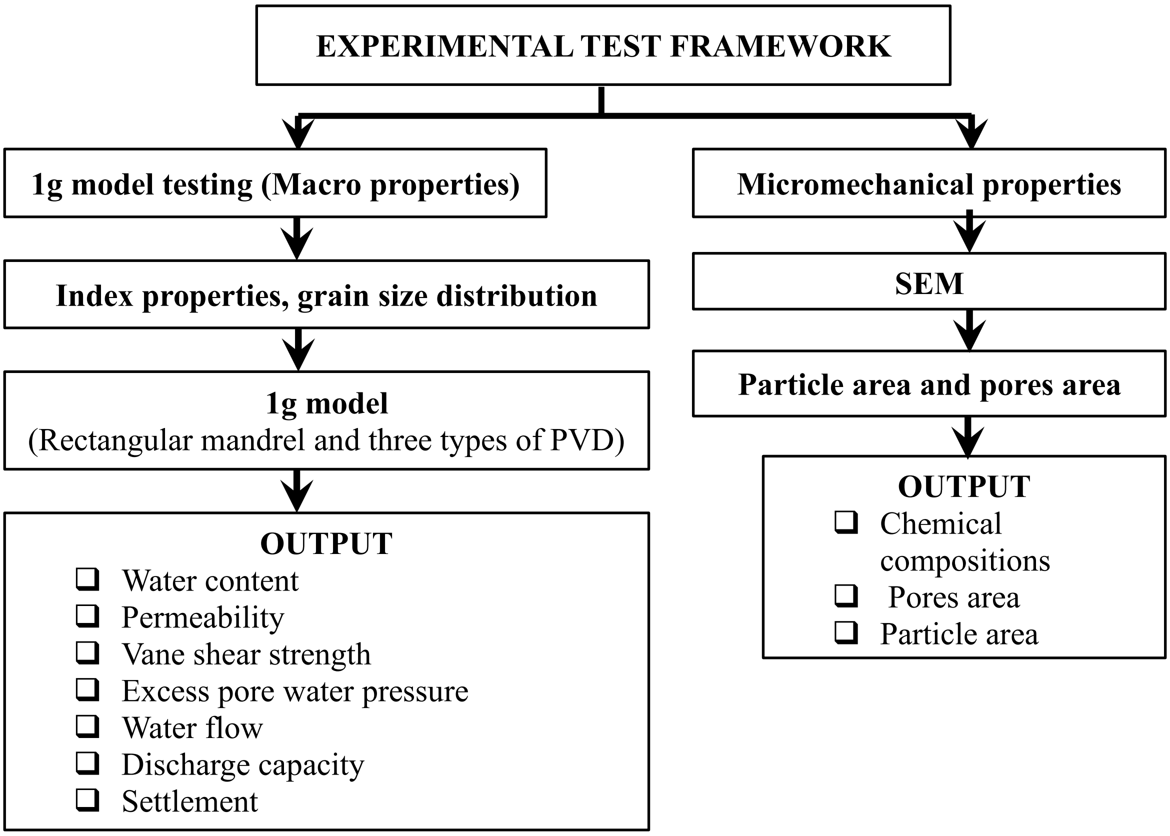

Figure 4. 15. Experimental framework outline.

Table 4. 5. The number of samples collected before PVD installation.

Testing	Information	Number of samples	Average value of samples
Water content, w		3	1
Vane shear strength, s_u	Before testing	3	1
Permeability, k		3	1
Scanning electron microscopy (SEM)	PVD structure	3	1
	Soil Structure	3	1

Table 4. 6. The number of samples collected after PVD installation.

Testing	Locations		Number of Samples			Average Value of Samples each PVD
			Type A	Type B	Type C	
Water content, w	A-A and B-B	Inner smear zone	36	36	36	3
		Transition zone	72	72	72	3
		Undisturbed zone	72	72	72	9

Table 4. 6. The number of samples collected after PVD installation (Continue).

Testing	Locations		Number of Samples Type A	Type B	Type C	Average Value of Samples each PVD
Excess pore water pressure	In the bottom of chamber (1 point)		3	3	3	3
The water flow rate (Q)			3	3	3	3
Vane shear strength, s_u	Oblique	Inner smear zone	6	6	6	3
		Transition zone	6	6	6	3
		Undisturbed zone	6	6	6	3
Permeability, k		Inner smear zone and Transition zone	4	4	4	2
		Undisturbed zone	4	4	4	2
Settlement	In the top of chamber (2 point)		2	2	2	1
Scanning electron microscopy (SEM)	PVD and soil	PVD	3	3	3	3
	Soil structure	Inner smear zone	3	3	3	3
		Transition zone	3	3	3	3
		Undisturbed zone	3	3	3	3

4.6 SUMMARY

This chapter focuses on describes the development of a large-scale consolidation (1g model) through laboratory testing and introduces the experimental setup and testing methodology of Scanning Electron Microscopy (SEM).

The experimental laboratory testing conducted in this research included: material of PVD including scaling law for 1g model was explained based on prototype to model test, soil properties, detailed apparatus of 1g model and SEM are explained including the functions and remarks. Additionally, the research also involved designing a rectangular mandrel driven PVD, three types of PVD, detailed distribution patterns of vacuum pressure determinations, and experimental test conditions. For Microstructure analysis the sample preparation of SEM and test procedure of SEM including ImageJ analysis method are shown in this chapter.

The testing procedures were explained, including physical characteristic tests, such as particle size distributions, plastic limit (w_p), liquid limit (w_L), plastic index (I_p), specific gravity (G_s), water content (w) before the improvement, permeability (k) before the improvement, shear strength (s_u) of soil before the improvement, and image process involves the ImageJ software to analyze the structure analysis before and after the testing (*n*) and (*n'*), which were conducted to obtain soil improvement data. Overall, this research provides important insights into the development of a large-scale consolidation model and microstructure analysis of physical characteristics of soil.

4.7 REFERENCES

Adriyati, M., Yasufuku, N., Ishikura, R., & Rifa, A. (2022b). Optimizing modified large-scale consolidation testing for describing smear zone caused by mandrel- driven prefabricated vertical drain. *2022 GeoAsia7 Conference & IGS First Young Engineers Conference (GeoAsia7)*, 5–8.

ASTM D 4648-00. (2000). *D 4648 – 00 ; Vane Shear Test for Saturated Fine - Grained Clayey Soil*.

ASTM D 6917-03 (2003). *D 6917-03; Standard Guide for Selection of Test Methods for Prefabricated Vertical Drains.*

Hansbo, S. (1979). Consolidation of clay by band-shaped prefabricated vertical drains. Ground Engineering, 12, pp. 16-25.

Indraratna, B., Rujikiatkamjorn, C., & Sathananthan, L. (2005). Radial consolidation of clay using compressibility indices and varying horizontal permeability. *Canadian Geotechnical Journal*, *42*(5), 1330–1341. https://doi.org/10.1139/t05-052

Long, R. P. ., & Covo, A. (1994). Equivalent diameter of vertical drains with an Oblong cross section. *Journal of Geotechnical Engineering*, *120*(9), 296–300. https://doi.org/https://doi.org/10.1061/(ASCE)0733-9410(1994)120:9(1625)

Pradhan, T. B. S., Imai, G., Murata, T., Kamon, M., Suwa, S. (1993). Experiment study on the equivalent diameter of a prefabricated band-shaped drain. *Proceeding 11th Southeast Asian Geotech. Conf.* 391-396.

Rixner, J. J., Kraemer, S. R., Smith, A. D. (1986). Prefabricated vertical drain. Vol. I, Engineering guidelines, FWHA/RD-86/168. Federal Highway Administration, Washinton, D. C.

The Japanese Geotechnical Society. (2015). Japanese Geotechnical Society Standards: Laboratory tesing standards of geomaterials, Vol.1. In *The Japanese Geotechnical Society* (Vol. 1, Issue July 2017).

The Japanese Geotechnical Society Standard, JGS 0131 Test method for particle size distribution of soil (JIS A1204).

Wood, D., M., Crewe, A., Taylor, C. (2002). Shaking table testing of geotechnical models. *International Journal of Physical Modelling in Geotechnics*, *1*, 01–13. https://doi.org/https://doi.org/10.1680/ijpmg.2002.020101

This Page Intentionally Left Blank

CHAPTER
V
EVALUATION OF PVD PERFORMANCE DUE TO SMEAR ZONE

5.1 INTRODUCTION

In this chapter evaluates the installation of PVD facilitates by pushing a mandrel into the soft soil layer, causing significant disturbance surrounding the drain, which is called a smear zone (Chung & Lee, 2010; Ghandeharioon et al., 2010; Indraratna & Redana, 1998). The soil surrounding the vertical drain disturbs the radial direction and reduces the consolidation rate. The unit cell condition to know how much the presence of a smear zone can significantly influence consolidation rate, and classical solution methods have been first proposed by (Hansbo, 1981). Therefore, modified optimizing apparatus large-scale consolidation testing beyond the scope of small conventional consolidation equipment to determine the methodology of the accuracy of the vertical drain during the consolidation process is an essential requirement.

This study aims to distinguish the basis of the terminology three-zone theory of large-scale consolidation technique by optimizing one designed rectangular iron mandrel due to PVD installation.

5.2 THREE-ZONE HYPOTHESIS

The three-zone hypothesis are shown Figure 5. 1, that introduced in this study to investigate the smear zone influence is determined in the smear zones are dependent on the size and shape of the mandrel (Sharma & Xiao, 2000). The inner smear zone, the transition zone, and the undisturbed zone is disturbed soil conditions (Madhave, et al., 1993). The values on the inner smear zone are essential to describe the effect of the smear zone due to PVD installation using a mandrel and during the consolidation process, which is determined:

$$s = \frac{r_s}{r_w} \quad (5.\ 1)$$

where r_s is the radius of the transition zone and r_w is the drain radius of the smear zone influence on PVD with mandrel.

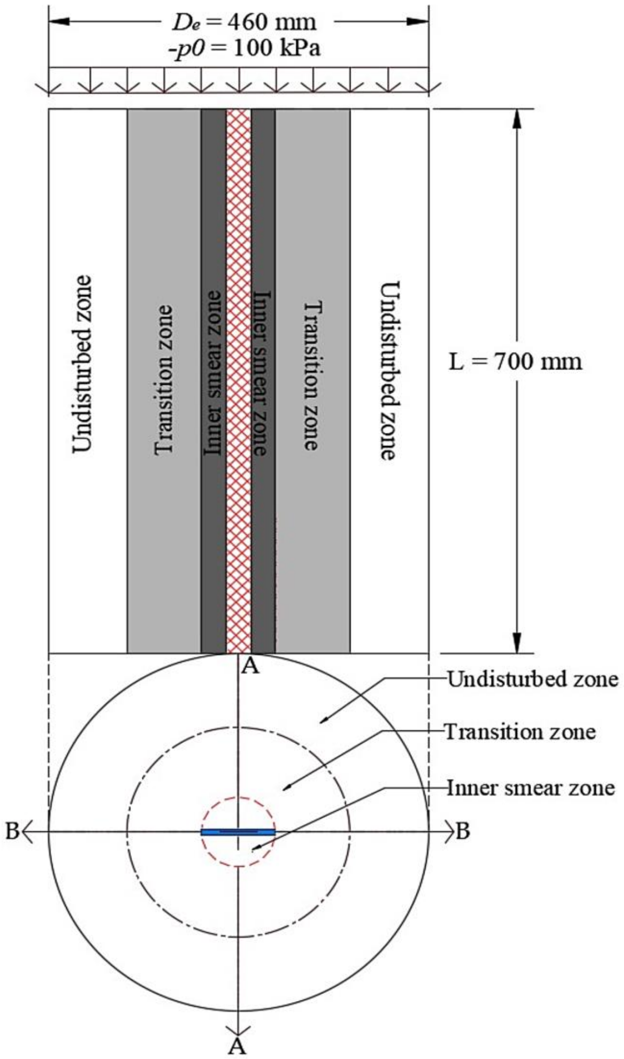

Figure 5. 1. The three zone.

Samples were collected from sections A-A and B-B following preloading and subsequently subjected to analysis. The monitoring procedures included measurement of pore water pressure and drainage. Further testing involved vane shear and permeability measurements, using samples with a diameter of 30 mm for water content measurement.

5.3 INFLUENCE OF PVD PERFORMANCE

5.3.1 Water content reduction effect of preloading

The normalized water content reduction measured along the short and long axes was evaluated, all average measurements are confined within a narrow band demarcating the smear zone from the relatively undisturbed outer zone.

This study examines the extent of the smear zone from the water content reduction after 24 hours from the initial water content of 135%. For this purpose, samples were collected vertically and horizontally from the chamber apparatus depth. The results from three types of PVD are shown in Figure 5. 2.

As a result, the variation of the water content in Type A shows that the water content at the 18.5 mm and 55.5 mm radial distance has decreased vertically and horizontally of 21% to 37% from all radial distance measurements. There is indicated in the radial distance the PVD is working to increase water content.

For Type B, a more uniform pattern is observed than Type A, with decreasing water content of 25% to 36% from all radial distances at 18.5 mm and 55.5 mm. On the other hand, the water content in Type C decreased from 30% to 47% in radial distances of 18.5 mm and 55.5 mm. The difference in Type C is that the water content significantly decreased around the middle of the chamber at 300 mm, with the lowest water content at 45% at the radial distance of 55 mm, resulting in a local buckling.

However, the uniformity of the result shows that Type B is the less disturbed PVD among all three. The indicated less smear zone occurs during the Type B installation. Another factor when the compressive load generates and sudden deflection changes the PVD structure, the buckling and migrating soil particles are small. Therefore, the differences in PVD shape influence the soil disturbance during installation with the mandrel, which affects the decreasing water content pattern. For PVD that works optimally, the water content decreases in the area smear and transition zone or near the PVD compared with the undisturbed zone. However, the water content is not significantly changing at a given depth in all radial locations as expected, implying reduced performance of PVD. The average and normalized water content in the radial distance is also analyzed and shown Figure 5. 3.

The average water content in the area close to the PVD is increased, proven when the normalized water content is also changing. The indication of reduced water content in (r_s) is 55.5 mm radial distance near PVD clarifies that inner smear zone (s) is 18.55 mm occurs due to ununiform water content in the radial distance. The results are linear with the analysis of the PVD depth. To understand the values in the transition area of extended smear zone in radius by effect rectangular mandrel and testing the equation 5. 1 is used, and the result is 18.5 mm in the radial distance. The apparent smear zone effect from the installation and the loading is insufficient to prove whether it can make an apparent effect in accelerating consolidation. However, analyzed the water content after the consolidation process proves that the effect on PVD performance differs from each measured height and radial distance.

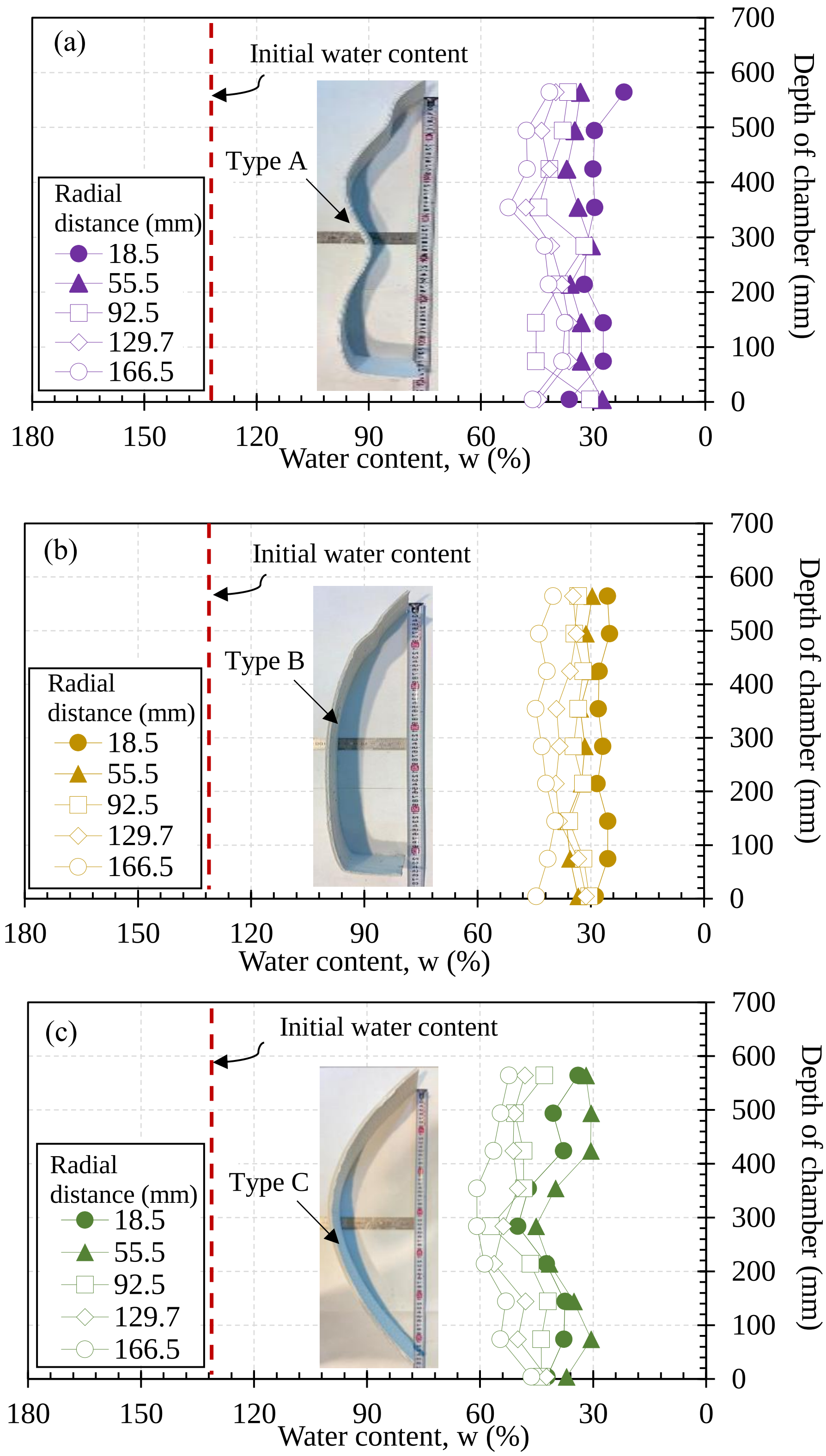

Figure 5. 2. The water content according to the depth of chamber due to vacuum preloading; (a) PVD type A, (b) PVD type B, (a) PVD type C.

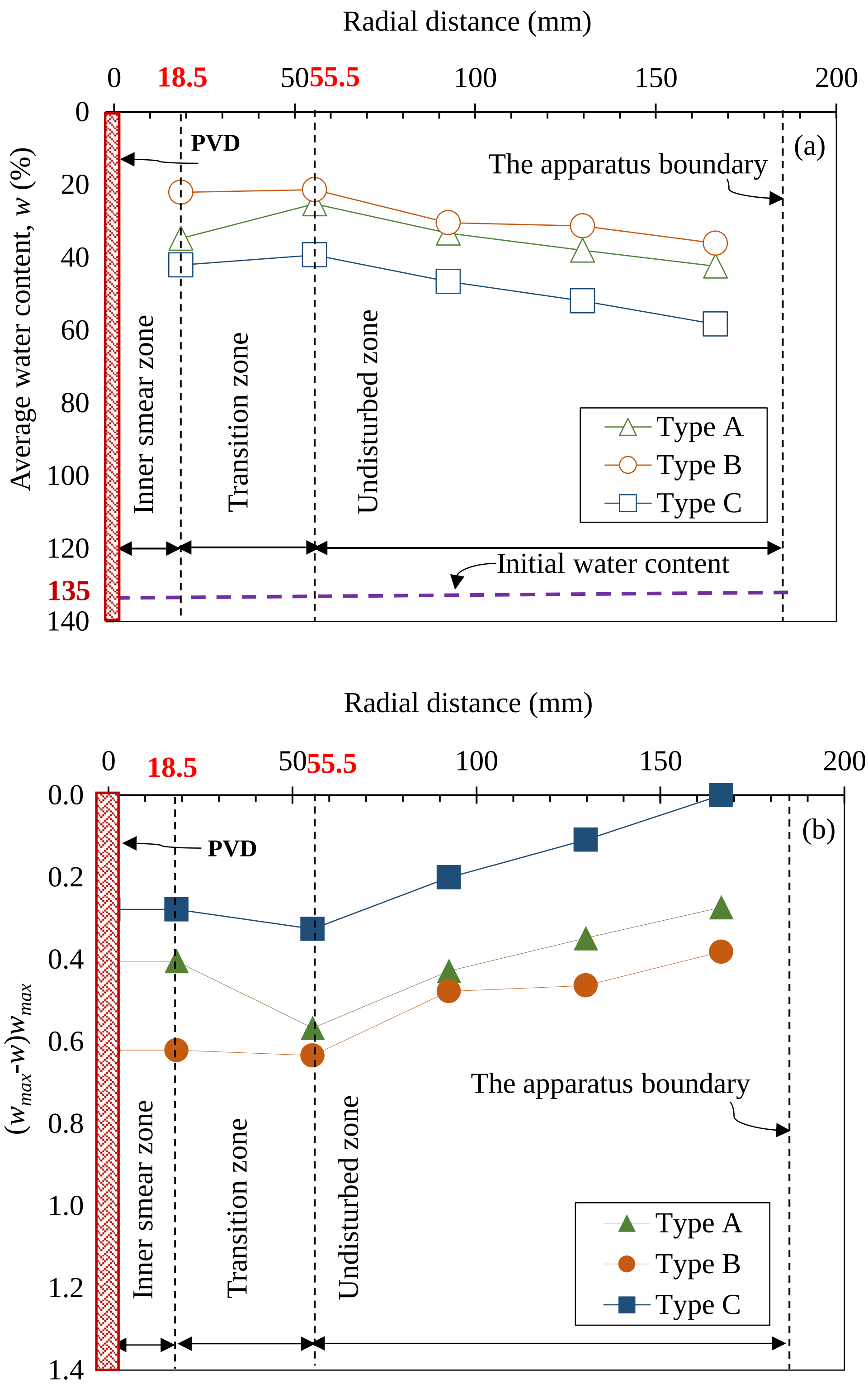

Figure 5. 3. (a) The average water content in radial distance due to vacuum preloading; (b) the normalized water content from the effect of PVD installation.

5.3.2 Shear strength of the soil

The vane shear equipment was used to measure the undrained shear strength before and after consolidation tests based on ASTM D 4648-00. The PVD combined with vacuum preloading improve the shear strength of soft soil (Mesri & Khan, 2011). The increased shear strength of soft clay deposits is subjected to a constant increase in effective vertical stress with depth, resulting from vacuum preloading in the filed measurements (J. Chai et al., 2006, 2007).

In this study, the shear strength was measured in a specified area before and after vacuum preloading in inner smear zone, transition zone, and undisturbed zone in radial distance. The vane shear blade was made of stainless steel; it was 20 mm in diameter and 40 mm in height. The adjustable stainless-steel rod diameter was 5 mm, capable of measuring the shear strengths at different locations; its height was 500 mm from the top of the chamber, 300 mm from the middle, and 100 mm from the bottom area. In the radial distance based on the three-zone hypothesis, the inner smear zone was 9.25 mm, transition zone was 46.25 mm, and undisturbed zone was 145.5 mm. The shear strength can be obtained, which is determined:

$$T = \frac{Spring\ constant}{180} + (Initial\ reading - final\ reading) \tag{5.2}$$

$$S = \frac{\mathrm{T}}{\pi\left(\frac{D^2H}{2} + \frac{D^3}{6}\right)} \tag{5.3}$$

where T is the torque, S is the shear strength of soil, D is the diameter of the vane (mm), and H is the height of the vane (mm).

The initial condition of the soft ground was measured using the vane shear test, and the results indicated a shear strength of 2 kPa. Furthermore, after consolidation, an increase in shear strength in the area close to the PVD was determined for the three types of PVD. It can be seen from Figure 5. 4 that the shear strength was affected by radial distance at each location and depth. After vacuum preloading, the variation in shear strength for the three types of PVD increased from 2 kPa to 14 kPa at different depths and radial distances. PVD type B led to an increase in shear strength from 10 kPa to 14 kPa in the smear zone at all depths compared with type A, where shear strength increased from 6.8 kPa to 14 kPa, and

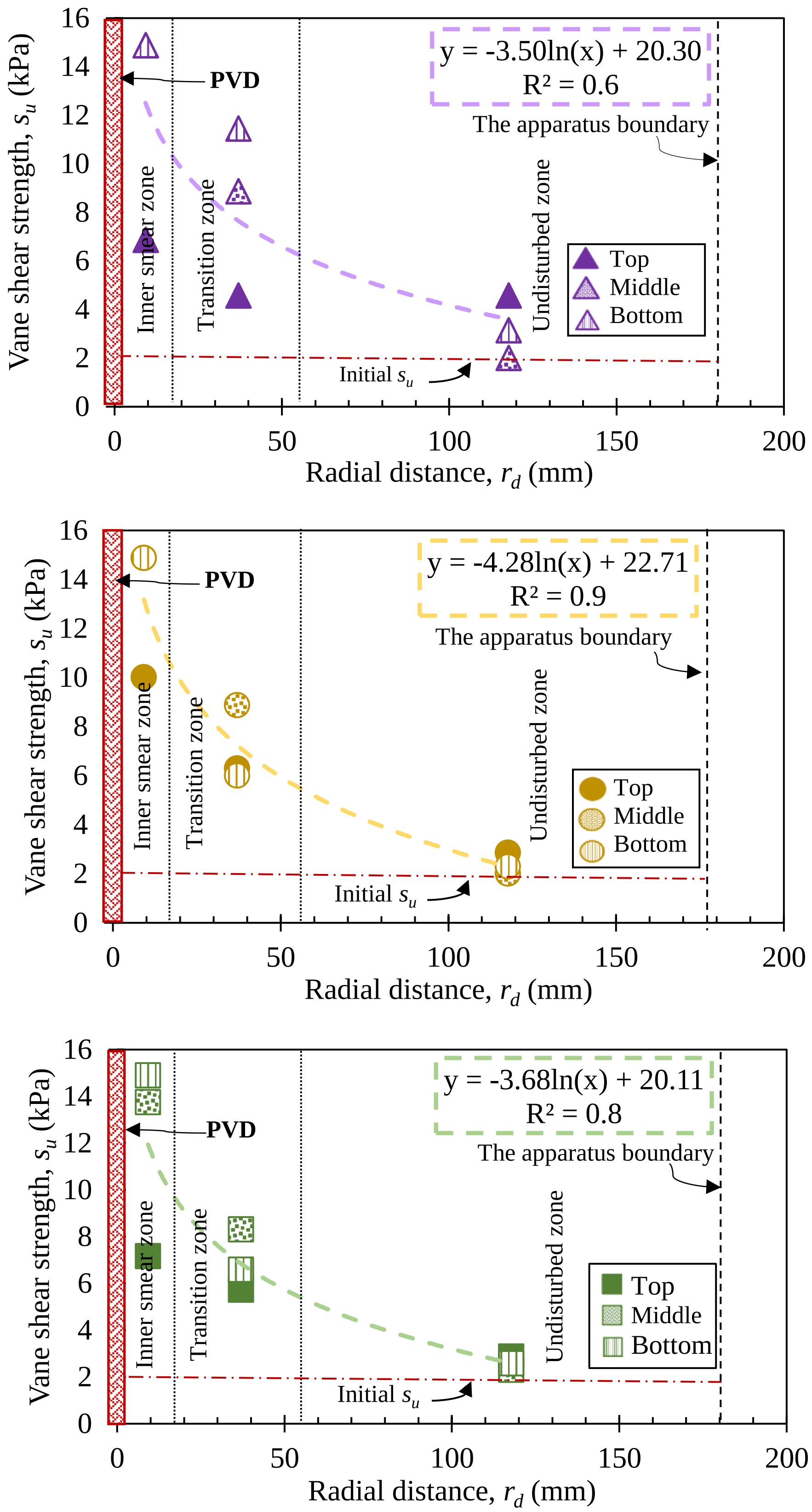

Figure 5. 4. The variation of shear strength of soil in radial distance: (a) PVD type A; (b) PVD type B; (c) PVD type C.

type C, where shear strength increased from 7 kPa to 14 kPa.

The soil shear strength decreased with increasing radial distance from the PVD, whereas it was highest in the soil close to the PVD, in line with the water content distribution properties. Furthermore, the study found that the PVD worked more effectively in the inner smear zone and transition zone than in the undisturbed zone with decreasing radial distance. The following general relationship was determined for the three types of PVD:

$$s_{u.cal} = \beta \ln r_{d0} + s_{u0} \tag{5. 4}$$

where β is the slope of the shear strength of soil, r_{d0} is the radial distance of the actual distance, and s_{u0} is the initial shear strength. The soil strength decreased significantly after being disturbed, which indicated that the structure of the soft soil was improved considerably by the reagent after vacuum preloading. The trend observed for the vane shear strength was comparable with the reduction in water content, indicating better consolidation in the inner smear zone and transition zone compared to the undisturbed zone.

The relationship between vane shear strength and depth is influenced by various factors. Studies have shown in Figure 5. 5 that the vane shear strength generally increases with depth in the inner smear zone, which is the disturbed zone closest to the PVD. Specially, type PVD A has been found to increase the vane shear strength near the PVD. Conversely, the vane shear strength may decrease in the undisturbed zone, which is further from the PVD. Considering these factors when investigating the relationship between vane shear strength and depth is important. Furthermore, it should be noted that vane shear strength testing is typically used for measuring the shear strength of clay soils and may not be appropriate for measuring other types of soil.

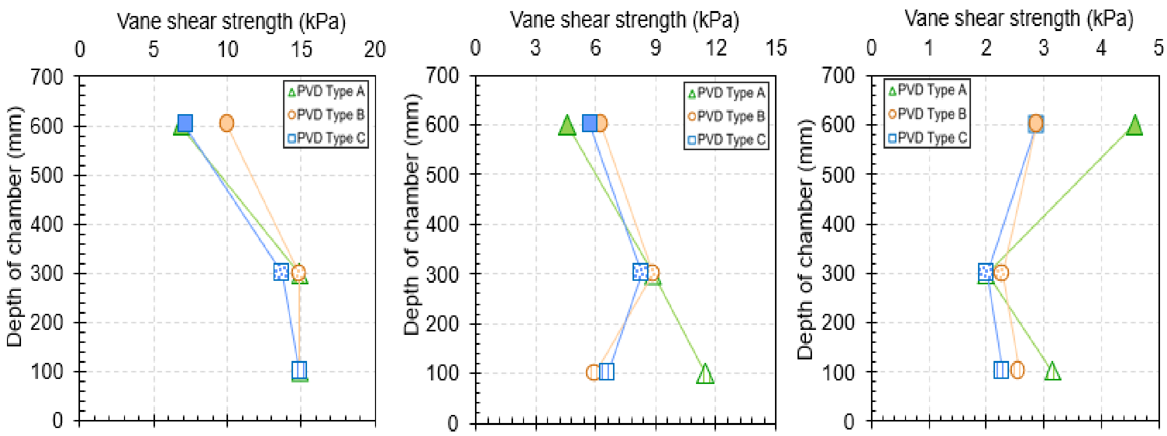

Figure 5. 5. The variation of shear strength of soil in depth: (a) inner smear zone; (b) transition zone; (c) undisturbed zone.

5.3.3 Permeability of the soil due to preloading

Soil permeability is a critical factor affecting the effectiveness of preloading in consolidating the soil. Soil permeability is an essential parameter in determining the effectiveness of preloading as a method of soil consolidation. One of the key factors that influence the permeability of soil during preloading is the installation of PVD. These drains reduce pore water pressure within the soil, enabling the consolidation process to occur more quickly and efficiently. Studies have shown that the increase in soil permeability during preloading is related to the distance from the PVD. The radial distance from the PVD affects the rate of water flow within the soil and influences the consolidation process. As the distance from the PVD increases further from the drain, the increase in soil permeability becomes less significant. However, it is important to note that the effectiveness of PVD in reducing pore pressure is not solely dependent on the radial distance from the drains but is also influenced by parameters such as the spacing, diameter, and depth of the PVD. The results in this study are shown in Figure 5. 6. The initial permeability before PVD installation are measured in laboratory is k as 7.81×10^{-4} cm/s.

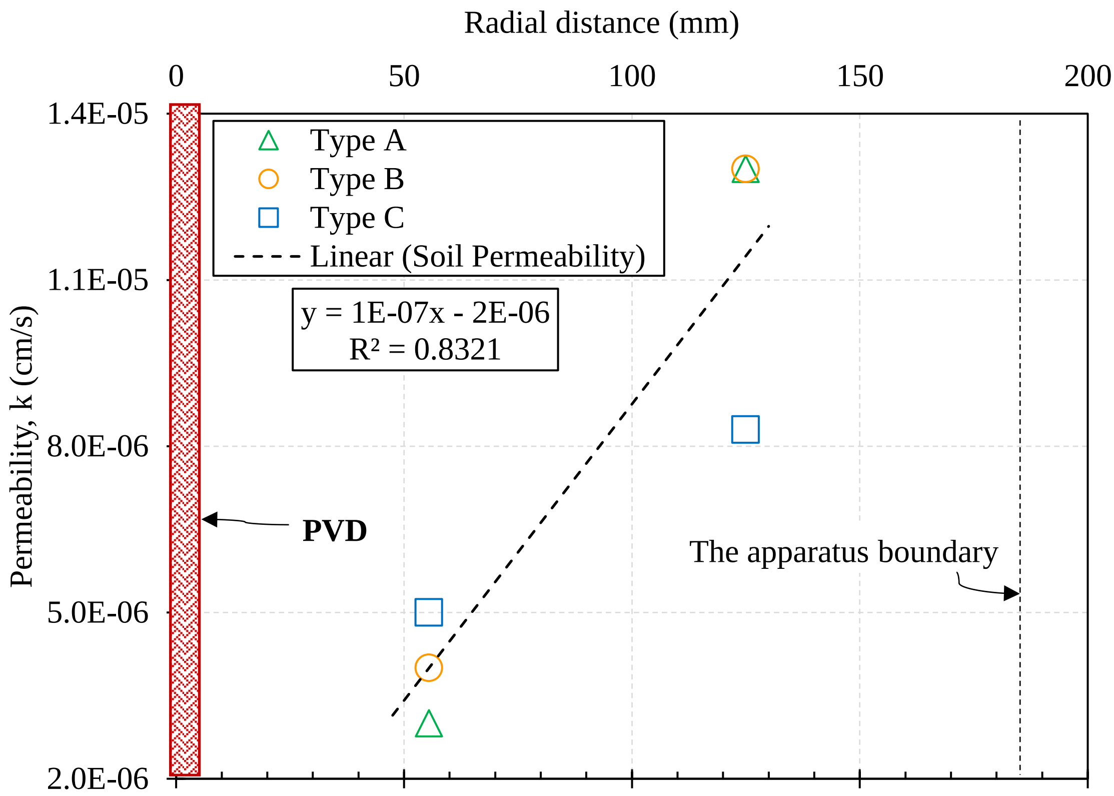

Figure 5. 6. The permeability of soil after preloading in radial distance.

The results of studies have also shown that the soil surrounding the PVD has low permeability. This phenomenon is due to soil stabilization, which is a result of the reduction in water content within the soil that occurs due to the installation of PVD.

Studies have shown that the installation of PVD can have a significant impact on the soil surrounding the drain. The results indicate that PVD types A, B, and C have a much greater influence on the transition zone and inner smear zone compared to the undisturbed soil area. As a result, the soil surrounding the PVD becomes more stable and less susceptible to failure. This improvement in soil stability and strength can reduce the risk of soil failure and ultimately improve the overall stability of the soil. Thus, the use of PVD can be an effective way to increase soil permeability during preloading, improving the consolidation process, especially in soft soils.

5.3.4 Water flow rate

This study is to understand the influence factors of PVD performance from the water flow rate tested in the laboratory. Therefore, to illustrate the ideal results of decreasing the amount of water flow with elapsed time, natural logarithm equations are used. The relationship between the amount of water flow and elapsed time was obtained for each type of PVD, and the results are determined in Figure 5. 7.

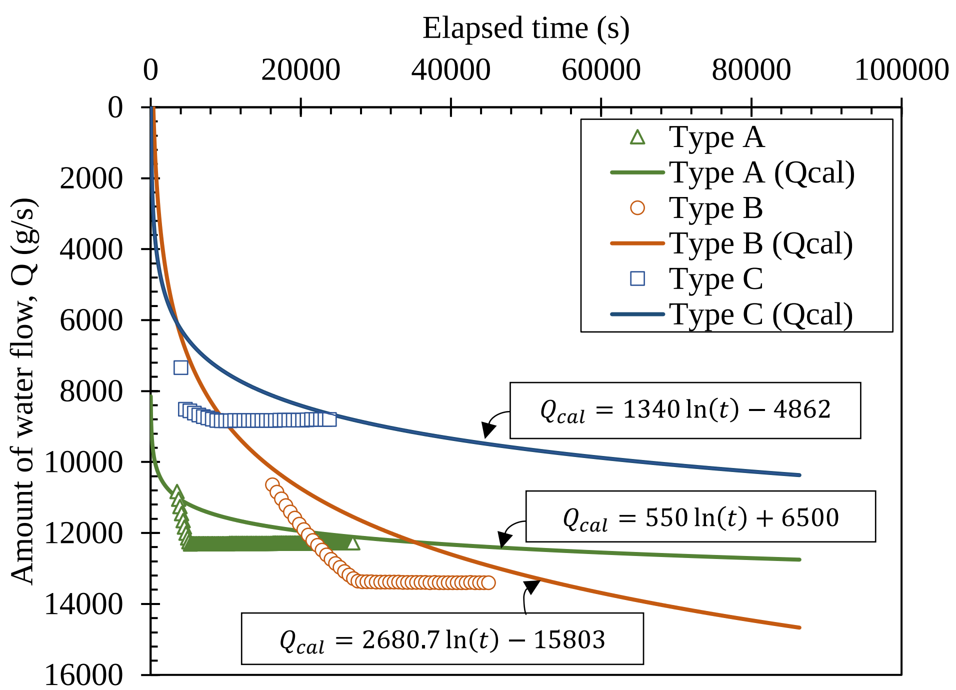

Figure 5. 7. The amount of water flow capacity during preloading

$$Q_{cal} = \beta \ln(t_0) + Q_{t_0} \tag{5. 5}$$

where β is the slope of the water flow rate, t_0 is the elapsed time of the actual water flow rate, and Q_{t_0} is the initial value or sort-term value of the water flow rate in elapsed time.

The result in Type A shows an extreme increment in the first few seconds of preloading but suddenly slowed in the amount of water flow. On the other hand, Type B shows a more stable result, and the amount of water flow constantly increases with each elapsed time. Although, Type C has a similar trend with Type A with lower water flow. After 24 hours, the amount of water flow for Type B is more significant and more optimum for discharging the water from the soft soil than Type A and Type C. Therefore, the results indicate that Type B has less disturbance during consolidation and the shape of the PVD is one of the crucial factors influencing water discharge from the soft soil.

The PVD core and a gap between PVD with the mandrel is one of the influence factors of the PVD performance in water flow rate. The PVD with a larger core area will allow water to flow more efficiently because of the larger volume allowance of water flow in general. However, the smear zone could be interfering the efficiently of the PVD core. From this study, natural logarithm equations are used and predicting the water flow rate.

5.3.5 Discharge capacity

In this study, the discharge capacity was analyses to understand the clogging effect on PVD performance. The discharge capacity is the most critical parameter affecting PVD performance based on the influence zone. Furthermore, the effects of the drain shape can be determined in the laboratory.

The discharge capacity is defined as the rate of water flow per elapsed time that can be conducted under a unit hydraulic gradient in the drain core (Adriyati et al., 2022b), which is determined:

$$i = \frac{\Delta h}{L} \tag{5. 6}$$

$$q_w = \frac{Q}{i} \tag{5. 7}$$

where i is the dimensionless hydraulic gradient, Δh is the head difference (m), L is the length of the chamber apparatus (m), q_w is the discharge capacity (m^3/s), and Q is the rate of water flow per unit of elapsed time (m^3/s).

Furthermore, the PVD was evaluated under the same loading and hydraulic gradient; the apparent varied discharge capacity values were obtained in different types of PVD. The exponential graph illustrates the ideal results of decreasing the discharge capacity with elapsed time. The regression method can be obtained by substituting the fitting curves expression when the clogs start. The actual data and calculated results are shown in Figure 5. 8.

As a result, PVD Type A is approximately discharge 20 mm^3/s in elapsed time of 1060 sec, and under deformation predicting is 45% based on changing the quality of discharge, whereas for PVD Type B is 171 mm^3/s in elapsed time of 320 sec and 55% during discharging. On the other hand, PVD Type C has a discharge 13 mm^3/s in elapsed time of 4280 sec and 75% of deformation prediction. Therefore, PVD Type A result reveals that clogging occur for a more extended period.

However, the deformation predicting the clogging in PVD Type B is more significant than in PVD Type A, but the time is shorter. The discharge capacity in PVD Type B only has one peak, meaning that PVD Type B has a most stable performance than the other two. PVD Type C has a dense portion of low discharge capacity and spans over a quite significant amount of elapsed time, implying that PVD Type C is the most unstable PVD among the three.

The discharge capacity of the PVD can be determined by factors other than the deformation and clogging particularly at areas where significant deformation is expected and can be generalize:

$$q_{w_{cal}} = q_{w_0} \mathrm{e}^{(-A_0 t)} \tag{5. 8}$$

where q_{w_0} is the initial value or sort-term value of the discharge capacity, A_0 is the coefficient with respect to the time-dependent discharge capacity in elapsed time.

The reduction in discharge capacity caused by drain deformation can be attributed to three factors. Firstly, the bending rigidity of the drain core significantly impacts its discharge capacity. While drains made of rigid plastic tend to have better discharge capacity, PVDs with low core bending rigidity are more likely to deform and lose capacity. Secondly, the size and shape of the drain core can also influence the discharge capacity, with larger cross-sectional areas typically performing better. The stiffness of the PVD filter and the soil around the drain can also affect its discharge capacity.

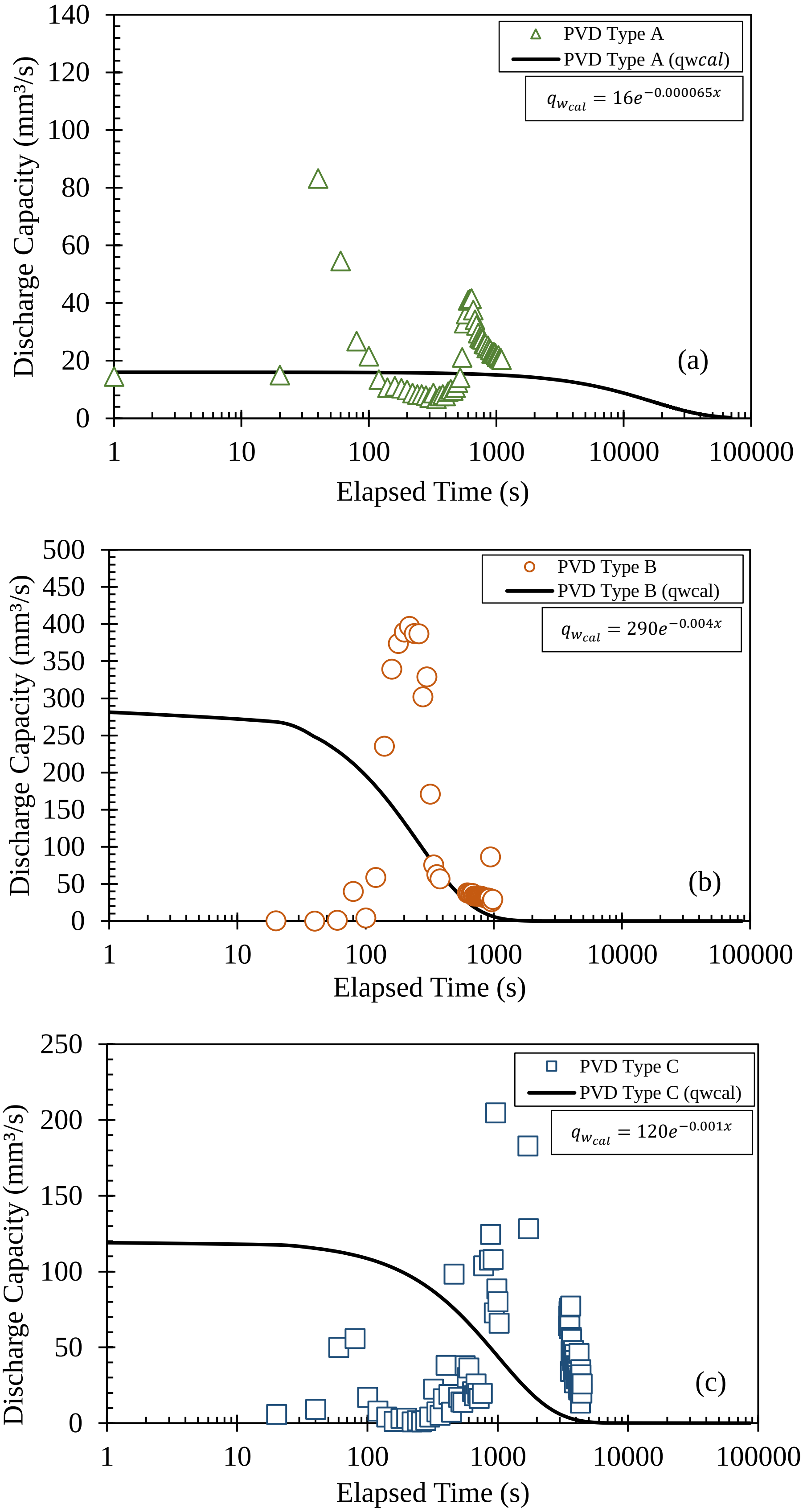

Figure 5. 8. Discharge capacity during preloading; (a) Type A; (b) Type B; (a) Type C.

However, PVD filters with higher stiffness values are preferred to maintain the drain's characteristic stiffness. Additionally, the stiffness of the soil affects deformation patterns around the drain. Less stiff soil may lead to larger soil deformation, which can increase the risk of clogging due to transmigration of fine particles. Lastly, soil stiffness also transfers pressure to the PVD, which can further cause deformation and disrupt the drain's stiffness.

5.3.6 Settlement

The settlement can be used to evaluate the quality of prefabricated vertical drain (PVD) combined with vacuum preloading. The degree of consolidation can be estimated using either settlement or pore water pressure. Monitoring changes in pore water pressure can provide valuable insights into the effectiveness of PVD and vacuum preloading in expelling excess water from the soil and increasing its density.

In this study, we collected results using LVDT on the surface of an acrylic mold at two locations close to PVD during vacuum preloading. The average of the settlement over time were plotted as shown Figure 5. 9 for three types of PVD.

As a results, average settlement measurements curves for each type of PVD show a sharp initial increase, followed by falling settling rates. The settlement at first reached approximately 0.32 cm, 0.6 cm, and 0.7 cm for PVD types A, B, and C, respectively. The curves then show settling rates that begin to fall between the time range of 140 s up to 2720 s, 540 s up to 14800 s, and 480 s up to 9260 s for PVD types A, B, and C, respectively. The final settlement values were 9.9 cm, 10 cm, and 8.8 cm for PVD types A, B, and C, respectively.

The curves show a sharp increase at the initial stage of vacuum preloading, then the corresponding settling rates began for fall for each type of PVD. This indicates a reduction in the rate of consolidation for each type of PVD.

However, the settlement measurement limitation is restricted to the surface of the PVD at the limitation point. Further analysis of settling rates could indicate the effectiveness of each type of PVD in achieving the desired consolidation rate. A piezometer or other equipment could be used for accurate measurement and to ignore the effect of boundary conditions

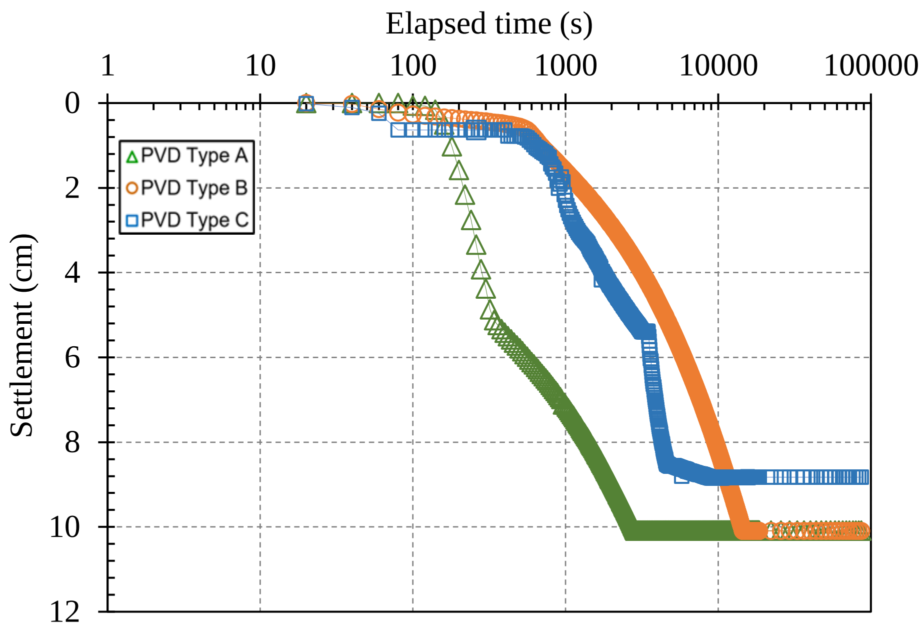

Figure 5. 9. Surface settlement varying with elapsed time.

5.3.7 Excess pore water pressure due to installation mandrel

The study investigates the trend of excess pore pressure dissipation towards the vertical drain during the installation of PVDs. The measurement of excess pore pressure during mandrel driving and withdrawal is shown in Figure 5. 10, which compares the use of closed-end and open-end mandrels in terms of their impact on the surrounding soft soil layer.

The results show the changes in the pore water pressure for different types of PVD. The excess pore water pressures reach their maximum values when the mandrel passes through the plane of the water pressure measurement ports. However, when the mandrel is withdrawn, the pore water pressure decreases rapidly. The closed-end mandrel causes significant lateral deformation and shear failure, contributing to the formation of the smear zone.

The study highlights the impact of smear zone effects and provides insights into the mechanism of PVD installation. This finding highlights the importance of using open-end mandrels, which can prevent the formation of a smear zone and enhance PVD performance. Overall, the findings from this study could help in optimizing PVD installation techniques for improved performance in geotechnical applications, leading to better and efficient soil improvement techniques.

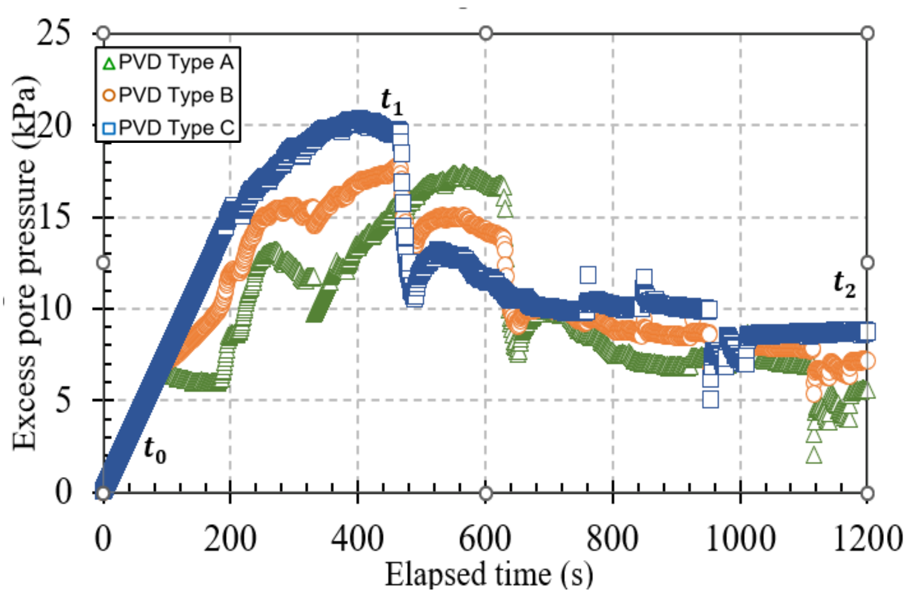

Figure 5. 10. Excess pore pressure response with time during installation mandrel for PVD Type A, Type B, and Type C.

5.3.8 Consolidation rates

The smear zone effect caused by installing PVD significantly impacts the consolidation rate (Barron R. A, 1948; Indraratna et al., 2005). To investigate the smear zone around the vertical drain on consolidation rate, the general equation used in literature is given by $U = 1 - e^{\frac{-8T}{\mu}}$. Furthermore, the extended inner smear zone in a radius of the transition zone is investigated in this study. The factor μ is modified to μ'. The modification version for average consolidation rate is determined:

$$U = 1 - e^{\frac{-8T}{\mu'}} \tag{5. 9}$$

where T is the time factor (non-unit) for consolidation due to radial drainage, μ' is the factor (non-unit) influencing extended inner smear zone in a radius of the transition zone. The consolidation is generally described in terms of the time factor as shown below:

$$T = \frac{c_h t}{{r_{w.eq}}^2} \tag{5. 10}$$

where c_h is the coefficient of consolidation in the horizontal direction, t is the elapsed time, and $r_{w.eq}$ is the dimensions of smear zone influence (mm) in this study given by equations 5.1 and for general form in a rectangular mandrel is determined in Chapter 4, The analytical solution for radial consolidation in above literature without effect smear zone is given by equations 5. 10 and the factor influencing the smear zone surrounding the PVD is shown in equations 5. 11 and 5. 12.

$$\mu = \ln n - \frac{3}{4} \tag{5. 11}$$

$$\mu = \ln\left(\frac{n}{m}\right) - \frac{3}{4} + \frac{k_h}{k_s}\ln m \tag{5. 12}$$

Furthermore, the factor influencing due to extended inner smear zone in a radius of the transition zone is determined as shown below:

$$\mu' = \ln\left(\frac{n}{m'}\right) - \frac{3}{4} + \frac{k_h}{k_s}\ln m' \tag{5. 13}$$

where $n = \frac{D_e}{r_{w.eq}}$, D_e is equivalent diameter of apparatus (mm), $m = \frac{s}{D_e}$ is modified to $m' = \frac{r_s}{D_e}$, s is the radius of the smear zone (mm), r_s is the radius of the transition zone (mm), k_h is the average horizontal permeability in the undisturbed zone (mm/s), and k_s is the average permeability in the smear zone (mm/s).

In this study, for the PVD Type A case the ratio of horizontal permeability in the undisturbed zone and smear zone.

In order to examine the effect of PVD influence in this study, evaluate the results, and compare with previous research are conducted. The Eq. (5.11) corresponds to no smear zone, Eq. (5.12) corresponds with a smear zone, and Eq. (5.13) corresponds to an extended smear zone in considering the radius of the transition zone.

The result in value of *T* is the time factor, corresponding to *U*=90%, is PVD Type A is 1.22 with smear zone and 0.75 with no smear zone, respectively, a difference of 61%. For PVD Type B is 1.21 with smear zone and 0.68 with no smear zone, respectively, a difference of 56%. The last types for PVD Type C are 1.18 with smear zone and 0.75 without smear zone, respectively, a difference of 63%. Therefore, the effect of the rectangular mandrel and PVD influences on consolidation rate are shown in Figure 5. 11.

As a result, the consolidation rate involving an extended inner smear zone in a radius of the transition zone is approximately close to the no-smear zone. By evaluating the extended inner smear zone, the mechanical component can be reliably evaluated with laboratory test results and understand the effect of the installation method for PVD using a mandrel. The value obtained for the rectangular mandrel has much less influence on the smear zone than the previous study. However, the boundary factor should be considered because the geometry of the mandrel in the PVD installation in the field is essential.

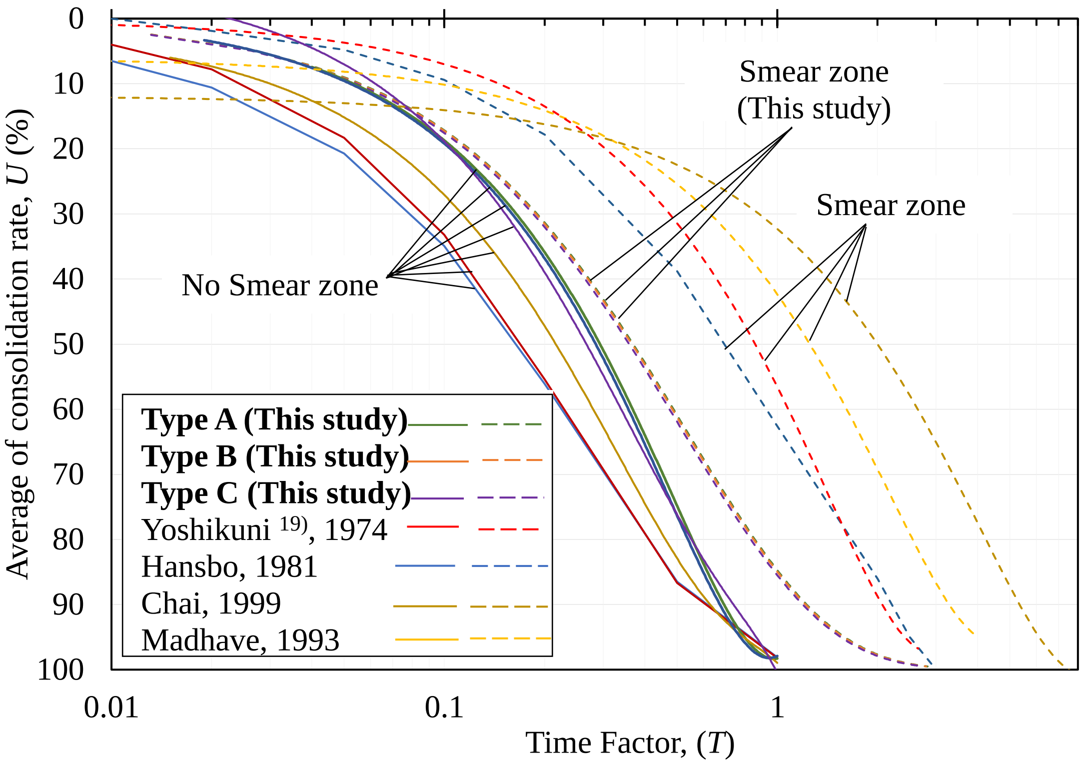

Figure 5. 11. Influence of PVD on consolidation rate.

5.4 SUMMARY

This study proposes a terminology based on the classic three-zone theory of large-scale consolidation technique utilizing three types of PVD and a rectangular mandrel. The focus of the investigation is on evaluating the effect of extended inner smear zone in transition zone on the consolidation rate using a 1g model test and empirical analysis, conducted with a specifically designed rectangular mandrel and the three types of PVD. The performance of PVD is examined in terms of their influence on effect of water content (w), shear strength of soil (s_u), permeability (k), water flow rate (Q), discharge capacity (q_w), settlement, excess pore water pressure , and consolidation rate (U) are discussed. The empirical analysis is employed to predict the optimal performance result for the PVD performance with Q and q_w used as indicator of performance. Furthermore, the modification factors that influence the performance of PVD is (μ') are proposed to understand the extended smear zone in transition zone on consolidation rate (U).

5.5 REFERENCES

Adriyati, M., Yasufuku, N., Ishikura, R., & Rifa, A. (2022b). Optimizing modified large-scale consolidation testing for describing smear zone caused by mandrel- driven prefabricated vertical drain. *2022 GeoAsia7 Conference & IGS First Young Engineers Conference (GeoAsia7)*, 5–8.

Barron R. A. (1948). Consolidation of fine-drained soils by drain well. *Transactions of ASCE*, *113*, 718–754.

Chai, J. C., & Miura , N. (1999). Investigation of factors affecting vertical drain behavior. *J. Geotech and Geoenviron Engrg*., Vol. 1, Balkema, Rotterdam, The Netherlands.

Chai, J., Miura, N., & Bergado, D. T. (2006). Preloading clayey deposit by vacuum pressure with cap-drain. *Geosyntetic Engineering Journal*, *3*, 45–52. https://www.jstage.jst.go.jp/article/jcigsjournal1998/21/0/21_0_45/_pdf

Chai, J., Miura, N., & Bergado, D. T. (2007). Preloading clayey deposit by vacuum pressure with cap-drain: Analyses versus performance. *Geotextiles and Geomembranes*, *26*(3), 220–230. https://doi.org/10.1016/j.geotexmem.2007.10.004

Chung, S. G., & Lee, N. K. (2010). Smear Effect and Well Resistance of PVD-Installed Ground Based on the Hyperbolic Method. *Journal of Geotechnical and Geoenvironmental Eng*, *136*(4), 640–642. https://doi.org/10.1061/(asce)gt.1943-5606.0000256

Ghandeharioon, A., Indraratna, B., & Rujikiatkamjorn, C. (2010). Analysis of Soil Disturbance Associated with Mandrel-Driven Prefabricated Vertical Drains Using an Elliptical Cavity Expansion Theory. *International Journal of Geomechanics*, *10*(2), 53–64. https://doi.org/10.1061/(asce)gm.1943-5622.0000027

Hansbo, S. (1981). Cosolidation of Fine-Grained Soils by Prefabrcated Drains. *10th International Conference on Soil Mechanics and Foundation Engineering*, 677–682. https://www.issmge.org/publications/publication/consolidation-of-fine-grained-soils-by-prefabricated-drains

Indraratna, B., & Redana, I. W. (1998). Laboratory Determination of Smear Zone due to Vertical Drain Installation. *J. Geotechnical and Geoenvironmental Engineering*, *124*(2), 180–184. https://doi.org/10.1061/(asce)1090-0241(1998)124:2(180)

Indraratna, B., Rujikiatkamjorn, C., & Sathananthan, L. (2005). Radial consolidation of clay using compressibility indices and varying horizontal permeability. *Canadian*

Geotechnical Journal, *42*(5), 1330–1341. https://doi.org/10.1139/t05-052

Madhave, R, M., Yeong-mog park, N. miura. (1993). Modelling and study of smear zones around band shaped drains. *Soils and Foundations*, *33*(4), 135–147. https://doi.org/https://doi.org/10.3208/sandf1972.33.4_135

Mesri, G., & Khan, A. Q. (2011). Increase in Shear Strength Due to Vacuum preloading. *2011 Pan-Am CGS Geotechnical Conference*, *October 2011*.

Sharma, J. S., & Xiao, D. (2000). Characterization of a smear zone around vertical drains by large-scale laboratory tests. *Canadian Geotechnical Journal*, *37*(6), 1265–1271. https://doi.org/10.1139/t00-050.

Yoshikuni, H. (1979). Design and constrcution control of vertical drain methods. Gihodo Tokyo, Found. Eng. Series (in Japanese).

CHAPTER VI
MICROSTRUCTURE ANALYSIS OF PVD AND SOIL

6.1 INTRODUCTION

The microstructure analysis is conducted to determine the clogging area of PVD due to vacuum preloading at the microscopic level. Scanning electron microscopy (SEM) and magnetograms were used to assess the relationship between soil structure and its mechanical behavior.

This chapter provides a thorough discussion of the analysis theory, hypotheses, and empirical analysis method following consolidation to enhance the understanding of the clogging effect and soil structure caused by vacuum preloading. The obtained results were carefully examined and interpreted, with particular attention to any chemical reactions occurring within the materials. ImageJ software was used to calculate pore area (*n*) and particle area (Ø) for structure analysis before and after testing.

The relationship between pore area and shear strength of the soil is complex and depends on various factors such as soil type, compaction, moisture content, and particle size distribution. Therefore, this chapter provides a detailed discussion of this relationship. Specifically, it highlights the complex and varying nature of the relationship between pore area and shear strength.

6.2 MICROSTRUCTURE ANALYSIS RESULTS

6.2.1 Chemical composition of soil

The soil sample used for this study is kaolinite because of its commercial availability, relatively high permeability, and the existing database of its engineering properties are available. Kaolinite is an aluminosilicate soft white mineral, have a chemical composition, the detail is shown in Figure 6. 1. Kaolinite is a type a clay mineral that has a chemical composition of AI_2Si_2O. This means that it contains atoms of aluminum (AI), silicon (Si), and oxygen (O).

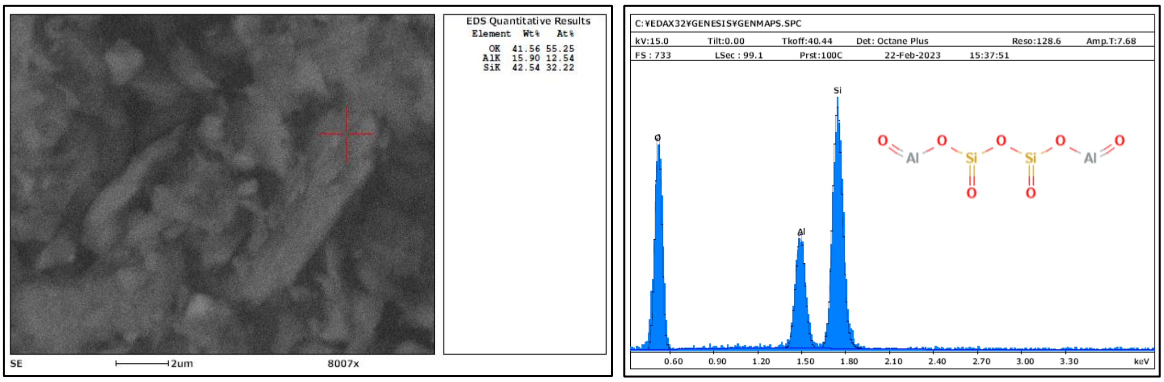

(a) (b)

Figure 6. 1. Chemical composition kaolinite: (a) SEM magnifications ×8007 with minimum particle 0.003 μm and maximum particles 194 μm , (b) Magnetograms.

6.2.2 Chemical composition of PVD

PVD consists of a drainage channel, filter, and core. The drains were made of Polypropylene core material, which was chosen for its specific properties related to drainage effectiveness, the detail is shown in Figure 6. 2.

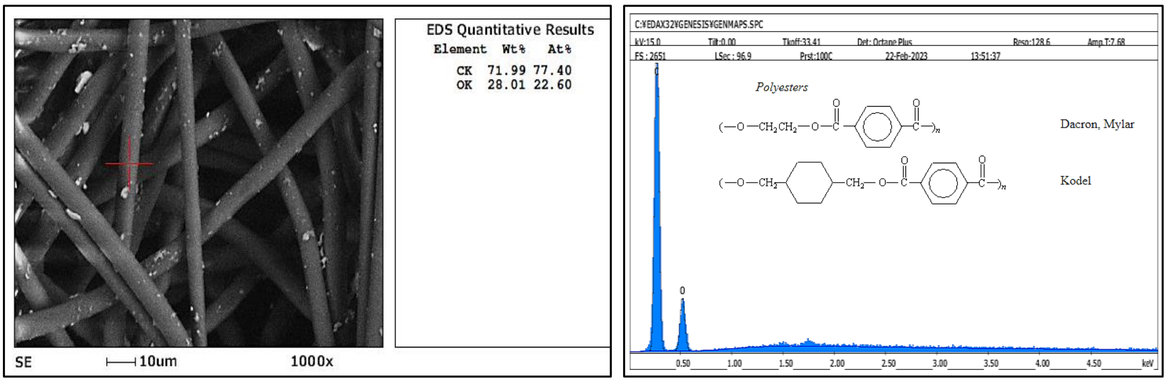

(a) (b)

Figure 6. 2. The PVD material: (a) SEM magnifications ×1000, (b) Magnetograms

The chemical composition of polyesters includes carbon (C) and oxygen (O) with specific ratio of the elements depending on the type of polyester and its manufacturing process. The chemical breakdown of polyesters through hydrolysis of the ester bonds in the main chain can result in the formation of small molecules such as glycols and dicarboxylic acids.

6.2.3 PVD structure

A PVD is typically composed of a geotextile filter-wrapped plastic band with molded channels designed to aid in the consolidation of soils. These serve as drainage pathways for pore water in soft compressible soils that consolidate more quickly when subjected to continuous vacuum preloading (Geng et al., 2011). The PVD filter should meet the filter design criteria as they are important for enhancing the PVD performance. A commonly used criterion was given in previous studies (Aydilek & Edil, 2004; Carroll, 1983; Chu et al., 2004).

The SEM pictures from the three types of PVD before vacuum preloading showed the arrangement of the straight filter and pore area. At 500× magnification, microscopic images in representative sections of the three types of PVD were captured, as shown in Figure 6. 3. The pore size or the apparent opening size (AOS) must be small enough to prevent the fine particles of the soil from entering the filter and the drain. The standards (Carroll, 1983; Chu et al., 2004), commonly used can be expressed:

$$O_{95} \leq (2-3)D_{85} \tag{6.1}$$

$$O_{95} \leq (4-7.5)D_{85} \tag{6.2}$$

$$O_{50} \leq (10-12)D_{50} \tag{6.3}$$

where O_{95} is the AOS of filter, D_{85} is the size which is larger than 50% of the fabric pores, and D_{85} and D_{50} refer to the sizes for 85% and 50% of particles in the soil by weight. $O_{95} \leq$ 0.075 m (or 75 mm) is often specified for a prefabricated vertical drain. As a result, to achieve the goals of the vacuum preloading effect, it is critical to select a suitable pore size of the filter. In addition, to interpret the SEM images, the pores and PVD filter size in the area were analyzed. At 500 magnification, microscopic images from SEM in representative sections of three types of PVD were captured, as shown in Figure 6. 3.

The results show that the pore size area of the filter for PVD types A, B, and C varied in the range of 0.1–12.136 µm. The average O_{95} values for PVD filters types A, B, and C of 83, 116, and 265 µm were employed in this study according to the criterion proposed in (Chu et al., 2004).

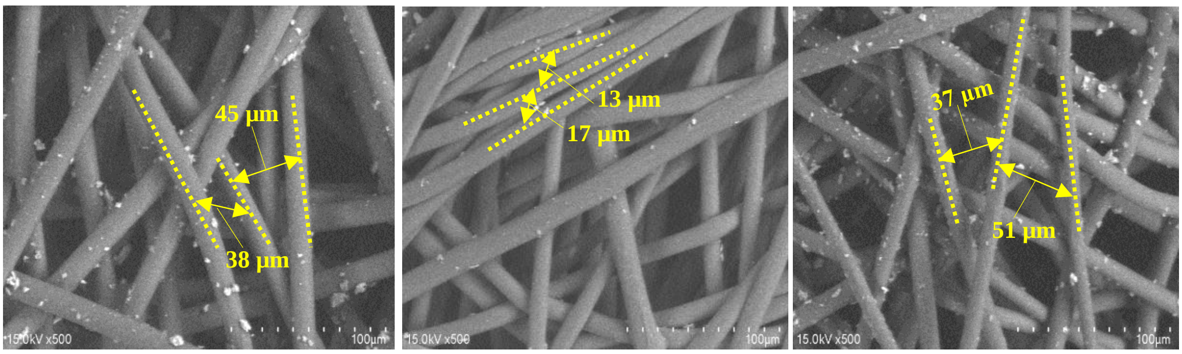

(a) (b) (c)

Figure 6. 3. The PVD results from SEM: (a) Type A, (b) Type B, (c) Type C.

In addition, to interpret the SEM images, the pores and PVD filter size in the area were analyzed as shown in Figure 6. 4. The quantitative analysis of the soil microstructure area showed that PVD type B had a large filter area of 55% and a pore area of 45%, whereas types A and C had a filter area of 43% and a higher pore area of 57%. Therefore, the SEM images could characterize PVD filters with different pore sizes. It is essential to observe the PVD type, and a large PVD filter ensures a higher drainage rate.

A large PVD filter area in percentage means that more filter material is present per unit area of soil, thus increasing the filtering capacity of the system and helping prevent soil particles from clogging the PVD (Xu et al. 2020). However, if the pore area is smaller in percentage, there is less space available for water to flow through the soil and into the PVDs; this can reduce the overall drainage capacity of the system and slow down the consolidation process.

The balance between the PVD filter and pore areas is important in designing an effective PVD system. The filter material must be sufficient to prevent clogging and maintain long-term performance. At the same time, the available pore space must be adequate to allow for efficient drainage and consolidation. Therefore, selecting the PVD type is essential to ensure its successful implementation in the field. According to this study, PVD type B over types A and C according to the PVD filter structure.

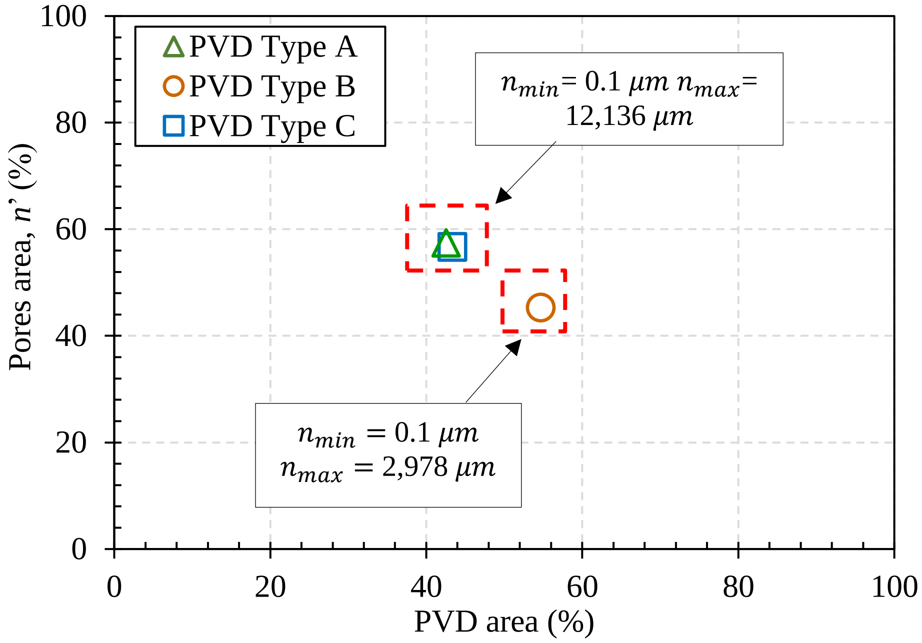

Figure 6. 4. The PVD area and pores area (n') in percentage.

6.2.4 Soil structures

Kaolinite is a type of clay mineral that is commonly found in soft soil with high water content. In Figure 6. 5 shown displays the soil conditions before the consolidation test, and Table 6. 1 describes the size distribution based on SEM image analysis. The SEM images of kaolinite specimens with different fabric arrangements are consistent with the conclusions obtained from sedimentation tests (Chow et al., 2019; Y.-H. Wang & Siu, 2006). However, various factors, such as sample preparation methods, imaging conditions, and material properties, may result in sample variations (Fischer et al., 2012).

In this study, SEM image may show a relatively smooth surface and uniform at lower magnifications with some voids and visible pores. The edges of the particles may appear slightly rounded or irregular due to the presence of water. At higher ×3000 magnifications, the SEM image may reveal a platy structure of the kaolinite particles that could be stacked or randomly arranged. The particles may be tightly packed, with minimal void spaces or more loosely packed with visible gaps and voids. Additionally, small particle aggregates may be present in some areas, indicating localized bonding between the particles and exhibiting textural variations such as cracks or fissures.

The SEM image can provide valuable insights into the microstructure and properties of the soil, which can help identify suitable engineering and construction strategies. Overall, the kaolinite soft soil with high water content may exhibit relatively homogeneous and uniform structures, with some variability in the particle arrangement and texture visible under higher magnification.

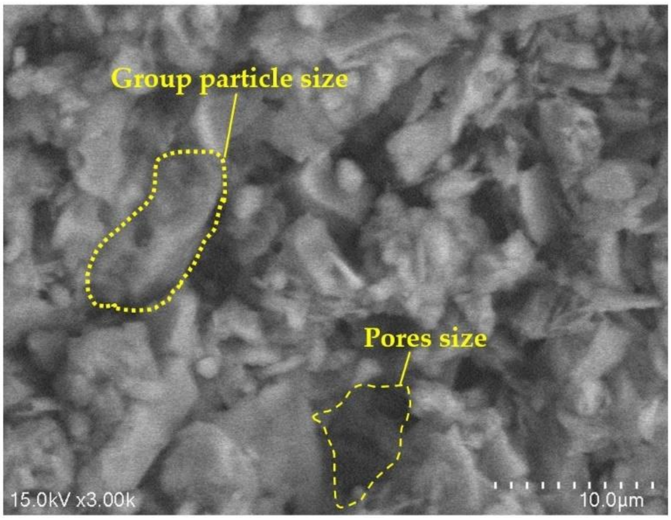

Figure 6. 5. The SEM image of kaolinite before the test.

Table 6. 1. Description of soil structure

Count	Pores (μm²)	Particle (μm²)
Min	0.0003	0.003
Mean	7.39	21.75
Max	194.49	557.30
Total area	525.09	717.73

6.3 INTERACTION PVD AND SOIL DUE TO CLOGGING EFFECT

The interaction between the PVD filter and the pores or known as clogging, which is caused by vacuum preloading depends on several factors, includes the properties of the soil, the filter material, and the drainage capacity of the system (Mesri & Khan, 2012; P. Wang et al., 2020; Xu et al., 2020). On the other hand, if the filter material has a low permeability or the PVD system is not designed correctly, the interaction between the PVD filter and pores may not be optimal (Bergado & Balasubramaniam, 1996).

During vacuum preloading, solid particles in the soil may become trapped in the pores of the filter sleeve, which can affect the overall pore structure and properties of the filter. This can impact the effectiveness of the preloading treatment, as a clogged filter may reduce the flow of water and air through the soil. However, the precise effects of bending or other specific factors on the pore structure and particle behavior may depend on the specific application and conditions of the vacuum preloading process. Therefore, it is crucial to understand the interaction between the PVD filter and the pores caused by vacuum preloading to optimize the design and properties of the system accordingly. Thus, the effectiveness of the PVD system during installation using a mandrel can be ensured in this part of study. After vacuum preloading, SEM images were captured of both the soil-facing and drain channel-facing sides. Additionally, the opening in the filter was filled with fine soil particles on both sides, with notable differences existing.

On the side contacting the soil, more fine particles are filled to the filter inter-spacing. The changing filter structure shows a change based on the vacuum preloading effect. In this study, the approach used is based on the shape of the deformation effect of the PVD. The PVD filter can occur in different structures after consolidation, including uniform, local, and sinusoidal bending referring to deformation modes in the previous study. Three types of PVD are described based on SEM image results and quantitative analysis. PVD type A shows in Figure 6. 6, Figure 6. 7, PVD type B shows in Figure 6. 8, Figure 6. 9, and PVD type C shows in Figure 6. 10, and Figure 6. 11 are leading to potential long-term stability issues.

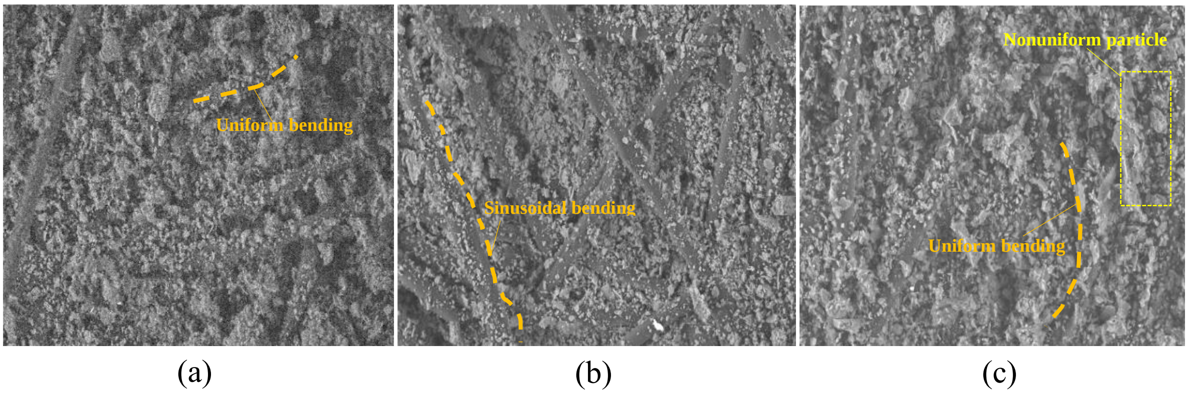

Figure 6. 6. The interaction PVD type A and soil ×300: (a) Top, (b) Middle, (c) Bottom.

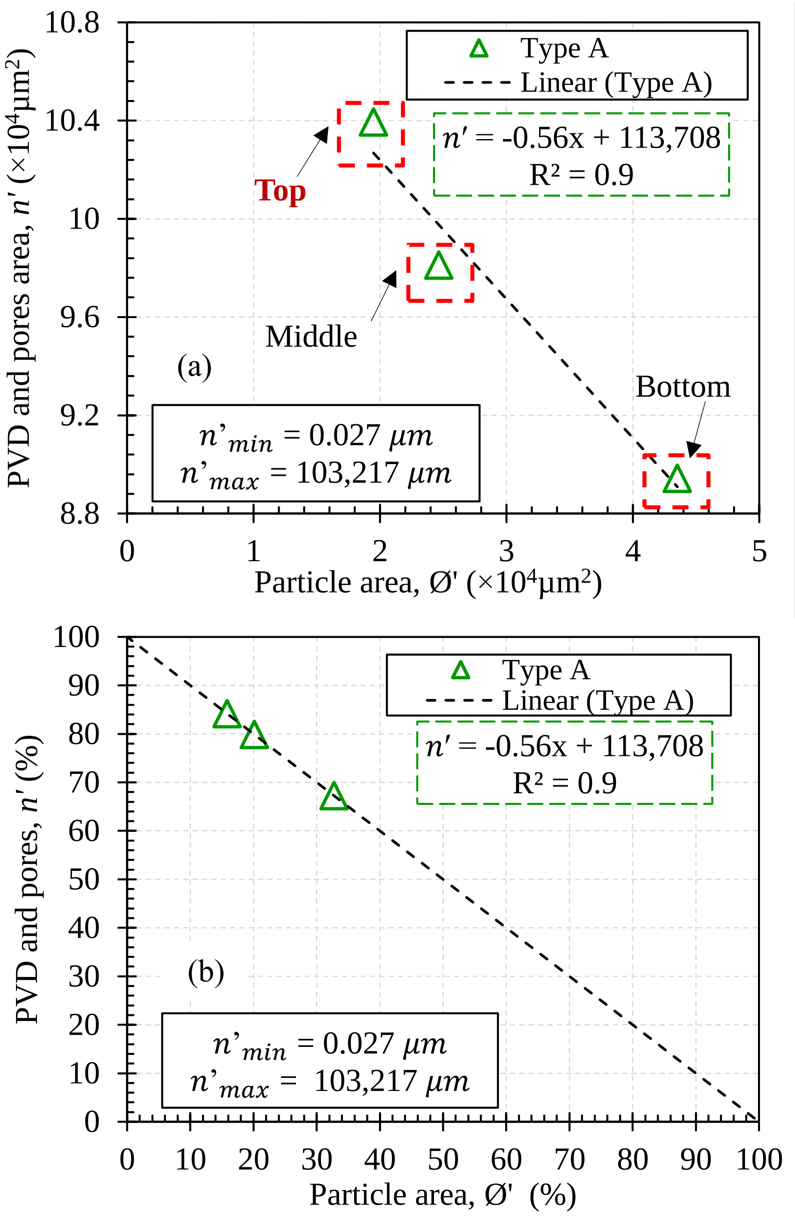

Figure 6. 7. The PVD type A: (a) Total pores and particle, (b) Percentage pores and particle.

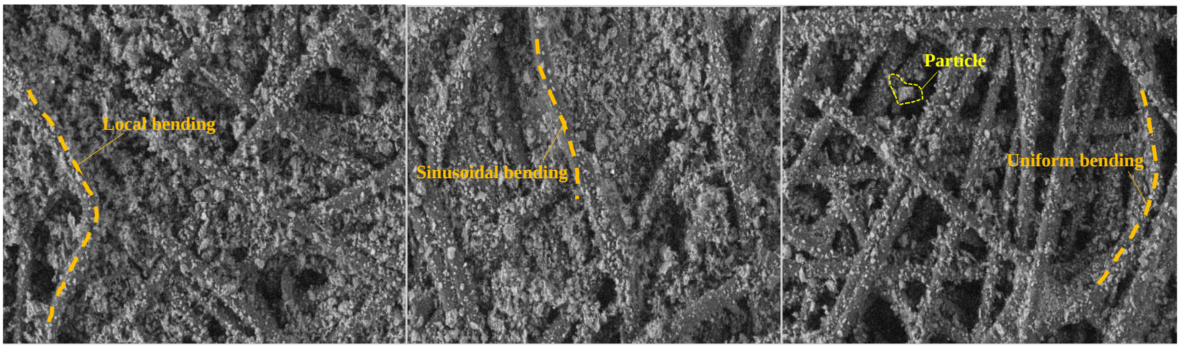

(a) (b) (c)

Figure 6. 8. The interaction PVD type B and soil ×300: (a) Top, (b) Middle, (c) Bottom.

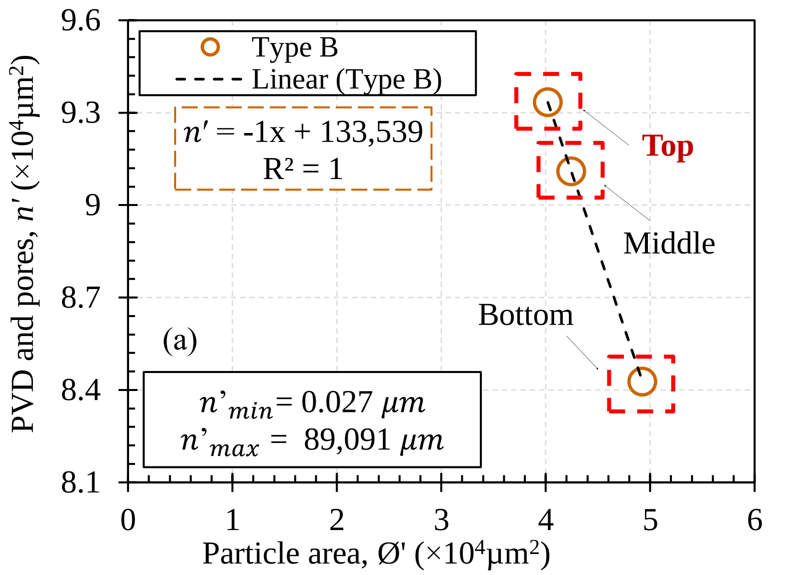

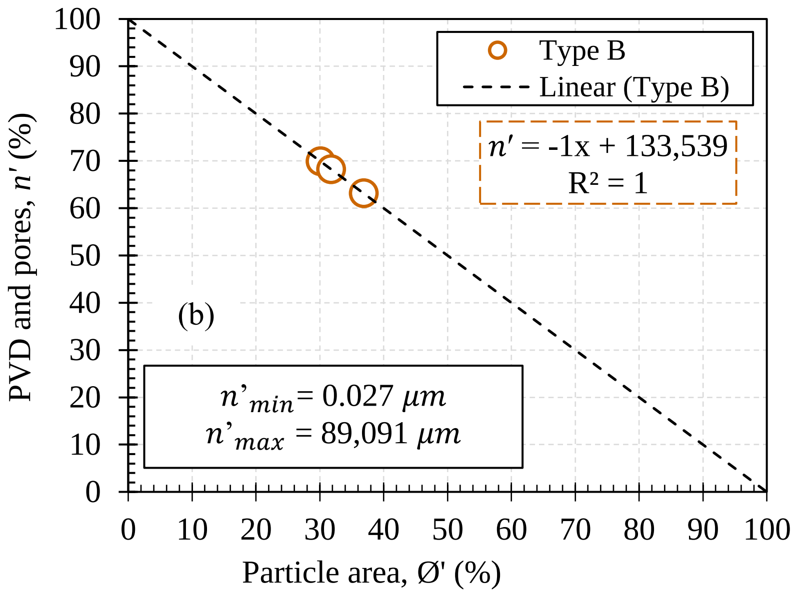

Figure 6. 9. The PVD type B: (a) Total pores and particle, (b) Percentage pores and particle.

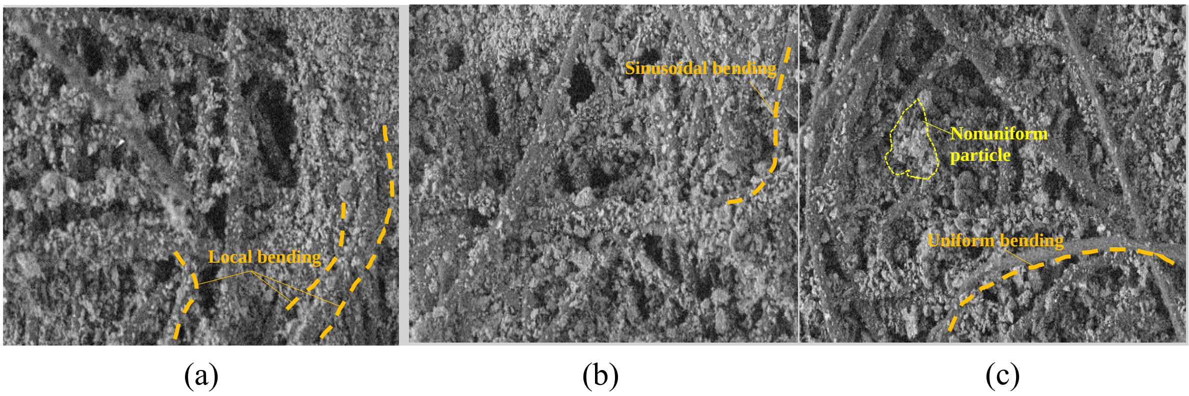

Figure 6. 10. The interaction PVD type C and soil ×300: (a) Top, (b) Middle, (c) Bottom.

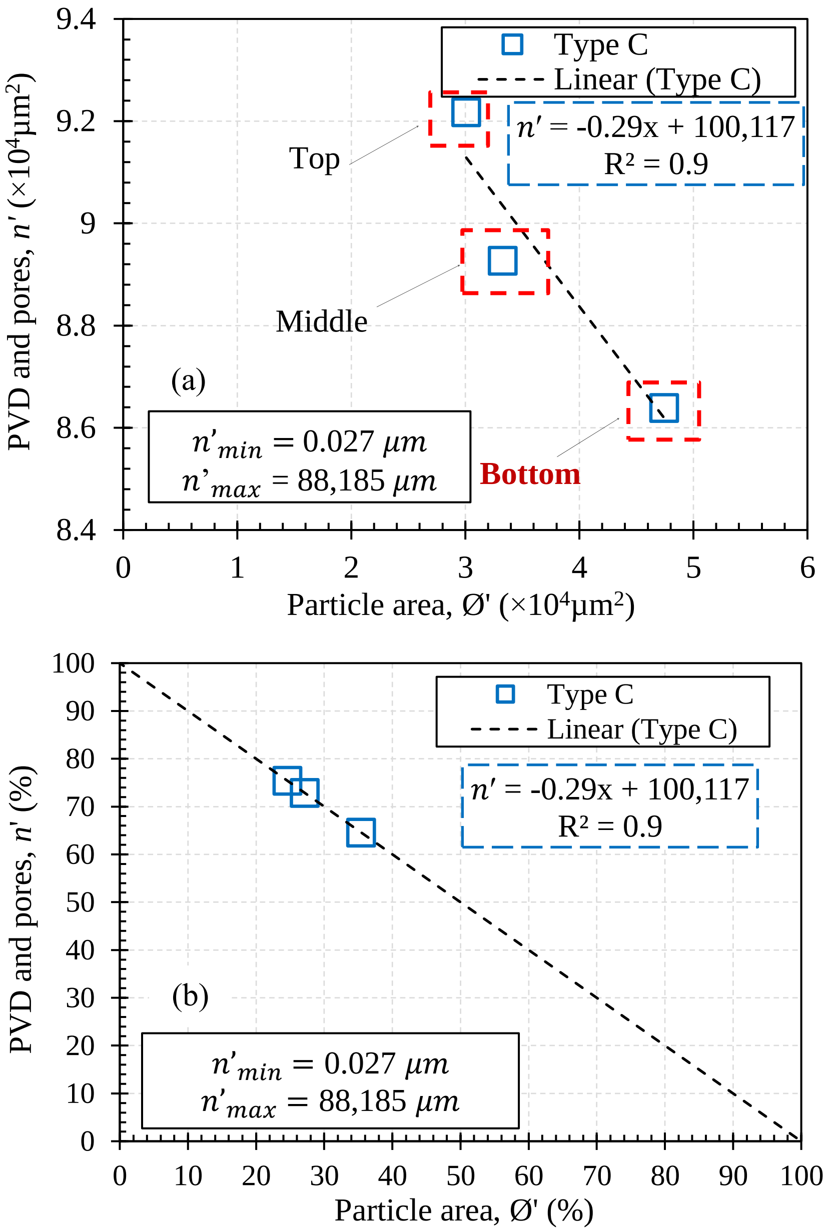

Figure 6. 11. The PVD type C: (a) Total pores and particle, (b) Percentage pores and particle.

The particles area was increasing in bottom effect area of PVD. The results show in Figure 6. 12 and Figure 6. 13 that the bottom area of PVD type A, the particle area is 4.3×10^4 μm^2 and pores area is 8.9×10^4 μm^2, type B is 4.9×10^4 μm^2 and 8.4×10^4 μm^2, type C is 4.7×10^4 μm^2 and 8.6×10^4 μm^2. These results, show that the bottom area of all PVD types in this study that higher particle area is due to vacuum preloading and using the PVD filter decreases pores size. These results indicate that the fine particle is moving to fill areas with large pores during vacuum preloading. Therefore, it is crucial to understand the meaning of the bending that occurs in the filter. Generally, effect of PVD filter due to vacuum preloading it is expected that small particles may become blocked in the pores of the filter membrane during the vacuum preloading process. This could affect the overall structure and properties of the filter, and potentially impact the effectiveness of the preloading treatment. This can lead to clogging of the filter and a reduction in the drainage capacity of the system. If this occurs, the consolidation process may be slowed down or ineffective, leading to potential long-term stability issues.

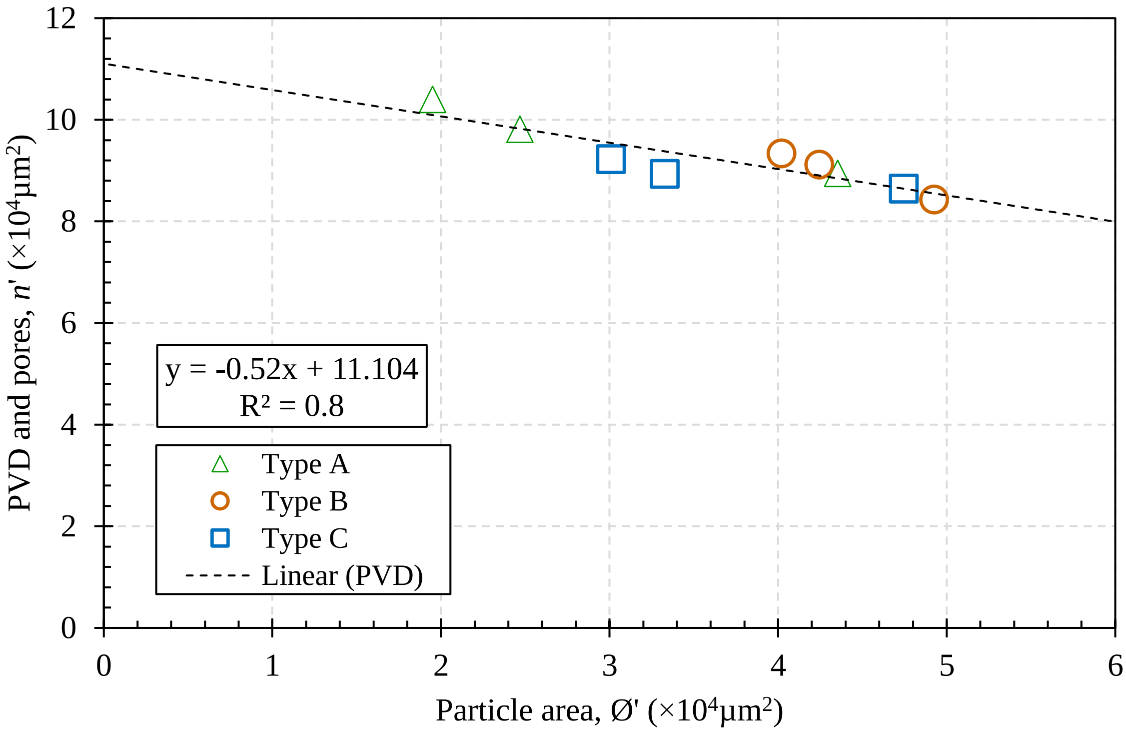

Figure 6. 12. Soil structure cause by vacuum preloading in pores and particle size analyses for all types of PVD.

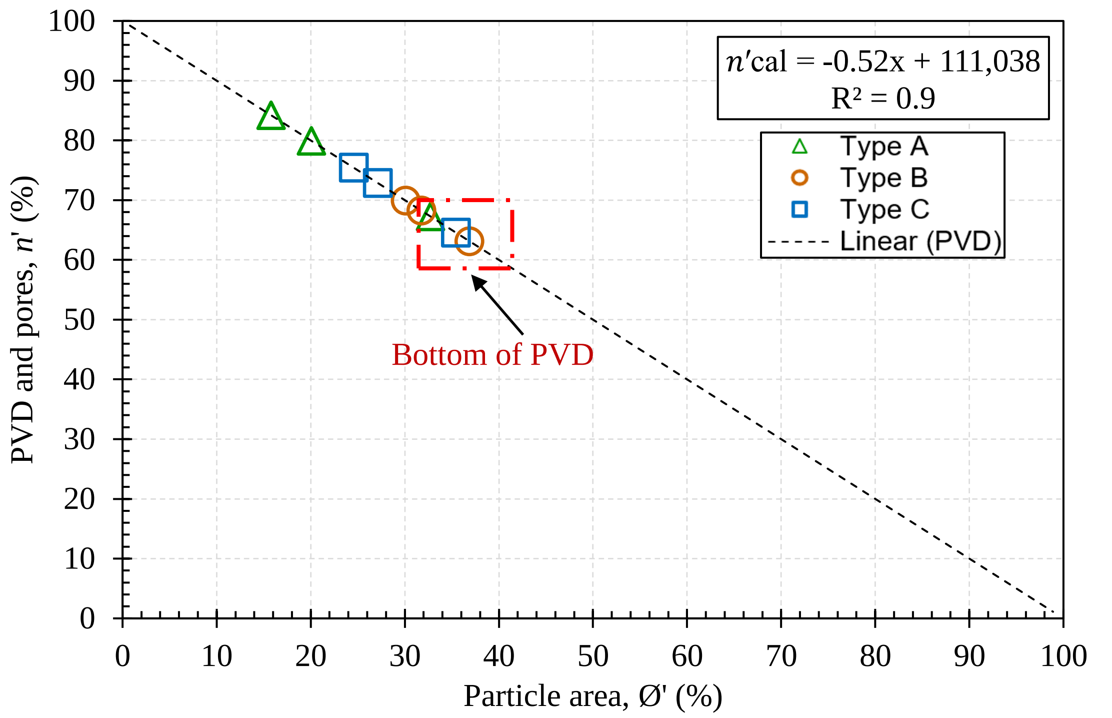

Figure 6. 13. The all PVD types in percentage

The general form of the PVD filter, pore, and particle areas was analyzed using ImageJ and expressed as follows:

$$n = n' = \alpha.\emptyset' + n'_0 \qquad (6.5)$$

where n is the pore area, n' is the PVD and pore area, α is the slope of the pore area, $\emptyset'$ is the particle area, and n'_0 is the initial PVD and pore area before the test.

In summary, the clogging effect on PVD filters caused by vacuum preloading was influenced by the filter's geometry, stiffness, and surrounding soil properties. The design and properties of the PVD filter should be optimized to ensure that it can withstand external loads and maintain its stability during installation and use.

6.4 SOIL STRUCTURE DUE TO VACUUM PRELOADING

6.4.1 Soil structures based on pores and particles

SEM images were used to study the changes in soil structure due to vacuum preloading (Penumadu & Dean, 2000; J. Wang et al., 2018; P. Wang et al., 2020; Xu et al., 2020). SEM can provide high-resolution images of soil particles and their arrangements, allowing us to observe the changes in the soil microstructure due to consolidation (Griffiths & Joshi, 1991; Nelson & Westrich, 1974; Yu et al., 2016).

Further analysis was necessary to understand the effect of PVD in three zone areas. Figure 6. 14, Figure 6. 15, and Figure 6. 16 shows the SEM image from three zone in effect of three types PVD due to effect of vacuum preloading following changes in soil structure. Based on PVD, pores, and particle results, the bottom location of PVD is determined as a clogging area. The soil particles become more tightly interlocked, resulting in a denser soil structure and face-to-face contact between particles and domains (Sachan, 2007). Furthermore, the morphology of soil particles can be affected by vacuum preloading (Ural, 2021; J. Wang et al., 2018).

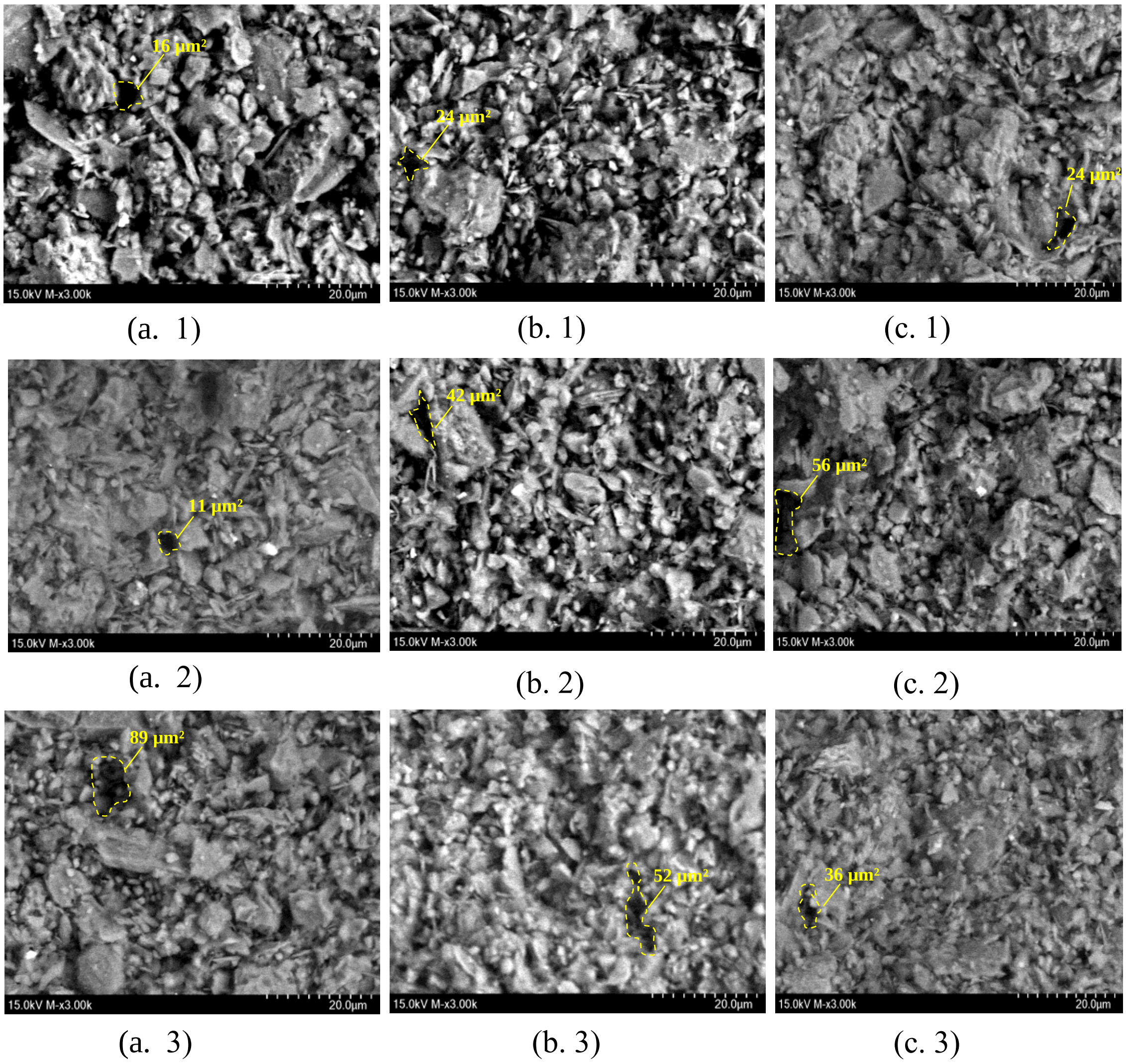

Figure 6. 14. Affect soil structure in the three zone for PVD type A; (a.1, a.2, a.3) Top, middle, and bottom in inner smear zone; (b.1, b.2, b.3) Top, middle, and bottom in transition zone; (c.1, c.2, c.3) Top, middle, and bottom in undisturbed zone

For example, clay particles may become more angular or irregularly shaped, indicating that the vacuum preloading has altered the soil particle properties. In this study the results shows that the pores and particle area of size for PVD type B with different scaled in inner smear zone 0.5×10^3 μm^2 and 0.7×10^3 μm^2, transition zone 0.3×10^3 μm^2 and 1.1×10^3 μm^2, and undisturbed zone 0.7×10^3 μm and 0.7×10^3 μm. Type A in inner smear zone 1.2×10^3 μm^2 and 2.4×10^3 μm^2, transition zone 0.9×10^3 μm^2 and 2.7×10^3 μm^2, and undisturbed zone 0.8×10^3 μm^2 and 2.7×10^3 μm^2. Type C in inner smear zone 1.2×10^3 μm^2 and 2.4×10^3 μm^2, transition zone 0.9×10^3 μm^2 and 2.7×10^3 μm^2, and undisturbed zone 1.9×10^3 μm^2 and 1.7×10^3 μm^2.

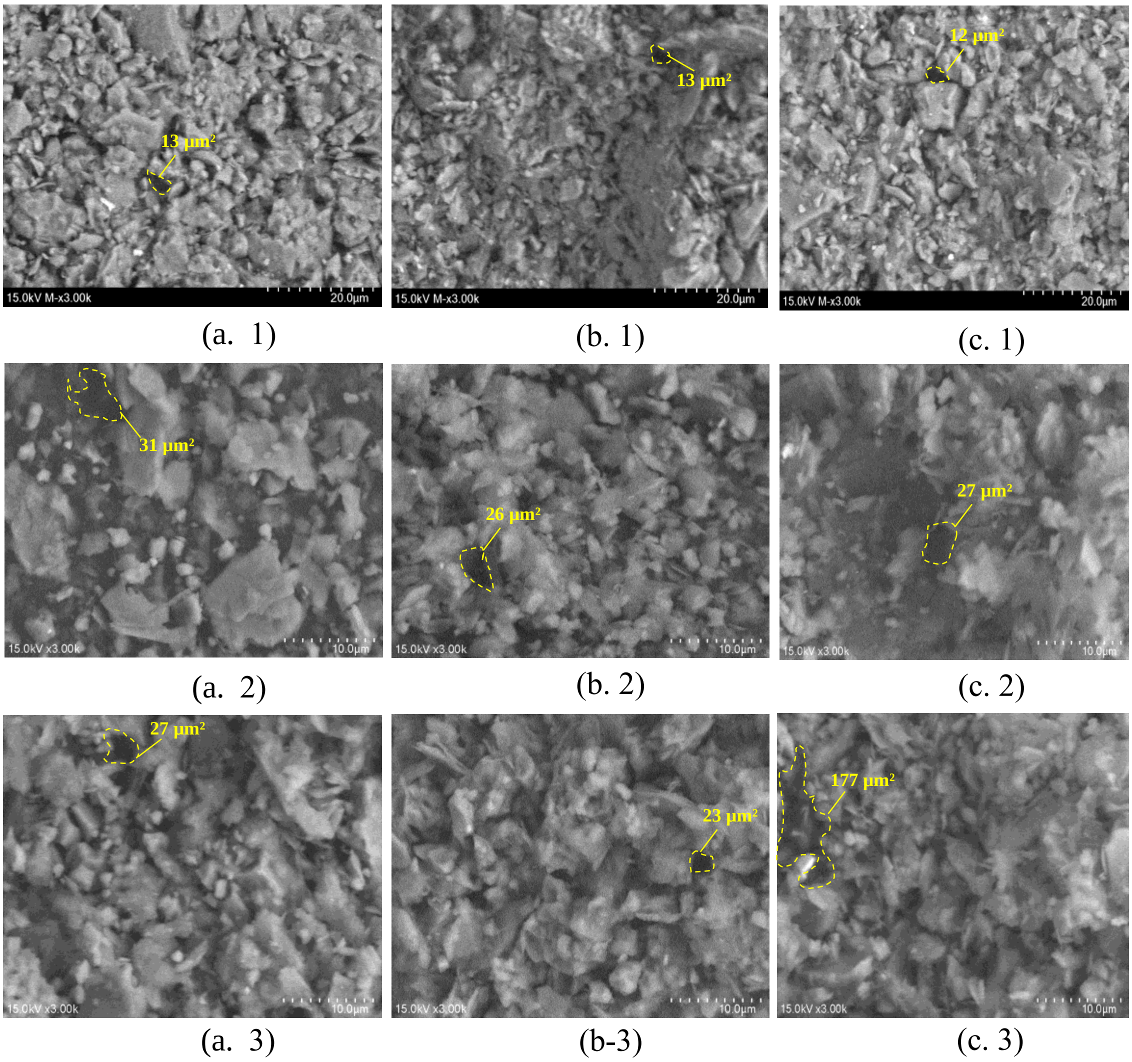

Figure 6. 15. Affect soil structure in the three zone for PVD type B; (a.1, a.2, a.3) Top, middle, and bottom in inner smear zone; (b.1, b.2, b.3) Top, middle, and bottom in transition zone; (c.1, c.2, c.3) Top, middle, and bottom in undisturbed zone.

The results shown that particles area increases when the pores decrease for all types of PVD. However, the size of the particles used in type B PVD were smaller than those used in PVD type A and C.

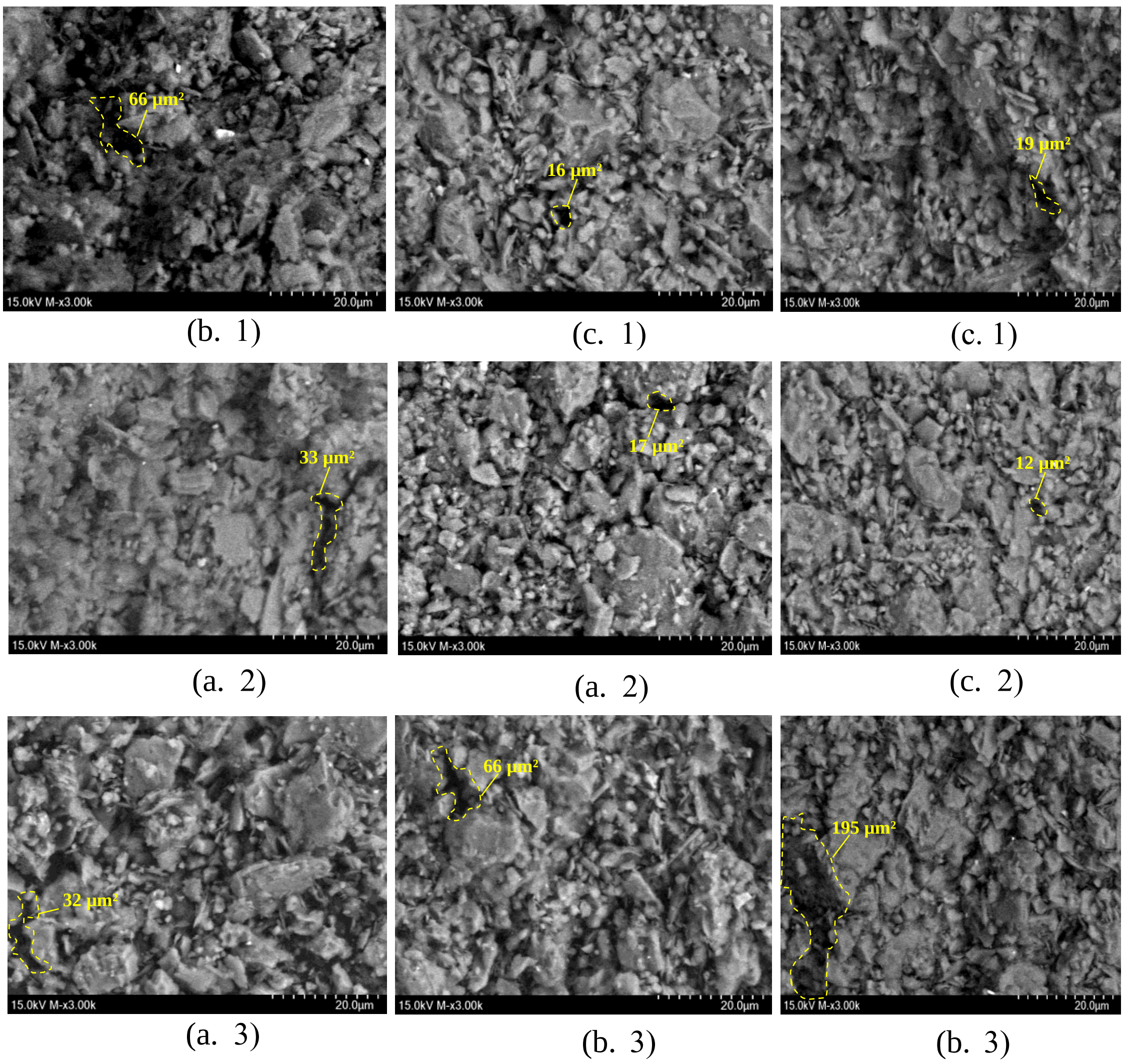

Figure 6. 16. Affect soil structure in the three zone for PVD type C; (a.1, a.2, a.3) Top, middle, and bottom in inner smear zone; (b.1, b.2, b.3) Top, middle, and bottom in transition zone; (c.1, c.2, c.3) Top, middle, and bottom in undisturbed zone.

To explain these results more clearly, an analytical approach is carried out for this study and shown in Figure 6. 17. The results indicates that the PVD B works optimally during the consolidation due to clogging effect. It was also proven that using type B the particles area was increased by 40% to 80%. This study found that a reduction in pores and particles size is shown with to impact soil structure. SEM images can reveal the changes in the soil fabric and provide insights into how these changes affect the soil properties. Overall, SEM can provide valuable insights into the changes in soil microstructure caused by vacuum preloading. This information can be used to understand the mechanisms of vacuum preloading and to optimize the technique for specific soil conditions.

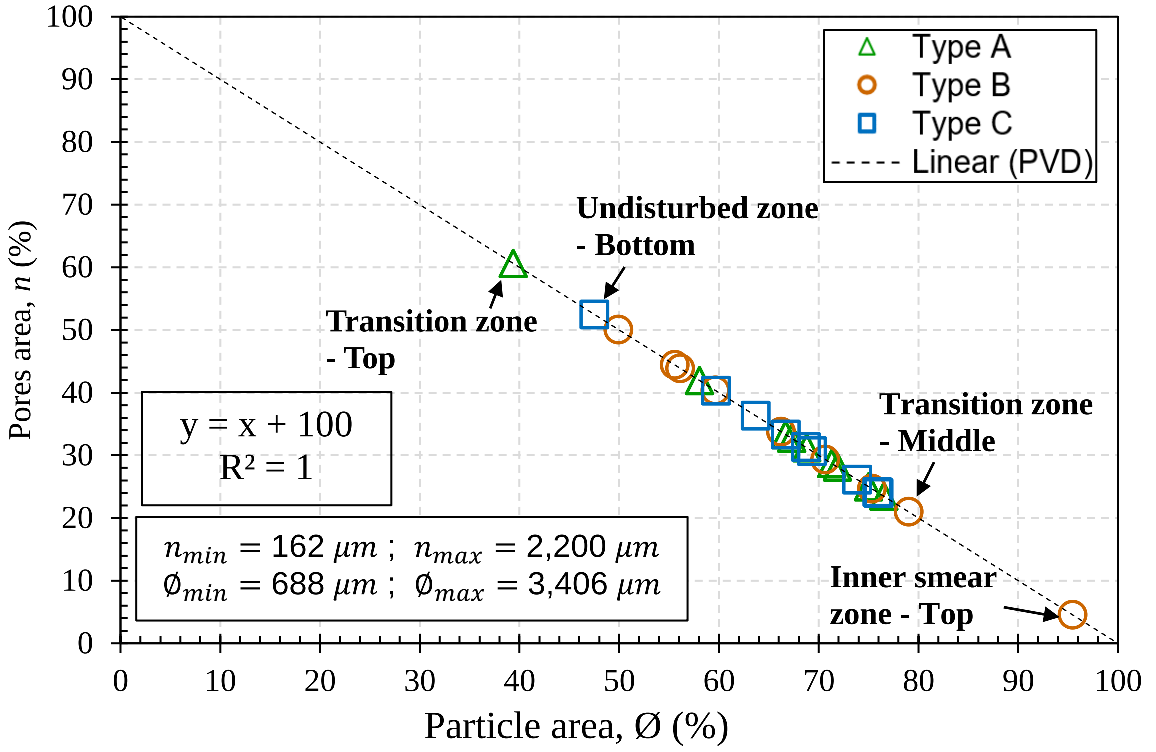

Figure 6. 17. The all PVD all types of percentage.

Soil permeability is a critical factor affecting the effectiveness of preloading in consolidating the soil. The increase in permeability during preloading is related to the increase in pore area within the soil. The pore area ratio varies in different zones of the soil, such as the inner smear zone, transition zone, and undisturbed zone. The inner smear zone, which is right beneath the preloading surface, experiences the most significant increase in pore area ratio due to the high-stress concentration. On the other hand, the undisturbed zone shows the smallest increase in pore area ratio because no new pores are being created. The results in this this study are shown in

6.4.2 Relationship of pores area and permeability

Many attempts have been made to find a relation between permeability and other measurable properties of porous materials such as particle-size and porosity or pores (Forestry, 1957; Ni et al., 2021).

In general, larger pores will correspond to higher permeability, which means that fluids can flow more easily through the material being considered. However, it is important to note that there can be many factors that affect permeability, including the size and shape of the pores, the fluid being considered, and any obstructions or barriers within the material.

Therefore, while there may be a general trend of increasing permeability with increasing pore size, it is possible for more complex relationships to exist between these variables. Additionally, in the context of prefabricated vertical drain clogging, changes in the size and structure of pores due to clogging can significantly impact permeability.

Figure 6. 18 shows that in this study the pores area increasing linier with the ratio of permeability in three zone area, inner smear zone, transition zone, and undisturbed zone. The study found that from three types of PVD. PVD type C has larger pores and higher ratio permeability. PVD type B has larger pores in area transitions zone. PVD type A has small pores are for inner smear zone, transition zone, and undisturbed zone. However, the other factors such as the filter material and drainage capacity can also affect the performance of the PVD. Therefore, a comprehensive comparison of PVD types should take into all these factors.

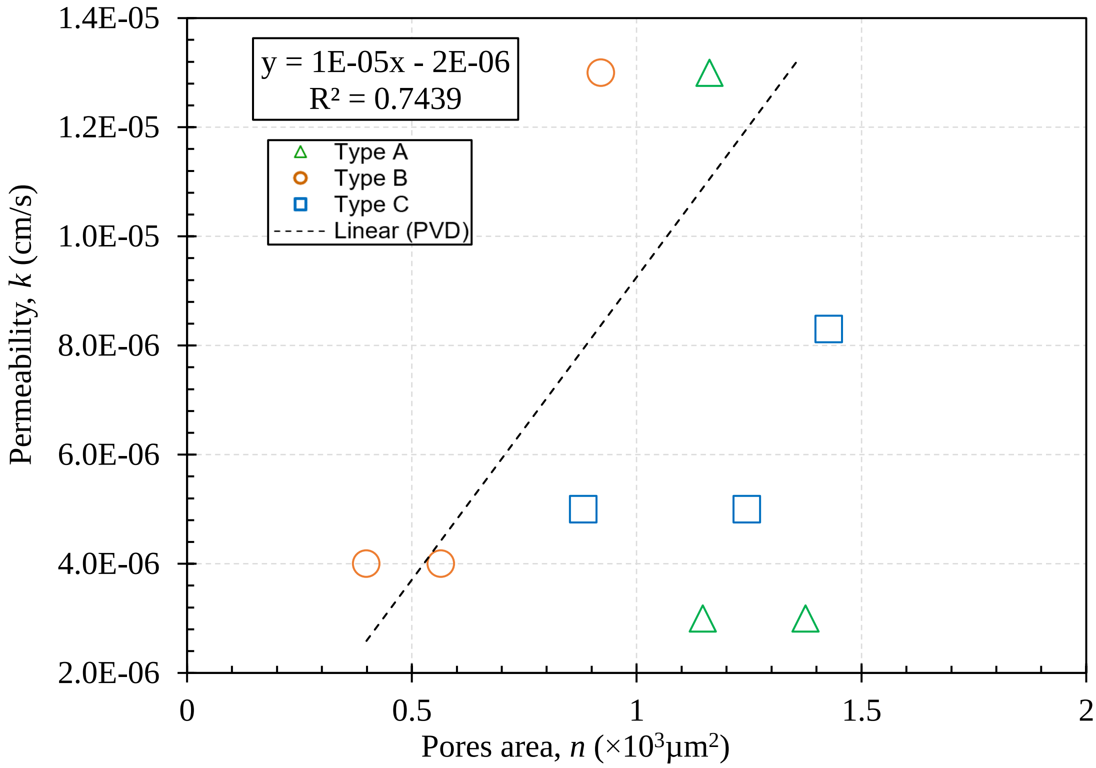

Figure 6. 18. The relationship between pores area and permeability.

The founding shows that there exists a linear relationship between the pore area ratio and permeability. When more pores are created due to preloading, the permeability increases linearly. This finding is consistent with the results of previous studies. However, it is important to note that the relationship between permeability and pore area ratio may vary depending on the type and composition of the soil. Therefore, understanding the specific relationship between pore area and permeability is essential to evaluating the effectiveness of preloading on a particular soil type.

In conclusion, soil permeability plays a crucial role in the preloading process, and the increase in pore area ratio caused by preloading is a key factor affecting soil permeability. The relationship between pore area and permeability is linear, and the magnitude of the increase in pore area ratio varies in different zones of soil. Thus, understanding these factors is essential in predicting the effectiveness of preloading for a particular soil type.

6.4.3 Correlation between pores area and vane shear strength

The relationship between the shear strength and pore structure of a soil structure can be affected by several factors such as soil composition, particle size, soil structure, and moisture content (Artidteang et al., 2011). In general, the shear strength of soil is influenced by the interlocking of soil particles and the bonding between them, which can be affected by the pore structure. Therefore, reduction in pores can improve soil stability and increase the shear strength of soil (Mitchell, 1993). Measuring the shear strength of soil towards to all PVD types in inner smear zone, transitions zone, and undisturbed zone as shown Figure 6. 19 and all area shown in Figure 6. 20.

The study results show that PVD type A has a higher shear strength of soil and smaller pores area in inner smear zone, transition zone, and undisturbed zone. In the inner smear zone, PVD type B has a greater influence on the shear strength of the soil compared to transition zone and undisturbed zone. Moreover, PVD type C in the inner smear zone, transition zone, and undisturbed zone has a high shear strength of soil. However, type C in area inner smear zone and transition zone has greater influence on the soil shear strength compared with undisturbed zone. Similar to the findings in (J. chun Chai et al., 2020), the results of this experiment indicate that consolidation the microstructures in an edge to face orientation increases the effectiveness of PVD installations method.

Smaller pores can increase the interlocking between the soil particles and improve the shear strength. On the other hand, soil pore structure can also affect its hydraulic properties, such as permeability and water retention characteristics. Large pores can increase the soil's permeability, allowing water to flow more easily. However, this can also lead to reduced water retention, which can affect the stability of the soil structure. The presence of smaller pores can improve water retention, which can improve the stability of the soil structure. The relationship between soil pore structure and shear strength is a complex phenomenon that requires careful consideration in soil engineering and geotechnical analysis. Soil models are commonly used to evaluate this relationship and can provide important information on the stability of soil structures. However, models must be designed with appropriate consideration of various soil properties and structures, including particle size and distribution, density, and moisture content.

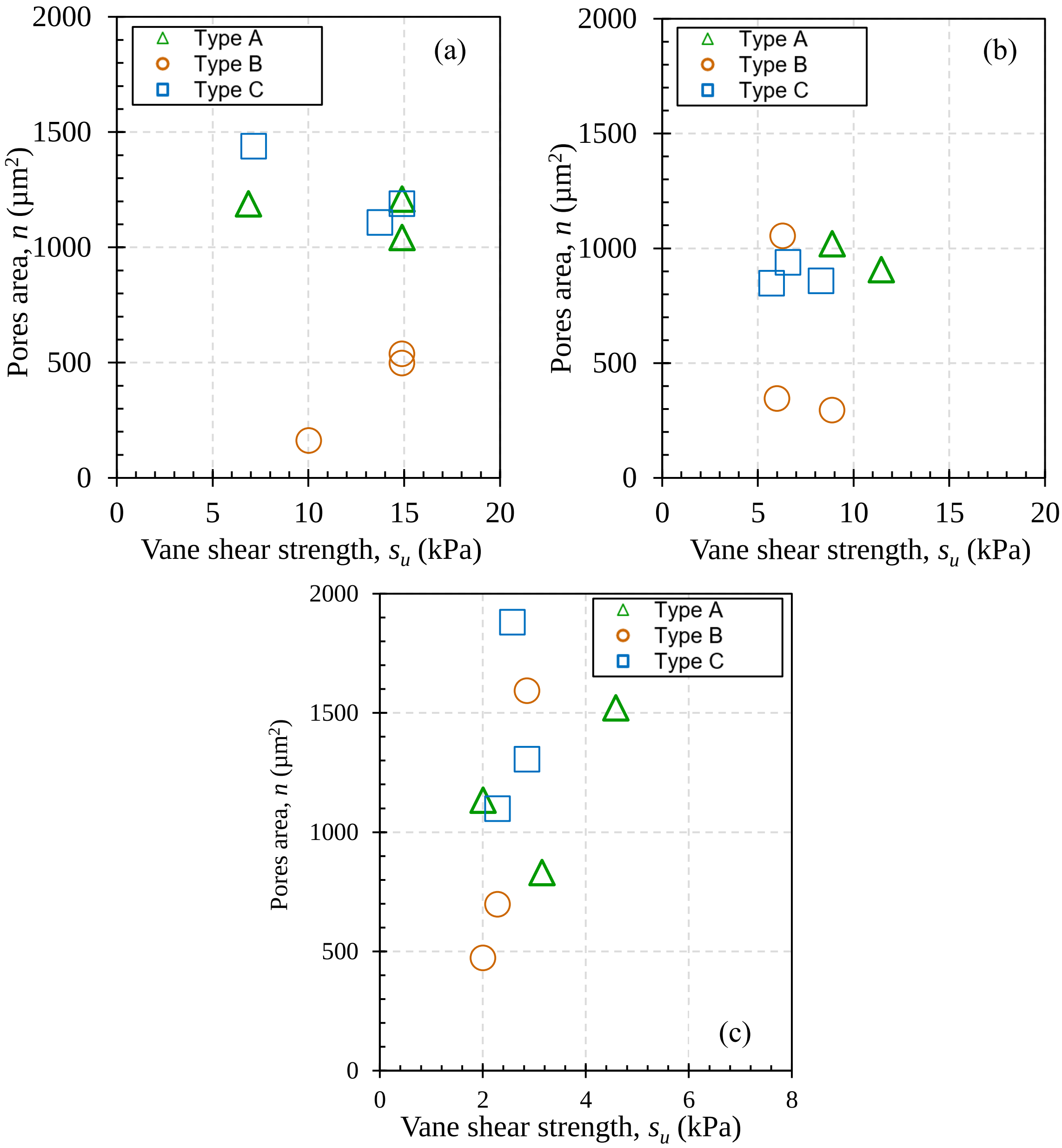

Figure 6. 19. The all PVD types in three zone area: (a) inner smear zone, (b) transitions zone, (c) undisturbed zone.

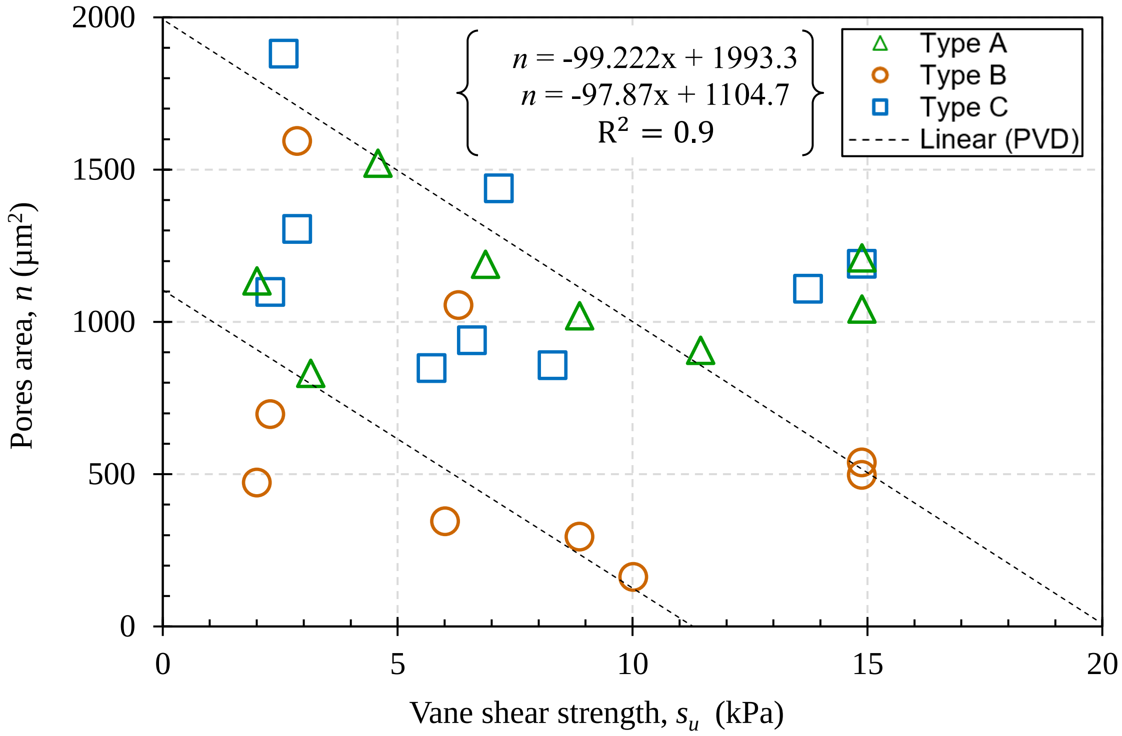

Figure 6. 20. The relationship of vane shear strength and pores area in three zone area.

In addition, the presence of structures such as aggregates and voids can significantly influence the soil's shear strength and stability.

Recent research has highlighted the importance of developing more accurate and effective models for evaluating the relationship between soil pore structure and shear strength. Such models can help ensure the safety and effectiveness of soil structures for various applications, from building foundations to infrastructure projects. Overall, developing better soil models requires a thorough understanding of the complex interactions between soil properties, structures, and the environment.

6.5 SUMMARY

This chapter provides an overview of the findings and methodology of a study investigating the effects of various PVD, mandrel system and vacuum preloading techniques on soft soil. The present study provides a comprehensive discussion on the analysis of microstructure and the interpretation of results, encompassing chemical reactions. The process of interpretation involves the utilization of the ImageJ software program to conduct an analysis of the structural components both prior to and subsequent to the testing phase. The parameter indicating the ability of a soil to allow fluids to pass through it, commonly referred to as soil permeability. A linear correlation between the pore area (*n*) and permeability (*k*) can be observed. The linear increase in permeability occurs due to the creation of additional pores through preloading. It is noteworthy that the correlation between permeability and pore area ratio could exhibit variability contingent upon the soil's type and composition. In order to evaluate the efficacy of preloading on a particular soil type, it is necessary to fully understand the specific relationship between pore area and permeability.

Moreover, the highest increase in shear strength (s_u) was observed in the smear zone and constantly decreased with increasing radial distance for each PVD type. The utilization of microstructure analysis facilitated the investigation of the phenomenon of clogging through the determination of the pore area (*n*) and particle area (Ø) of the structure resulting from preloading. The observed correlation between shear strength (s_u) and pore area (*n*) indicates that a decrease in pore area is associated with an increase in shear strength.

The findings suggest that the correlation between (s_u) and (*n*), as well as (*k*) and (*n*), may serve as a means of ascertaining the impact of the mandrel system and vacuum preloading. The research established a correlation between the area of pores and shear strength, whereby the strength exhibited an upward trend as the pore area decreased. In addition, the study demonstrates that selecting the optimal mandrel system is crucial for improving the ground quality in geotechnical engineering design.

6.6 REFERENCES

Artidteang, S., Bergado, D. T., Saowapakpiboon, J., Teerachaikulpanich, N., & Kumar, A. (2011). Enhancement of efficiency of prefabricated vertical drains using surcharge, vacuum and heat preloading. *Geosynthetics International*, *18*(1), 35–47. https://doi.org/10.1680/gein.2011.18.1.35

Aydilek, A. H., & Edil, T. B. (2004). Evaluation of Woven Geotextile Pore Structure Parameters Using Image Analysis. *Geotechnical Testing Journal*, *27*(1), 1–12. https://doi.org/10.1520/GTJ11070

Bergado, D. T., & Balasubramaniam, A. (1996). Filtration Criteria for Prefabricated Vertical Drain Geotextile Filter Jackets in. *Geosynthetics International*, *3*(January), 63–83. https://doi.org/10.1680/gein.3.0054

Carroll, R. . (1983). *Geotextile Filter Design*. Transportation Research Recors, 916: 46-53. https://onlinepubs.trb.org/Onlinepubs/trr/1983/916/916-008.pdf

Chai, J. chun, Fu, H. tao, Wang, J., & Shen, S. L. (2020). Behaviour of a PVD unit cell under vacuum pressure and a new method for consolidation analysis. *Computers and Geotechnics*, *120*, 103415. https://doi.org/10.1016/j.compgeo.2019.103415

Chow, J. K., Li, Z., & Wang, Y. H. (2019). Comprehensive microstructural characterizations of 1-D consolidated kaolinite samples with fabric tensors and pore elongation factors. *Engineering Geology*, *248*, 22–33. https://doi.org/10.1016/j.enggeo.2018.10.016

Chu, J., Bo, M. W., & Choa, V. (2004). Practical considerations for using vertical drains in soil improvement projects. *Geotextiles and Geomembranes*, *22*(1–2), 101–117. https://doi.org/10.1016/S0266-1144(03)00054-2

Fischer, E. R., Hansen, B. T., Nair, V., Hoyt, F. H., & Dorward, D. W. (2012). Scanning Electron Microscopy. *Current Protocols in Microbiology*, *25*(1), 1–47. https://doi.org/10.1002/9780471729259.mc02b02s25

Forestry, I. (1957). *NATURE September 28, 1957*. *1*.

Geng, X., Indraratna, B., & Rujikiatkamjorn, C. (2011). Effectiveness of partially penetrating vertical drains under a combined surcharge and vacuum preloading. *Canadian Geotechnical Journal*, *48*(6), 970–983. https://doi.org/10.1139/t11-011

Griffiths, F. J., & Joshi, R. C. (1991). Change in pore size distribution owing to secondary consolidation of clays. *Canadian Geotechnical Journal*, *28*(1), 20–24. https://doi.org/10.1139/t91-003

Mesri, G., & Khan, A. Q. (2012). Ground Improvement Using Vacuum Loading Together with Vertical Drains. *Journal of Geotechnical and Geoenvironmental Engineering*, *138*(6), 680–689. https://doi.org/10.1061/(ASCE)GT.1943-5606.0000640

Mitchell, J. (1993). *Fundamentals of Soil Behaviour*. Wiley and Sons, New York,. https://doi.org/10.2136/sssaj1976.03615995004000040003x

Nelson, J. A., & Westrich, R. M. (1974). *Scanning Electron Microscopy for Microstructural Analysis James*. *1*, 41–54.

Ni, H., Liu, J., Huang, B., Pu, H., Meng, Q., Wang, Y., & Sha, Z. (2021). Quantitative analysis of pore structure and permeability characteristics of sandstone using SEM and CT images. *Journal of Natural Gas Science and Engineering*, *88*(February), 103861. https://doi.org/10.1016/j.jngse.2021.103861

Penumadu, D., & Dean, J. (2000). Compressibility effect in evaluating the pore-size distribution of kaolin clay using mercury intrusion porosimetry. *Canadian Geotechnical Journal*, *37*(2), 393–405. https://doi.org/10.1139/cgj-37-2-393

Sachan, A. (2007). Variation in geometric arrangement of particles in kaolinite clay due to shear deformation using SEM technique. *Current Science*, *93*(4), 515–522. https://www.scopus.com/record/display.uri?eid=2-s2.0-34548682579&origin=inward

Ural, N. (2021). The significance of scanning electron microscopy (SEM) analysis on the microstructure of improved clay: An overview. *Open Geosciences*, *13*(1), 197–218. https://doi.org/10.1515/geo-2020-0145

Wang, J., Cai, Y., Fu, H., Hu, X., Cai, Y., Lin, H., & Zheng, W. (2018). Experimental study on a dredged fill ground improved by a two-stage vacuum preloading method. *Soils and Foundations*, *58*(3), 766–775. https://doi.org/10.1016/j.sandf.2018.02.028

Wang, P., Han, Y., Zhou, Y., Wang, J., Cai, Y., Xu, F., & Pu, H. (2020). Apparent clogging effect in vacuum-induced consolidation of dredged soil with prefabricated vertical drains. *Geotextiles and Geomembranes*, *48*(4), 524–531. https://doi.org/10.1016/ j.geotexmem.2020.02.010

Wang, Y.-H., & Siu, W.-K. (2006). Structure characteristics and mechanical properties of kaolinite soils. I. Surface charges and structural characterizations. *Canadian Geotechnical Journal*, *43*(6), 587–600. https://doi.org/10.1139/t06-026

Xu, B. H., He, N., Jiang, Y. Bin, Zhou, Y. Z., & Zhan, X. J. (2020). Experimental study on the clogging effect of dredged fill surrounding the PVD under vacuum preloading. *Geotextiles and Geomembranes*, *48*(5), 614–624. https://doi.org/10.1016/ j.geotexmem.2020.03.007

Yu, C. Y., Chow, J. K., & Wang, Y. H. (2016). Pore-size changes and responses of kaolinite with different structures subject to consolidation and shearing. *Engineering Geology*, *202*, 122–131. https://doi.org/10.1016/j.enggeo.2016.01.007

CHAPTER
VII
CONCLUSIONS AND FUTURE WORKS

7.1 CONCLUSIONS

The main objective of this dissertations is to evaluate the performance of the prefabricated vertical drain (PVD) due to installation with designed rectangular mandrel on soft ground. This research was conducted to simulate the field condition by numerical analysis including calculated the embodied CO_2 emission, model testing by optimization large scale consolidation apparatus (1g model), and microstructure analysis by using SEM. The main conclusions can be drawn as follows:

1. The study based on field condition focuses on accurately predicting settlement by evaluating different PVD spacings through assessing soil parameters. It has been found that different spacings lead to different settlement durations and that the combined ground improvement method such as surcharge or vacuum preloading can accelerate consolidation settlement. However, the study acknowledges the limitations of the numerical study model and highlights the importance of monitoring the settlement plate to better understand the influence effect. By taking into account environmental impacts. The ground improvement projects can become more sustainable. Additionally, the study calculated the emissions coefficient for runway construction using the ICE database and presented the accuracy of the estimate for the total embodied CO_2 emissions for construction materials including PVD material. Overall, the study calculated the embodied CO_2 emission found that the PVD material had higher saving CO_2 emission comparing with other ground improvement based on this study, it also highlights the importance of monitoring and understanding the influence effect. Finally, the study demonstrates how incorporating environmental factors can make ground improvement projects more sustainable.
2. Development of a 1g model testing in laboratory and SEM analysis explains the experimental laboratory testing conducted in this research. The results describe the experimental approach employed to test the performance of prefabricated vertical drains (PVD). The experiments were performed using a large-scale consolidation model at 1g model, with SEM analysis used to examine the soil microstructure. The testing procedure

includes a detailed description of the PVD material, soil properties, scaling laws, apparatus functions, and mandrel driven PVD design. Three types of PVD were tested, and the distribution patterns of vacuum pressure were studied under four experimental conditions. The following subsections elaborate on each aspect of the experimental setup and testing procedure, including physical characteristic tests such as particle size distribution, plastic limit, liquid limit, plastic index, specific gravity, water content, permeability, and shear strength of the soil. The SEM images were analyzed using ImageJ software to investigate the pore area and microstructure. Overall, the experimental method provides a detailed account of the experimental setup and procedures implemented in the present study to evaluate the performance of PVDs in ground improvement.

3. The study proposes a new terminology based on the classic three-zone theory of large-scale consolidation technique and evaluates the effect of an extended inner smear zone in the transition zone on consolidation rate using a 1g model test. The study also examines the effect of water content, water flow rate, discharge capacity, and consolidation rate to determine the performance of the PVD. The empirical analysis shows that the use of the rectangular mandrel and three types of PVD can predict the ideal result for optimal PVD performance during testing. The performance can also be examined using the water flow rate and discharge capacity. A modification factor is proposed to understand the effect of the extended smear zone in the transition zone on consolidation rate. Overall, the study provides insights into improving PVD performance and understanding the factors that can influence.
4. In most design the study found a correlation between pore area and shear strength in soft soil. Specifically, the results indicated that as pore area decreased, shear strength increased. The study also highlighted the importance of selecting the optimal mandrel system for improving ground quality in geotechnical engineering design. This could have practical implications for engineers and designers who are involved in ground improvement projects, as they may need to consider the pore area and select the appropriate mandrel system to achieve the desired shear strength. Overall, this study contributes to the understanding of the relationship between pore area and shear strength in soft soil and provides insights into optimizing ground improvement techniques.

7.2 FUTURE WORKS

This research has been accomplished the objectivities and necessities described in Chapter 1. However, further detailed studies are needed to investigate certain scopes and issues, listed as follows:

1. The recommendation for construction project could focus on further refining the numerical model, exploring other ground improvement techniques, and adopting sustainable practices to make ground improvement projects environmentally friendly. Additionally, the use of emissions coefficients for other pollutants could also be explored to improve sustainability by exploring other predictive techniques for calculating CO_2 savings
2. Future work in this area could focus on improve the testing procedures and explore the use of alternative materials and techniques
3. Future research could further explore the use of this terminology and modification factor in practical applications and investigate other factors that may impact the performance of PVD systems in different soil types. Additionally, continued development of empirical analysis techniques could enhance the ability to predict the behavior of PVD systems in the field.
4. Future research could explore additional factors affecting shear strength in various soil types and refine ground improvement techniques by exploring different mandrel systems.